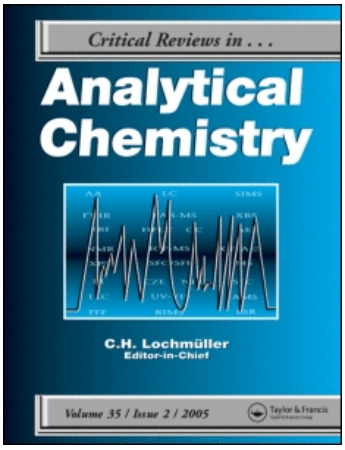


**Critical Reviews in Analytical Chemistry**
Publication details, including instructions for authors and subscription information:
http://www.informaworld.com/smpp/title~content=t713400837

# Differential Absorption Lidar Techniques in the Determination of Trace Pollutants and Physical Parameters of the Atmosphere

Eugenio Zanzottera[a]
[a] Laser and Lidar Section of CISE S.p.A., Milano, Italy

**To cite this Article** Zanzottera, Eugenio(1990) 'Differential Absorption Lidar Techniques in the Determination of Trace Pollutants and Physical Parameters of the Atmosphere', Critical Reviews in Analytical Chemistry, 21: 4, 279 — 319
**To link to this Article: DOI:** 10.1080/10408349008051632
**URL:** http://dx.doi.org/10.1080/10408349008051632

# Differential Absorption Lidar Techniques in the Determination of Trace Pollutants and Physical Parameters of the Atmosphere

*Eugenio Zanzottera*

Referee: Walter L. Zielinski, Ph.D.
Center for Analytical Chemistry
National Institute of Standards and Technology
Gaithersburg, Maryland

## LIST OF SYMBOLS

$A$ = area ($cm^2$)

$B$ = bandwidth of the receiver (Hz)

$c$ = velocity of light = $3 \times 10^{10}$ cm/s

$d$ = average speckle diameter (m)

$D$ = telescope diameter (m)

$e$ = electron charge = $1.6 \times 10^{-19}$ C

$f$ = frequency (Hz)

$E$ = electric field (V/m)

$F_l$ = local oscillator electric field (V/m)

$E_s$ = signal electric field (V/m)

$E_i^t$ = transmitted laser energy at frequency i (J)

$E_o$ = energy of the lower state of a transition (J)

$F_i(r)$ = overall transmitting and collecting efficiency of the optics for signal at frequency i from distance r

$G$ = photomultiplier gain

$h$ = Planck's constant = $6.626 \times 10^{-34}$ Js

$i(t)$ = heterodyne detector current (A)

$I$ = detector current (A)

$I_b$ = solar background current (A)

$I_d$ = dark current (A)

$I_n$ = noise current (A)

$I_s$ = signal current (A)

IF = Intermediate frequency (Hz)

$k$ = Boltzmann's constant = $1.381 \times 10^{-23}$ J/K

$m$ = molecular mass (Kg)

$M$ = number of speckles

$n$ = refractive index

$N$ = concentration of a molecular species ($cm^{-3}$)

$N(r)$ = concentration of a molecular species at range r ($cm^{-3}$)

$\Delta N$ = minimum detectable concentration ($cm^{-3}$)

NEP = noise equivalent power (W)

$p$ = pressure (atm)

$p_o$ = pressure of 1 atm

$P_b$ = background optical power (W)

$P_i(t)$ = signal power at frequency i detected at time t (W)

$P_i(r)$ = signal power at frequency i detected from distance r (W)

$P_i^t(t)$ = transmitted laser power at frequency i, at time t (W)

$P_l$ = local-oscillator power (W)

$P_s$ = signal power (W)

$r$ = range (cm)

$\Delta r$ = range resolution (cm)

$R$ = detector load resistor (Ohm)

$R_i$ = differential back-reflectivity at frequency i ($sr^{-1}$)

$s$ = laser spot diameter (m)

$S$ = intensity of an absorption line (cm)

**E. Zanzottera** earned his Laurea in Physics at the Università degli Studi di Milano, Italy, in 1976. Presently, Dr. Zanzottera is with the Laser and Lidar Section of CISE S.p.A., P.O. Box 12081-I 20134 Milano-Italy.

SNR = signal-to-noise ratio

t = time (s)

$T_l$ = laser pulse duration (s)

T = temperature (K)

$T_o$ = temperature of 273 K

V = visibility range (km)

$\alpha$ = volume scattering (extinction) coefficient ($cm^{-1}$ or $km^{-1}$)

$\alpha_i$ = volume scattering (extinction) coefficient at frequency i ($cm^{-1}$ or $km^{-1}$)

$\beta_i(r)$ = volume backscattering coefficient at frequency i ($cm^{-1}$ $sr^{-1}$ or $km^{-1}$ $sr^{-1}$)

$\gamma_N$ = natural half-width at half maximum (HWHM) of an absorption line ($cm^{-1}$)

$\gamma_L$ = collisional HWHM of an absorption line ($cm^{-1}$)

$\gamma_D$ = doppler HWHM of an absorption line ($cm^{-1}$)

$\delta$ = depolarization factor

$\eta$ = detector quantum efficiency

$\theta$ = laser divergence (rad)

$\lambda$ = wavelength (nm or $\mu$m or m)

$\upsilon$ = wavenumber ($cm^{-1}$)

$\upsilon_o$ = wavenumber at absorption line center ($cm^{-1}$)

$\sigma$ = normalized root-mean-square of signal fluctuation

$\sigma$ = cross section ($cm^2$)

$\Delta\sigma$ = differential absorption cross section ($cm^2$)

$\sigma_i$ = absorption cross section at frequency i ($cm^2$)

$\sigma(\upsilon)$ = absorption cross section at frequency $\upsilon$ ($cm^2$)

$\sigma_\pi$ = Rayleigh backscattering cross section ($cm^2$ $sr^{-1}$)

$\tau$ = lifetime of an excited state (s)

$\omega_l$ = angular frequency of local-oscillator (rad/s)

$\omega_s$ = angular frequency of received signal (rad/s)

$\Omega$ = solid angle (sr)

## I. HISTORICAL BACKGROUND

Optical remote sensing, remote analysis by means of light, is a two-step analysis: the first step consists in a proper excitation of the medium under study by sending into it radiation at optical frequencies; the second step consists in collecting from it a suitable light signal which has the property of being a direct or indirect carrier of the information needed about the interaction. Therefore, we need a suitable light source as a light transmitter. It can be a natural source, for example, the sun, in the passive techniques or it can be a lamp or a laser, in the active techniques. The receiving antenna is a lens or a telescope. It has the task to collect the light on a detector for the conversion of the optical signal in an electrical signal which is much easier to handle. If the light source is able to emit short pulses, then this configuration is identical to that of radio detection and ranging (radar), whose principles, applications, and utility are well known. This instrument is able to remotely detect an object and evaluate its distance by measuring the time delay between the emission of the electromagnetic pulse and the return of the echo radiation. Radar was utilized very early in the meteorological field, but in this particular application, the radar principle was first utilized at optical frequencies. In fact, in 1938, a group of French researchers was able to measure the height of the cloud base by utilizing light pulses generated by electric sparks.[1] Their device, subsequently utilized for routine measurements, can be considered the ancestor of the actual light detection and ranging (lidar) i.e., the optical analog of radar.

The subsequent discovery of the laser, which offers superior performances in terms of radiance and monochromaticity, has lead scientists to devise many possible applications in atmospheric research. The first laser application in this field is due to Fiocco and Smullin,[2] who sounded the mesosphere with a ruby laser in 1963, and to M. H. G. Lygda at Stanford Research Institute, who contemporary sounded the troposphere.[3] These systems were utilized for the detection of aerosol backscattering of clouds, hazes, and plumes. The structure of these first instruments was very simple: they consisted of the laser as a transmitter, a photomultiplier coupled to a telescope as a receiver, and an oscilloscope for signal display.

The detection of the main gaseous constituents of the atmosphere was attempted a few years later by means of Raman scattering. With this technique, Leonard[4] detected Raman scattering of $O_2$ and $N_2$ with a nitrogen laser in 1967. A year later, Cooney[5] made range-resolved measurements of nitrogen up to an altitude of 3 km with a ruby laser, and in 1970, Inaba and Kobayasi[6,7,8] with the same type of laser, performed spectral analyses of Raman echoes of nitrogen, oxygen, and several pollutants.

The subsequent progress made in lidar technology was mostly due to the discovery of new types of lasers which offered new

possibilities in terms of wavelength tunability and bandwidth. Thanks to this evolution, in 1969, Bowmann[9] was able to detect for the first time the fluorescence of stratospheric sodium utilizing a flashlamp pumped-dye laser tuned to the D1 line at 589 nm.

The technique utilizing the spectral absorption properties of gases was the last to be widely utilized in atmospheric remote sensing because of the requirement of laser tunability and emission at two different wavelengths. A pioneer in this field was Schotland, who made the first experimental[189] and theoretical[190] analysis of the Differential Absorption Lidar (DIAL) method. In 1966, he performed the first measurements of humidity vertical profiles utilizing a ruby laser thermally tuned around a water vapor absorption line. The first detection of an atmospheric pollutant is due to Rothe et al.[10] who detected nitrogen dioxide in a long-path measurement (at distances up to 4 km) over the town of Cologne in 1973. A year later, the same authors[11] reported range-resolved differential absorption measurements of $NO_2$ by horizontally scanning the lidar. In the same year, Grant et al.[12] reported calibrated measurements of $No_2$ obtained by firing the laser through a chamber containing a known amount of gas. This last experience was also important because it was obtained with an experimental setup that is now standard (see Figure 1), i.e., in this experiment, use was made of digital recording of lidar echoes and computer data acquisition. This structure permits the utilization of lidar acquisition. This structure permits the utilization of lidar techniques for quantitative measurements and also to perform real time data processing and analysis that are indispensable for routine field measurements.

After this pioneering work, many further possible applications have been demonstrated and several DIAL systems developed for routine measurements. Times are now propitious

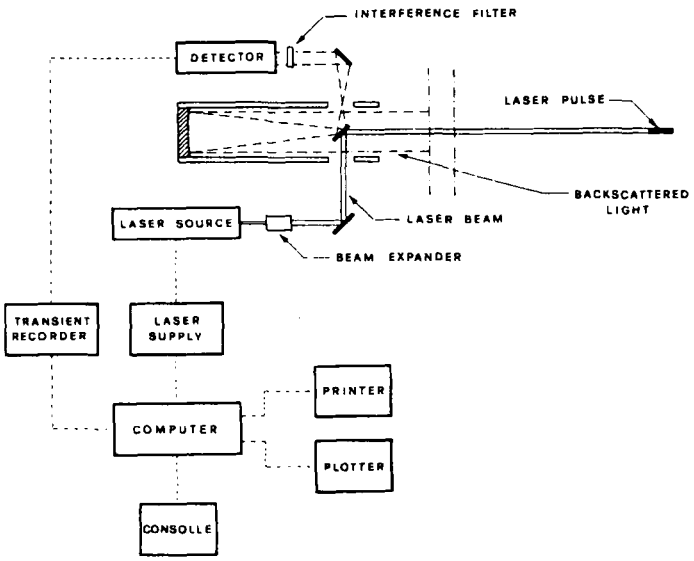


**FIGURE 1.** Block diagram of a DIAL system.

for a critical review of the real potential and usefulness of the DIAL technique and of laser remote sensing in general, which, 20 years ago, was enthusiastically accepted as a technique capable of performing many kinds of measurement. This analysis will be completed by a description of the main features of the differential absorption technique, an evaluation of its sensitivity in comparison with other methods, and a short treatment of the instrumental apparatus required. Exhaustive information about this field can be found in References 129 through 134 and 186, and, in particular, in the excellent book by Measures[129] and in the early review *Laser Monitoring of the Atmosphere.*[131]

## II. LASER REMOTE SENSING OF THE ATMOSPHERE

Light can interact with atmospheric gases and aerosols in two ways: it can be scattered or absorbed. The former interaction can be divided into elastic and inelastic scattering.

Elastic scattering (see Section V.C) is concerned with Mie and Rayleigh scattering (by aerosols and by molecules) and with resonance scattering (often identified with resonance fluorescence, to which it is associated). It is characterized by the fact that there is no energy absorption by the medium and excitation and scattered light are at exactly the same wavelength. There is only a small Doppler shift in the frequency of the received light due to the motion of the scatterers with respect to the laser source or to the receiver. This property, due to the thermal motion of molecules for Rayleigh scattering and to the wind in the case of scattering by aerosols, can be used to derive information about atmospheric temperature (which is, however, also measurable with the DIAL method: see Section VIII about meteorological lidars and wind speed, respectively.

In inelastic scattering, energy absorption by the molecule occurs so that the return light is characterized by typical frequency shifts in the case of Raman scattering, which are useful to recognize the scattering species,[75] or by emission at the same or at a lower frequency in the case of resonance and nonresonance fluorescence. Fluorescence is a two-step process: it consists in the absorption of a quantum of light and in the subsequent radiative deexcitation. This process is characterized by a typical decay time, while resonance scattering is instantaneous; moreover, the fluorescence is highly damped by collisions at standard temperature and pressure. Both phenomena are typical of metal vapors[103] in which the relevant cross section is very high. From the point of view of lidar detection, the distinction between resonance scattering and fluorescence is unimportant.

Absorption of radiation in the atmosphere can be attributed to many factors. Scattering of radiation alone is responsible for the attenuation of laser beams simply because it removes from the optical path part of the light. This property, while useful on one hand because it provides a distributed reflector

which generates most of the lidar signal, limits, on the other hand, the useful operating range in the case of low visibility conditions. Particulate absorption is responsible for modifying the aerosol-scattering behavior and can be accompanied by a noticeable fluorescence. Gas absorption, which occurs for every species at typical wavelengths and is a standard analytical tool in laboratory measurements, is also very useful in remote sensing.

Raman scattering and fluorescence directly supply a light signal that is proportional to the intensity of the excitation light and to the concentration of the gas to be analyzed. The absorption methods instead require a bistatic geometry, as in Figure 2A (in which transmitter and receiver are facing on the opposite sides of the area to be monitored), or some kind of reflective targets, as in Figure 2B. These targets can be naturally occurring topographic reflectors, such as buildings, hills, and terrains, or a real optical mirror placed at the end of the area under study or a distributed reflector constitued by backscattering particles, as in Figure 2C. In the first two cases,

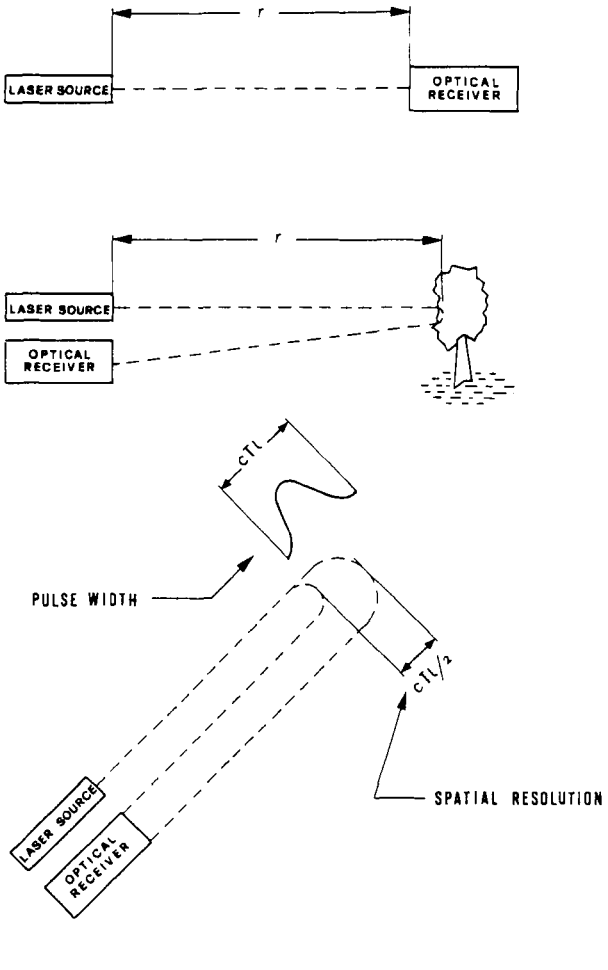


**FIGURE 2.** Configurations adopted for atmospheric absorption measurements. A: Bistatic lidar, B: Monostatic lidar with back-reflector, C: Monostatic lidar with distributed reflector.

only the average concentration of the gas in the optical path can be measured, while the third system is able to give range-resolved measurements, that is to measure concentration as a function of the distance. In all these measurement schemes, the light signal is affected by *a priori* unknown quantities, such as atmospheric transmission, target reflectivity, or atmospheric backscattering. In order to cancel these effects, which are slow functions of wavelength, a differential approach is usually adopted. This approach consists in utilizing two wavelengths so close to each other to be identically subjected to all these parameters but corresponding to maximum and minimum spectral absorption for the species investigated. The ratio of the relative return signals is then a function only of the gas concentration multiplied by the range (see Section III).

This method is usually named DIAL; the term DASE[189,190] (Differential Absorption of Scattered Energy) was also used. DIAL is utilized to indicate instruments with range-resolution capabilities as well as systems requiring topographic reflectors. With the last configuration, a continuous wave laser source can also be used. A further subdivision among DIALs can be made between systems utilizing direct detection of the optical signal or heterodyne detection; this item is dealt with in Section VI.

## III. PRINCIPLES OF THE DIAL METHOD

Let's now evaluate the optical signal power $P_i(t)$ received at time t with the scheme of Figure 2B, utilizing a topographic target:

$$P_i(t) = P_i^t\left(t - \frac{2r}{c}\right)F_i(r)R_i\frac{A}{r^2}$$

$$\exp\left\{-2\int_o^r dr'\left[\alpha_i(r') + \sigma_i N(r')\right]\right\} \qquad (1)$$

where

| | | |
|---|---|---|
| $P_i^t(t)$ | = | transmitted optical power (W) |
| r | = | distance (cm) |
| c | = | speed of light = $3 \times 10^{10}$ cm/s |
| $F_i(r)$ | = | overall receiver and transmitter optical efficiency |
| $\sigma_i$ | = | gas absorption cross section ($cm^2$) |
| A | = | receiver area ($cm^2$) |
| $\alpha_i(r)$ | = | scattering attenuation coefficient ($cm^{-1}$) |
| $R_i$ | = | target back-reflectivity per solid angle ($sr^{-1}$) |
| i | = | suffix to denote wavelength i |
| N(r) | = | concentration of the gas ($cm^{-3}$) |

The reflectivity $R_i$ can be taken equal to the total scattering coefficient divided by $\pi$ if the reflector is assumed to be lam-

bertian. The reflectivity can be higher if a nonisotropic reflector (for example, the reflectors utilized for road signs, which back-reflect the light in a narrow cone of few degrees) with enhanced backward scattering is utilized. $F_i$ takes into account the losses on the optical components and the collecting optical efficiency which is a function of range.

Let i = 1 and 2 to indicate wavelength of maximum and minimum absorption (for example, $\lambda_{on}$ and $\lambda_{off}$ of Figure 3). Let's also indicate with $\Delta\sigma$ the differential absorption cross-section:

$$\Delta\sigma = \sigma_1 - \sigma_2 \qquad (2)$$

The absorption cross-section is customarily expressed in square centimeters or square meters; the concentrations are expressed in number of molecules per unit of volume. Also often utilized are the units $atm^{-1}\ cm^{-1}$. In this last case, the gas concentration is expressed in terms of partial pressure or in parts per million (ppm) or parts per billion (ppb). As shown in the following sections, the absorption cross-section is characterized by two parameters: the transition intensity and the linewidth. The former is dependent on temperature only, while the latter is also a function of pressure. The coefficient expressed in units $atm^{-1}\ cm^{-1}$, in addition, depends on temperature through the molecular density (number of molecules per cubic centimeter), which is evaluated by means of the perfect gas law. Therefore, care should be taken in selecting the appropriate coefficient with reference to the atmospheric conditions.

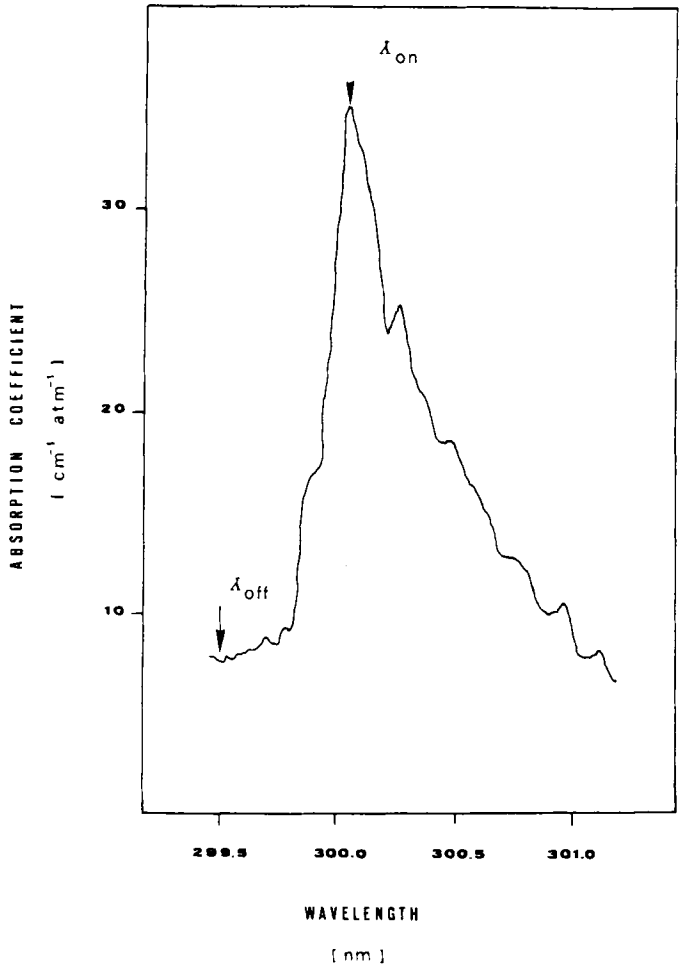


**FIGURE 3.** Absorption spectrum of sulfur dioxide from 299.5 to 301 nm; showing an example of a pair of wavelengths utilized for DIAL detection.

Expression 1 must be inverted in order to evaluate the gas concentration. In the differential absorption scheme, the following approximations are assumed to hold:

$$\alpha_1 = \alpha_2 \qquad R_1 = R_2 \qquad (3)$$

These assumptions are justified only if the two wavelengths can be chosen very close and if the pulses are emitted at the same time. As it will be shown later, there are a few significant exceptions. From Equations 1, 2, and 3, the average gas concentration between the lidar position and the reflector can be easily calculated as follows:

$$N = \frac{-1}{2r\Delta\sigma} \ln\left(\frac{P_1 P_2^t F_2}{P_1^t P_2 F_1}\right) \quad [cm^{-3}] \qquad (4)$$

where, for the sake of clarity, the time dependence of transmitted and received powers have been dropped.

In the case of the distributed reflector, the lidar signal obtained with a short laser pulse at wavelength i, emitted at time t°, can be described by the following equation.[13]

$$P_i(r) = E_i^t \frac{c}{2} F_i(r)\beta_i(r) \frac{A}{r^2} \exp\left\{-2\int_o^r dr'\left[\alpha_i(r') + \sigma_i N(r')\right]\right\} \qquad (5)$$

where $E_i^t$ is the transmitted energy, $\beta_i(r)$ is the backscattering coefficient ($cm^{-1}\ sr^{-1}$), and r is the range, corresponding to the time t: $r = c\,(t - t°)/2$. Equation 5 is identical to Equation 1 with the substitution of $R_i$ with $\beta_i(r)$. The spatial resolution, i.e., the length element sounded at a given instant, is imposed by laser-pulse duration $T_l$ and is $cT_l/2$. The spatial resolution is also limited by the time response of the receiver and detection electronics. In general, $T_l$ must be substituted by the overall effective response time of the system. A more general form of the lidar return, which takes into account laser-pulse duration and detector response time, can be found in Reference 34.

The average concentration in the path between r and r + $\Delta r$ can be obtained from Equation 5 in the earlier approximations by assuming that $\beta_i(r)$ is nearly constant for the small

frequency shift and that $F_i(r)$ has the same behavior vs. range for the two wavelengths. In this case, we obtain:

$$N(r \div r + \Delta r) = \frac{-1}{2\Delta\sigma\Delta r} \ln\left(\frac{P_1(r + \Delta r)P_2(r)}{P_1(r)P_2(r + \Delta r)}\right) \quad [cm^{-3}] \tag{6}$$

From this expression it can be noted that only the two lidar waveforms are needed for the evaluation. Hence, in principle, this technique does not require other calibrations except for wavelength calibration and detector linearity. In Figure 4, a typical example of lidar signals and relevant concentration vs. range is reported.

## IV. SENSITIVITY OF THE DIAL METHOD

The sensitivity of the DIAL method, generally expressed as the minimum amount of a given chemical or physical quantity that can be distinguished from noise, has to be evaluated in terms of range and spatial resolution, and cannot be defined independently. In fact, the measurement errors depend on the signal-to-noise ratio characteristic of the lidar return which, in turn, is strongly dependent on range. The signal-to-noise ratio is also influenced by the electrical bandwidth of the receiver (being inversely proportional to the square root of the bandwidth, as shown in Equations 20, 21, and 36, which is inversely proportional to spatial resolution). Moreover, the concentration is evaluated according to Equation 6, in which the spatial resolution term $d_r$ appears in the denominator; this also means that the concentration error is inversely proportional to $d_r$. Taking into account these two terms, the concentration error is inversely dependent on the spatial resolution with a power exponent of 1.5.

In Section VI, dealing with the error analysis of the DIAL technique, emphasis is given to these terms since they constitute an upper limitation to the precision of measurement. Other factors arising from practical instrumental limits or from the particular features of the experience are outlined in some typical cases.

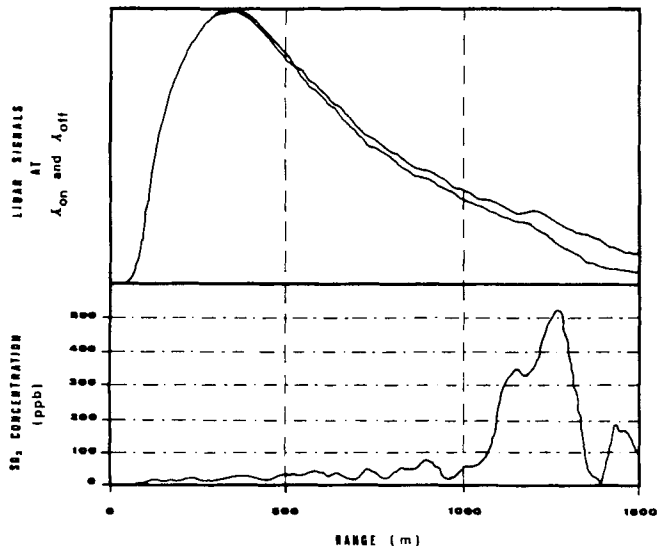


**FIGURE 4.** DIAL detection of sulfur dioxide in a plume of a power plant. The two lidar signals (arbitrary unit) at the wavelengths of Figure 3 and the measured concentration (ppb) are shown. The signals have been detected by a photomultiplier with gain modulation so that the tails of the signals are more amplified and appear much larger than they really are.

## V. OPTICAL PROPERTIES OF THE ATMOSPHERE

### A. Atmospheric Windows

The DIAL measurements of a particular gas are obviously possible only if the signal transmission through the atmospheric path is reasonably high, i. e., if the standard atmospheric constituents or other possible pollutants have a reasonably low absorption in the frequency range of the measurements and the gas to be analyzed is characterized by a sufficiently high-absorption cross-section. According to the atmospheric composition (which is a function of height, geographic position, season, etc.), measurements are possible only within the so-called atmospheric windows, located outside the absorption bands of the main constituents. These regions, and the corresponding detection possibilities, are examined here:

**Ultraviolet (220 to 400 nm)** —This region is limited by the absorption of oxygen[146] below 220 nm and contains the absorption spectra of many interesting gases and vapors (see Figure 5): sulfur dioxide,[137-140,144,145] ozone,[78,92] hydrogen sulfide, OH, chlorine,[142] mercury,[125,151] nitric oxide,[138,143] nitrogen dioxide,[141] aromatic molecules,[111] etc.

**Visible (400 to 700 nm)** —The visible is rather free from absorption features, only a few molecules have spectra here of use for DIAL, notably nitrogen dioxide,[140,141] chlorine,[142] iodine, and low-intensity ozone[78] (at 600 nm) and water vapor bands (see Figures 5 and 6).

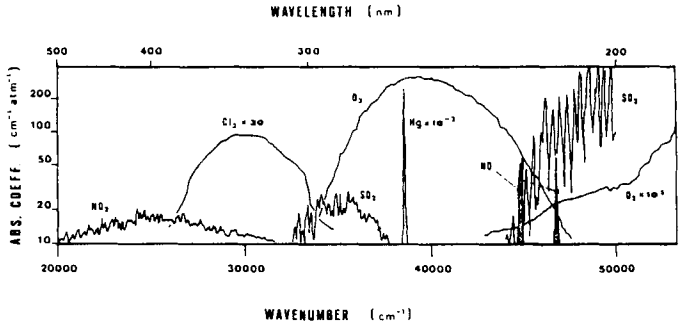


**FIGURE 5.** Absorption spectra and absorption coefficients (in units $cm^{-1}$ $atm^{-1}$) of some gases in the range 200 to 500 nm (20,000 to 50,000 $cm^{-1}$): $SO_2$,[137-140,143-145] $NO_2$,[140-141] $Cl_2$,[142] NO,[138,143] $O_2$,[146] Hg,[151] $O_3$.[78,192]

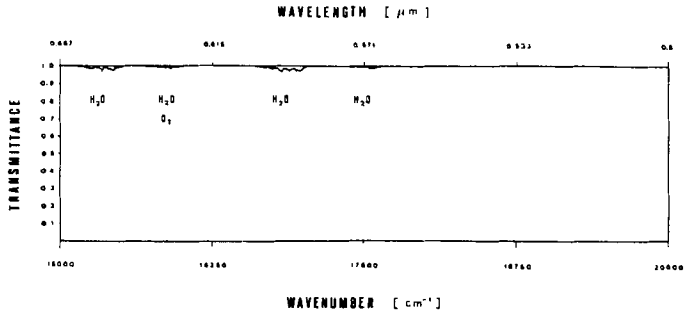


**FIGURE 6.** Atmospheric transmission spectrum from 500 to 666 nm (15,000 to 20,000 $cm^{-1}$ over a 1-km path in a standard atmosphere at sea level (at 293 K, 1 atm, and 60% relative humidity). The spectrum is computed with the data contained in AFGL tape.[28,90]

**Near infrared (700 to 2500 nm)** —Overtone and combination vibrational bands of many gases are found here, but their intensities are about two orders of magnitude smaller in comparison with the fundamental bands so that a good detection sensitivity is generally not possible except for long range. This range is then suitable for the monitoring of gases that are present in a relatively high concentration (carbon dioxide, water vapor, carbon monoxide, oxygen, etc.) and not for trace species (see Figures 7 to 9).

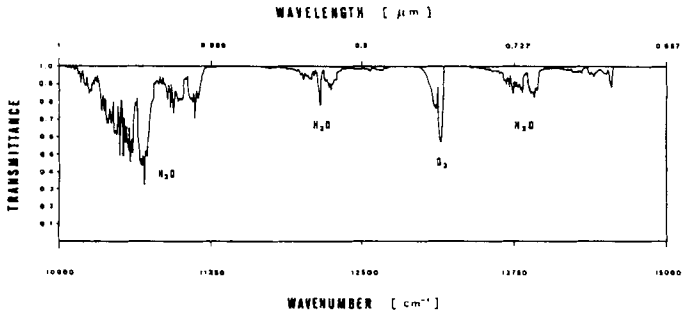


**FIGURE 7.** Atmospheric transmission spectrum from 666 to 1000 nm (10,000 to 15,000 $cm^{-1}$) over a 1-km path in a standard atmosphere at sea level (at 293 K, 1 atm, and 60% relative humidity). The spectrum is computed with the data contained in AFGL tape.[29,90]

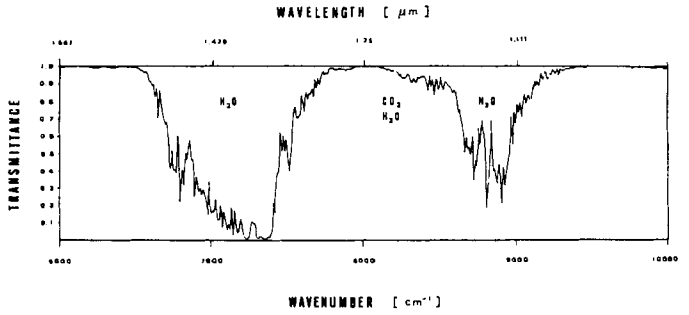


**FIGURE 8.** Atmospheric transmission spectrum from 1000 to 1666 nm (6,000 to 10,000 $cm^{-1}$) over a 1-km path in a standard atmosphere at sea level (at 293 K, 1 atm, and 60% relative humidity). The spectrum is computed with the data contained in AFGL tape.[28,90] Spectral ranges useful for pollutant detection are shown.

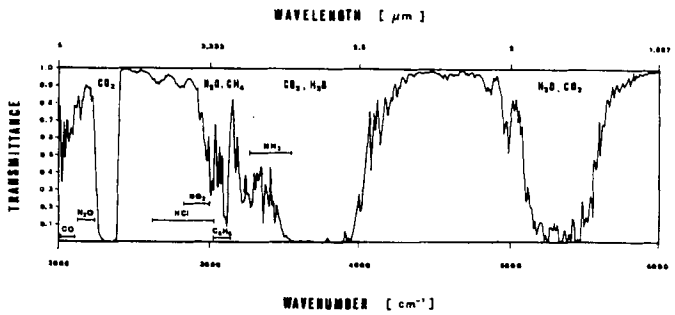


**FIGURE 9.** Atmospheric transmission spectrum from 1666 to 5000 nm (2,000 to 6,000 $cm^{-1}$) over a 1-km path in a standard atmosphere at sea level (at 293 K, 1 atm, and 60% relative humidity). The spectrum is computed with the data contained in AFGL tape.[28,90] Spectral ranges useful for pollutant detection are shown.

**Middle infrared (2500 to 25,000 nm)** —The middle infrared is particularly rich of spectral features and indeed is commonly used for standard laboratory chemical analysis. Carbon dioxide and water vapor absorptions, however, strongly limit the useful ranges (particularly the water vapor in the troposphere), as seen in Figures 9 and 10.

**Far infrared (0.025 to 0.5 mm)** —This region is not advantageous because of the lack of suitable tunable laser sources and because of the presence of intense rotational bands of water vapor.

## B. Characteristics of the Absorption Spectra of Gases

As is well known, absorption spectra in the infrared are due to roto-vibrational molecular transitions; such transitions give origin to a spectrum of lines which can be well separated (as is the case of simple molecules at low pressure, e.g., $CH_4$) or can be overlapped when their density is high in comparison to their width, e.g., methanol. The absorption cross-section utilized in the DIAL method generally corresponds to the peak of the absorption line (when a continuously tunable laser is available). If a discretely tunable laser is utilized, for example,

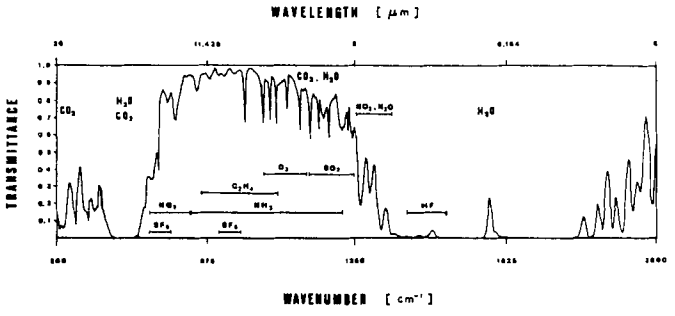


**FIGURE 10.** Atmospheric transmission spectrum from 5000 to 20,000 nm 500 to 2,000 $cm^{-1}$) over a 1-km path in a standard atmosphere at sea level (at 293 K, 1 atm, and 60% relative humidity). The spectrum is computed with the data contained in AFGL tape.[28,90] Spectral ranges useful for pollutant detection are shown.

a gas laser, there may be an accidental coincidence between an absorption line and a laser line. Typical is the case of a $CO_2$ laser, whose emission can be tuned in the spectral range from 9 to 11 μm (depending on the isotopical composition of the $CO_2$ gas), on a set of tens of narrow lines with a linewidth of less than 0.001 wavenumbers and spacing between the lines of about 2 wavenumbers.

In the ultraviolet and visible regions, absorption is due to electronic transitions, resulting in single lines in the case of atomic species (for example, alcali metals or mercury) or in complicated roto-vibrational bands in the case of poliatomic molecules. The resulting line overlapping can bring to the nearly continum spectrum of ozone or to the more structured spectra of sulfur dioxide or nitrogen dioxide, characterized by broad peaks of a few nanometers. The DIAL wavelength separation must necessarily be of the same order.

A separate line is characterized by three parameters: the position of the peak, the absorption cross-section, and the linewidth. For an isolated atom or molecule, not taking into account its relative motion with respect to the light source, the linewidth is only due to the lifetime of the energy states involved in the transition. In this case, the line profile is lorentzian and its half-width at half maximum (HWHM), $\gamma_N$, is proportional to the reciprocal of the lifetime $\tau$:[110]

$$\gamma_N = \frac{1}{2\pi\tau c} \quad [cm^{-1}] \tag{7}$$

In standard tropospheric conditions, linewidth depends on both pressure and temperature. The cause of broadening is mostly due to collisions between molecules (pressure broadening), also in this case, the lineshape is assumed to be Lorentzian, described by the following expression:[110]

$$\sigma(\nu) = \frac{S}{\pi} \frac{\gamma_L}{(\nu - \nu_o)^2 + \gamma_L^2} \quad [cm^2] \tag{8}$$

where

$\sigma$ = cross section ($cm^2$)
$\upsilon$ = wavenumber ($cm^{-1}$)
$\upsilon_o$ = line center wavenumber ($cm^{-1}$)
s = intensity of the line (cm)
$\gamma_L$ = collisional HWHM ($cm^{-1}$)

$\gamma_L$ depends on pressure and temperature through the formula:

$$\gamma_L = \gamma_o \left(\frac{p}{p_o}\right)\left(\frac{T_o}{T}\right)^b \quad [cm^{-1}] \tag{9}$$

where

p = pressure (atm)
$p_o$ = 1 atm
$T_o$ = 273 K
T = temperature (K)
$\gamma_o$ = collisional HWHM at $p_o$ and $T_o$ ($cm^{-1}$)

$\gamma_o$ depends on the type of gas and the composition of the atmosphere in which it is mixed; its value is in the range 0.05 to 0.1 $cm^{-1}$ for most gases. The exponent b, usually assumed equal to 0.5 according to kinetic theory, is in reality a varying parameter, even for different transitions of the same gas. For example, for the $O_2$ molecule, a value of 0.7 is usually adopted,[67] according to experimental data, and for $H_2O$, a value of 0.62 is generally assumed.[70]

Line intensity S is the integral of cross-section over frequency. This term is dependent on temperature only; its value is generally reported relative to 273 K and can be extrapolated at other temperatures according to[28]

$$S(T) = S(T_o)\left(\frac{T_o}{T}\right)^j \exp\left(\frac{-E_o}{kT - kT_o}\right) \quad [cm] \tag{10}$$

where

k = Boltzmann's constant = $1.381 \times 10^{-23}$ J/K
$T_o$ = 273 K
$E_o$ = energy of the lower state of the transition (J)
T = temperature (K)
j = 1 for linear molecules
= 1.5 for nonlinear molecules

Absorption line parameter compilations[28,90] usually report for each spectral line, together with line frequency, intensity, and relative quantum numbers, also the value of $E_o$ and $\gamma_o$; from these data, transmission spectra can be easily computed.

Other important collisional effects are the dramatic reduction of a lifetime of excited states to values of nsec or less, and the quenching of fluorescent emission ranging from $10^3$ to $10^5$, depending on the type of molecule.[75] This fact has different consequences: on one hand, it reduces the sensitivity of the detection system based on fluorescence and, on the other hand, the shorter lifetime allows a better spatial resolution and avoids saturation problems connected with high-intensity laser beams. In a DIAL system, the quenching of fluorescence is useful because it eliminates this extra term in the interpretation of lidar returns (see Reference 151 about the DIAL detection of mercury, which possesses a high fluorescence efficiency.)

At high altitudes in the stratosphere at low molecular density, collisions are not the dominant broadening mechanism, which is now mainly due to the Doppler effect, i.e., to the random thermal motion of the molecules. In this case, the line profile is described by a Gaussian function:

$$\sigma(\nu) = \frac{S}{\gamma_D}\sqrt{\frac{\ln 2}{\pi}} \exp\left(\frac{-(\nu - \nu_o)^2 \ln 2}{\gamma_D^2}\right) \tag{11}$$

where $\gamma_D$ is the Doppler half-width given by

$$\gamma_D = \frac{\nu_o}{c}\sqrt{\frac{2kT\ln 2}{m}} \quad [cm^{-1}] \qquad (12)$$

where

c = velocity of light ($3 \times 10^8$ m/s)
m = molecular mass (kg)

The Doppler linewidth, being proportional to the frequency of the transition, is higher in the visible than in the infrared, while collisional broadening is about the same over all frequency ranges. In the middle and far infrared, for tropospheric measurements, Doppler broadening is negligible; in the near infrared, it is about a factor of 5 smaller than the pressure term. For example, for oxygen lines at 766 nm at 273 K (proposed for lidar measurements of temperature and pressure), the Doppler HWHM is 0.0136 cm,$^{-1}$ to be compared with a collision broadening coefficient (in air) of 0.035 to 0.06 $cm^{-1}$ $atm^{-1}$.[69,71] For water vapor lines at about 725 nm, the pressure broadening coefficients are in the range 0.08 to 0.11 $cm^{-1}$ at $m^{-1}$,[70,72] and the Doppler HWHM is 0.02 $cm^{-1}$. In these cases, in particular when measurements have to be taken from the ground level up to several kilometers in height (where pressure and temperature are lower) or from a satellite pointing downwards, it is very important to define, for every altitude, a correct lineshape, represented by a convolution of the two profiles, i.e., the Voigt profile.[73] This line profile is particularly useful for the lidar measurements of atmospheric temperature[66,67] and pressure[68] because, especially in this last case where the wings and not the center of the oxygen absorption lines are utilized, it represents a better approximation.

Another effect related to pressure (therefore dependent on altitude) and important for the previously described applications is the line shift, which is proportional to pressure, with coefficients in the range $-0.001$ to $-0.008$ $cm^{-1}$ $atm^{-1}$ for the A-band of oxygen[71] and ranging between $+0.002$ and $-0.04$ for water vapor in the 720-nm region.[74] In Figure 11, the combined effect of pressure broadening and pressure shift on a water vapor line is shown.

A compilation of spectral line parameters for the evaluation of these spectra has been done by AFCRL (afterwards become AFGL) in 1973.[28] These data are the collection of the experimental results obtained by the scientific community and are continuously updated and extended not only to the standard atmospheric gases, but also to other molecular species of interest in the field of atmospheric monitoring. The latest version[90] contains the spectra of 28 gases, mostly in the IR.

Spectral data are useful not only in the definition of the best operative wavelength for the detection of a particular pollutant, but also for avoiding spectral interferences by other gases.

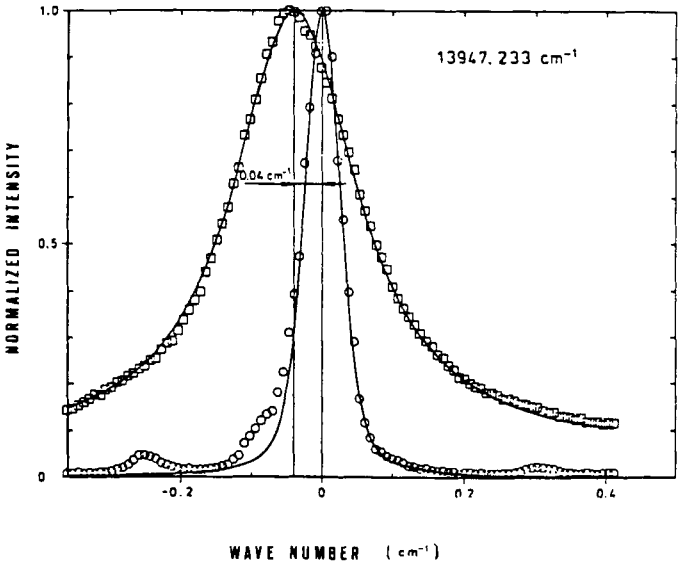


**FIGURE 11.** Pressure broadening and pressure shift of a water vapor absorption line (13947.233 $cm^{-1}$) at two different pressures: with water vapor only (narrow line) and with nitrogen at 1013 mbar total pressure and 290 K (broad line). The experimental data are fitted with Voight functions.[75] (Reproduced from Bösenberg, J. *Appl. Opt.*, 24, 3531, 1985. With permission.)

## C. Aerosol and Molecular Scattering

Atmospheric light scattering is a sum of many contributions: Raman, molecular, and aerosol. The laser beam attenuation due to the Raman term is negligible, being at least three orders of magnitude lower than the molecular scattering term and therefore, will no longer be considered. Molecular scattering (Rayleigh scattering) is a parameter completely defined in terms of the refractive index of the medium. For air, the Rayleigh cross-section is expressed by[22,129,162]

$$\sigma = \frac{8\pi^3}{3}\frac{(n^2-1)^2}{N^2\lambda^4}\left(\frac{6+3\delta}{6-7\delta}\right) \quad [cm^2] \qquad (13)$$

where n is the refractive index, N is the number of gas molecules per unit volume, and $\delta$ is the depolarization factor of the scattered radiation, defined as the ratio between the intensity of the scattered radiation at 90° with polarization orthogonal and parallel to that of the incident beam, respectively. According to Elterman,[16] $\delta$ is equal to 0.035 for the standard air mixture. A characteristic feature of Rayleigh scattering is the fourth-power dependence of frequency which is responsible for the blue color of the sky. This behavior, as verified by many authors, holds over visible and infrared up to 10 μm, with only a slight deviation due to dispersion effects.[15]

The backscattering cross section per unit of solid angle is related to the total scattering cross-section by the following expression:

$$\left(\frac{d\sigma}{d\Omega}\right)_\pi = \sigma_\pi = \frac{3\sigma}{8\pi} \quad [cm^2\ sr^{-1}] \qquad (14)$$

A useful numerical formula is given by Collis and Russel:[14]

$$\sigma_\pi = 5.45\left(\frac{\lambda(\text{nm})}{550}\right)^{-4} \times 10^{-28}\ \text{cm}^2\ \text{sr}^{-1} \qquad (15)$$

Atmospheric aerosol extinction is characterized by a much lower wavelength dependence in comparison with gaseous absorption or Rayleigh scattering. It is composed of two terms: scattering, which is most important in visible and near infrared, and absorption, which is noticeable only at longer wavelengths. Scattering by particles can fall in the Rayleigh scattering regime for particle sizes much smaller than the wavelength of light. In the opposite case (i.e., with ice and snow crystals, rain drops, or mists), the scattering is nearly independent of wavelength. For sizes of the same order of magnitude (i.e., in the case of atmospheric dust, smogs, hazes, clouds, etc.), the scattering is described by a complicated function of refractive index and scattering parameters; it was first treated in detail by Mie in 1908 for the case of dielectric spheres.[17] Mie scattering for a single particle has an oscillatory wavelength and angular behavior which is smoothed when the contribution of the scattering of a continuous distribution of sizes is taken into account.

A comprehensive description of Mie scattering can be found in many text books.[18-20] In order to apply these results to lidar work, however, it is necessary to make some assumptions about the size distribution and refractive index of the aerosol. To this purpose, the result of research efforts made during many years, (in particular the systematic work made by researchers of AFCRL and then of AFGL[15,16,21-27] in the field of optical transmission of the atmosphere) have established models which take into account most atmospheric situations. The main features of these models are[25]

1. The atmosphere is divided into regions: boundary layer (i.e., below 2 km), upper troposphere, stratosphere (10 to 30 km), and upper atmosphere (above 30 km).
2. In the boundary layer, the aerosol concentration is highly variable. In order to take into account many possible situations, it was found useful to define them in terms of meteorological range or visibility, defined as the distance at which the atmospheric transmission at 550 nm falls down to 0.02. The models generally utilized refer to the haze regime, corresponding to a visibility larger than 1.2 km which represents the transition to fog[24]. In comparison, the pure Rayleigh regime, based on the standard atmosphere (1015 mbar and 15°C), corresponds to a visibility of 336 km. Hence, the aerosol contribution to scattering is dominant in the visible, while molecular scattering dominates only in the ultraviolet with good atmospheric visibility conditions.
3. Boundary layer aerosols are described by three models: rural, urban, and maritime, representing three different distributions of particle sizes and chemical compositions. The rural model is adopted to represent continental aerosols in pollution-free regions that are far from towns or industrial areas. Their compositions are made of dusts picked up from the soil and particles produced by the reactions of atmospheric gases. The distribution law adopted by Shettle and Fenn[25] for this model is a sum of two log-normal distributions; the first principal distribution being mainly due to particle sizes in the range of 0.1- to 1.0-μm diameter and the secondary one corresponding to sizes between 5 and 100 μm. The urban model utilizes the same particle size distribution, but with a different composition, taking into account aerosol coming from combustion or industrial plants. It supposes a mixture of 65% rural aerosols (composed by ammonium and calcium sulfate, water soluble substances, dusts, etc.) and 35% carbonaceous aerosols. The maritime model considers a mixture of sea spray aerosol (salt particles) and rural aerosols depleted of the largest particles. The size distribution is largely dependent on atmospheric conditions since humidity can grow the hygroscopic salt particles and wind can increase their production. It should be noted that near pollution sources, the aerosol composition can be largely different from those predicted by these models.
4. The upper troposphere is described by a model which is less sensitive to the particular geography and meteorological and seasonal variations. It is described by a rural model depleted of the large particles.
5. The stratospheric models assume a global, uniformly distributed background of aerosols which are assumed to be composed of sulfate particles. Volcanic eruption can increase the aerosols content up to a factor of 100. The volcanic particles are then dispersed all over the world by stratospheric winds; their lifetime is typically 1 year. Besides the standard background, two volcanic aerosol-size models are considered: fresh volcanic or aged volcanic, depending on whether they refer to a recent eruption or an old one. Four different vertical distributions are generally considered: background and three volcanic profiles, depending on the amount of volcanic materials injected into the stratosphere (moderate, high, and extreme).
6. The upper atmosphere is poor of aerosols in comparison with the other layers. They are mainly composed by meteroic or cometary dusts and give origin to a negligible attenuation of light.

In conclusion, once the appropriate aerosol model has been chosen, thus defining size distribution and refractive index of the particles, one can utilize the Mie theory in order to calculate the scattering coefficients. This task has been undertaken by many authors, and their results form the basis of computer

codes for the evaluation of light transmission through the atmosphere.[15,26,30,31] Other input data necessary for these codes are gaseous composition, temperature, and density of the atmosphere with the height for various latitudes and seasons. These data[32] are important for evaluating Rayleigh scattering coefficients and the transmission spectra of atmospheric gases.

In order to define a set of scattering coefficients and give an illustrative example, one can rely upon a formula[33] which is often used in the evaluation of lidar performances and which is supposed to be a good approximation, particularly for visibilities not larger than 6 km:

$$\alpha = \frac{3.91}{V}\left(\frac{550}{\lambda}\right)^{g} \quad [km^{-1}] \qquad (16)$$

with $g = 0.585^{q}$

and $q = V^{1/3}$

Here, V, the visibility, $\alpha$, the extinction coefficient, and $\lambda$, the wavelength, are expressed in km, $km^{-1}$, and nm, respectively. As can be seen in this formula, the dependence of the scattering coefficient on wavelength is flat since the value of g is unity for useful visibility ranges. A similar behavior can be found in more sophisticated aerosol models.[15,22] For DIAL measurements of most gases, the two frequencies used for the measurements are so close that the corresponding differential absorption due to scattering is negligible in comparison with the differential absorption due to the gas.

This is not true in only a few cases, such as for ozone measurements in the ultraviolet where the absorption band of the gas is so flat and structureless that an appreciable differential cross-section corresponds to a pair of wavelengths 5 or 10 nm apart. This value is high when compared with the 280 to 300 nm at which the two wavelengths are centered. A further complication arises because in this spectral region, Rayleigh scattering (which depends inversely on the fourth power of wavelength) is comparable with aerosol scattering. As a result, this particular kind of measurement requires a correction[35-38] which can be performed only after a reliable determination of the visibility range. Milton[113] evaluated corrections of the order of 10 to 20 ppb for measurements of ozone in typical tropospheric environments when the wavelength separation is about 5 nm and relevant differential absorption coefficients are in the range of 20 to 40 $atm^{-1}$ $cm^{-1}$ (see Section X.A). In the case of a typical pollutant such as sulfur dioxide, instead, the wavelength difference can be as low as 0.5 nm (see Figure 3), with a differential absorption cross section larger than 20 $atm^{-1}$ $cm^{-1}$. The corrections are therefore one order of magnitude lower and are generally neglected.

The volume backscattering cross-section can be determined starting from the earlier scattering coefficients. For isotropic scattering, it is possible to write[39-41]

$$\beta = \frac{\alpha}{4\pi} \quad [km^{-1}\ sr^{-1}] \qquad (17)$$

The scattering is, however, generally enhanced in the forward direction.[133,205] In some cases (clouds, fogs, or precipitations), it is concentrated on a narrow angular cone around it. For a rough evaluation of the intensity of the backscattered light for DIAL applications in the troposphere, a better approximation, confirmed by experiments in plumes[29] and by calculations[42] is to take half of the value expressed in Equation 17.

## VI. BACKSCATTERED SIGNAL POWER: SIGNAL-TO-NOISE EVALUATION

### A. UV-Visible

With the scattering data calculated with Equation 6 and the system parameters defined in Table 1, it is possible to evaluate return optical power according to Equation 5. We will make the assumption that only scattering contributes to signal attenuation, that no other interfering gas is present, and that the pollutant to be measured is present in trace concentration so that to give a small absorption. Figure 12 shows the optical signals calculated for three visibility ranges: 2, 5, and 10 km. In Figure 13, the relevant signal-to-noise ratios (SNR) are shown; they are calculated assuming that the detector is a photomultiplier, as is the case in the visible and UV. The noise current $I_n$ and the SNR have been evaluated according to well-known formulas[64]

$$I_n = \sqrt{2eB(I_s + I_b + I_d) + 4kTB/RG^2} \quad [A] \qquad (18)$$

$$SNR = I_s/I_n = \frac{I_s}{\sqrt{2eB(I_s + I_b + I_d) + 4kTB/RG^2}} \qquad (19)$$

where

$I_n$ = noise current referred to the photocathode (A)

e = electron charge = $1.6 \times 10^{-19}$ C

B = detector bandwidth (Hz)

G = photomultiplier gain

$I_s$ = $P_s$ $\eta e/h\nu c$ photocathode signal current (A)

$I_b$ = $P_b$ $\eta e/h\nu c$ photocathode current due to solar background (A)

$I_d$ = dark current referred to photocathode (A)

$P_s$ = signal optical power (W)

**Table 1**
**Typical System Parameters of a UV-Visible DIAL (CISE-ENEL and IIE Systems)**

| | |
|---|---|
| Transmitter | |
| Laser type: | Nd:YAG pumped-dye laser |
| Pulse energy: | 10 mJ at 280 to 300 nm |
| Pulse duration: | 10 ns |
| Laser bandwidth: | 0.1 $cm^{-1}$ |
| Laser divergence: | 0.5 mrad |
| Repetition rate: | 20 Hz |
| Receiver | |
| Telescope configuration: | newtonian |
| Telescope diameter: | 0.6 m |
| Telescope focal length: | 1.6 m |
| Field of view: | 1 to 2 mrad |
| Detector type: | PMT Philips XP2020Q |
| Detector quantum efficiency: | 20% |
| Detector gain: | $10^4$ to $10^7$ with $t^2$ modulation |
| Detector bandwidth: | 3 Mhz |
| Transient Recorder | |
| Type: | Tektronix 390AD |
| Nominal precision: | 10 bit |
| Selected sampling rate: | 10 MHz |
| Computer Configuration | |
| Computer type: | GPX Vaxstation |
| Internal memory: | 5 Mbytes |
| External memory: | 70 Mbytes hard disk<br>90 Mbytes streamer tape |
| Consolle: | High resolution graphic display |
| Graphic hard copy: | Plotter with A3 format<br>Graphic printer |
| Overall Specifications | |
| Range: | Up to 3 km |
| Range resolution: | 15 to 240 m |
| Sensitivity: | 20 ppb of ozone or sulfur dioxide |

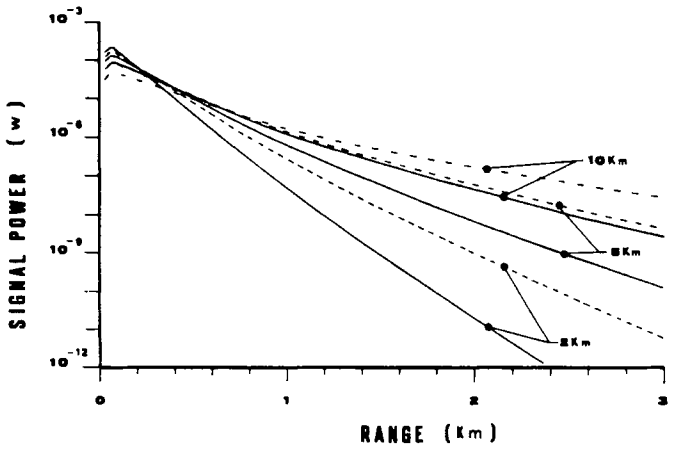


**FIGURE 12.** Computer evaluation of the backscattered light power collected by a typical DIAL system for three visibility ranges: 2, 5, and 10 km. The data are reported for two wavelength: at 300 nm (solid lines) and at 500 nm (dashed lines). The system parameters are reported in Table 1.

$P_b$ = solar background radiation power (W)

$\eta$ = photocathode quantum efficiency

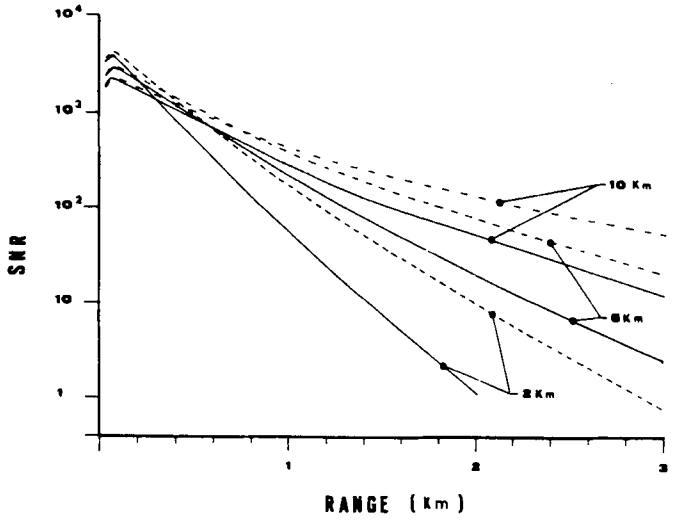


**FIGURE 13.** Signal-to-noise ratios relevant to the signals in Figure 12.

h = Planck constant = $6.626 \times 10^{-34}$ Js

$\upsilon$ = light frequency (wavenumber) ($cm^{-1}$)

k = Boltzmann constant = $1.381 \times 10^{-23}$ J/K

T = ambient temperature (K)

R = photomultiplier load resistor (Ohm)

In tropospheric DIAL systems, where the integration times are a few hundred nanoseconds (corresponding to the required spatial resolution of the order of a few tens of meters), the digitized signal is generally equivalent to the integration of many photoelectrons and the dark current is negligible. This term is only important when photon counting techniques are utilized; for example, for ground-based stratospheric ozone measurement.[35,61]

The resistor noise term is usually negligible if the photomultiplier gain is high enough. The background radiation term is important for daylight measurements and can be limited (but not always eliminated) with the utilization of narrow-band filtering and by reducing the telescope field of view. It is an important factor limiting the measurement range for measurement in the visible, the near infrared, and sometimes the ultraviolet. In the case that $I_s$ is predominant with respect to the other terms in Equation 18, then Equation 19 can be rewritten as follows:

$$SNR = \sqrt{\frac{P_s \eta}{2h\upsilon cB}} \quad (20)$$

which is the expression for shot noise-limited detection.

As it can be seen in Figure 4, the signal intensity is nearly zero at short distance because the collecting telescope is ob-

scured by the obstruction of the last transmitting mirror of the laser beam. This is a standard feature for a lidar system and depends on parameters such as beam divergence, telescope field of view, collinear or noncollinear configuration, etc.; these arguments are dealt with in the section describing receiving optics.

In an homogeneous atmosphere, the signal maximum is reached at a distance dependent on these parameters; the amplitude of the maximum is proportional to the backscattering cross-section, which, in the visible, is roughly inversely dependent on visibility. The tail of the signal has a decay which is the product of the exponential attenuation due to the aerosols, multiplied by the inverse quadratic dependence on the distance (i.e., on the time). The dynamic range of the signal, for the combined effect of these factors, is of many decades, i.e., much larger than the dynamic range of any digitizer (see Figure 12). This feature, which represents a practical limitation to the precision and range of the measurements, is discussed later. The SNR, which is proportional to the square root of the signal itself, represents the ultimate physical limit to the precision of the measurements.

Averaging over many laser pulses is the technique usually adopted for reducing the signal fluctuations. With temporally uncorrelated measurements, improvements of the precision proportional to the square root of the number of shots is obtained.[91] However, this procedure is useful in case of short-term fluctuations or in case of white noise; slow drifts of the atmospheric conditions or the instrumental parameters cannot be compensated in this way.[43,54]



## B. Infrared

For infrared detection, the Lidar signal is described by Equation 5, but the detector has a different noise behavior. An important distinction must be made in this case between direct or heterodyne detection. This choice has indeed a strong influence on the configuration of the laser, detector, and associated signal processing hardware on the transmitting and receiving telescope and on the SNR characteristics, which are deeply different in the two cases.

## C. Infrared Direct Detection

Infrared direct detection is characterized by detector noise, usually described by a noise figure, the detectivity, indicated with D* (for avalanche photodiodes, in particular for silicon devices utilized in the NIR range up to 1100 nm; also, the excess noise term[112] should be considered). From it, one can easily calculate the Noise Equivalent Power (NEP), i.e., the optical input power equivalent to detector noise:[187,188]

$$\mathrm{NEP} = \frac{\sqrt{AB}}{D^*} \quad [\mathrm{W}] \qquad (21)$$

where

A = detector sensitive area ($cm^2$)

B = detector bandwidth (Hz)

D* = detectivity (cm $Hz^{1/2}$ $Watt^{-1}$)

The SNR is evaluated by simply dividing the signal optical power by the NEP. In this case, the SNR is directly proportional to received optical power. A comparison with the performances of a typical UV-visible lidar provides the following results:

1. The lidar signal is much lower in the infrared because of the lower scattering cross-sections.
2. For the same reason, the signals in the IR are less attenuated by aerosols.
3. The infrared detectors have much more noise.
4. The SNR has a steeper behavior with range in the IR because of the linear dependence on signal amplitude. In the UV-visible instead, according to Equation 20, the SNR is proportional to the square root of the received optical power.
5. The SNR values are much lower than the correspondent values of a UV-visible system with the same laser energy and telescope size.

For this reason, it is difficult to use a direct-detection IR system for range-resolved measurements and, in fact, generally they have been utilized for integrated path concentration measurements with the help of a topographic reflector,[49,53-58,104] Only a few exceptions to this rule are reported: the DIAL system based on powerful $CO_2$ lasers[44,45,50] (able to produce energies per pulse of the order of 1 J) and a system based on a DF laser.[46]

In Reference 50, an evaluation of the system parameters required for range-resolved measurements with a $CO_2$ laser at 10-km range is made: 15 J per pulse and a 1.2-m diameter telescope are required for a SNR of 50 in a single shot (a comparison between direct and heterodyne detection can also be found in Reference 65). Coherent detection instead typically requires only a 0.1 J with a 28-cm telescope,[51,52] with the drawback of a larger sensitivity to turbulence effects and speckle noise.[47-49,51,59,60,184] The $CO_2$ laser systems, nothwithstanding their high emission energy, are now generally converted to heterodyne detection that offers superior performances, thanks to the quantum noise-limited operation, at a cost of a much more expensive and complex system. Direct detection is generally limited to short-range applications, where it still maintains a superiority; it should be utilized only when a detection SNR larger than one is expected. Recently, research on laser preamplifiers at $CO_2$ frequencies[117-119] has shown that the SNR of direct detection can be improved by a factor up to 700 using this method. Even if this is a very good result, up to now, this solution is too cumbersome to be practical because it requires a multiple transmission of the received signal in a $CO_2$ tube,

kept at constant gain for a long time (tens of microseconds) before the detection.

It should be noted that detectors at $CO_2$ frequencies are particularly not advantageous because they suffer high thermal noise, about one order of magnitude larger in comparison with a detector at HF or DF laser wavelength (3 to 4 μm). Moreover, in this spectral region, the backscattering coefficients are also lower. On the other hand, $CO_2$ lasers are much more powerful than any tunable laser.

### D. Heterodyne Detection

The principle on which optical heterodyne detection is based is described in many textbooks. (For a more detailed presentation, see References 62 and 63.) An exhaustive analysis of this technique in a DIAL application has been made by Hardesty.[51] Here, only the more important features are outlined.

The optical block diagram of heterodyne detection is shown in Figure 14. The lidar return signal is collimated and coherently mixed on a detector, with the radiation coming from another laser (local oscillator or LO). Coherent mixing means that every part of the LO and signal beams must be in phase on the detector surface and with the same polarization. The emission frequency of the local oscillator is generally shifted a few MHz with respect to the other laser or can be identical if the same laser is used as LO and a transmitter. In this last case, the system is more appropriately indicated with the term homodyne. Homodyne detection suffers 1/f noise, which, instead, is eliminated by the frequency offset in heterodyne detection. Optical detectors are sensitive to the intensity of the radiation field, i.e., to the square of the electric field. The total electric field, E(t), on the detector is the sum of the two electric fields:

$$E(t) = E_l\cos(\omega_l t) + E_s\cos(\omega_s t) \quad (22)$$

where l and s denote local oscillator and signal, respectively, and ω is the angular frequency (rad/s). The current i(t) on the detector is proportional to the square of E(t):

$$i(t) = aE(t)^2 \quad (23)$$

$$E(t)^2 = E_l^2\cos^2(\omega_l t) + E_s^2\cos^2(\omega_s t) + E_lE_s\cos[(\omega_l + \omega_s)t] + E_lE_s\cos[(\omega_l - \omega_s)t] \quad (24)$$

where a is a proportionality constant. By taking the time average of 24 over many periods, the third term vanishes so that

$$i(t) = a\left(\frac{E_l^2}{2} + \frac{E_s^2}{2} + E_sE_l\cos[(\omega_l - \omega_s)t]\right) \quad (25)$$

The current i(t) is simply the sum of the contributions of the intensities of the two signals plus a term representing the beat between them. By filtering around the intermediate frequency IF = $(\omega_l - \omega_s)$, the first two DC terms vanish. The remaining term, i.e., the useful signal at IF, can then easily be expressed in terms of $P_l$ and $P_s$ which are the optical powers of local oscillator and light signal on the detector:[62]

$$I_s = \frac{\eta e}{h\nu c} 2\sqrt{P_sP_l}\cos[(\omega_l - \omega_s)t] \quad (26)$$

The evaluation of the SNR starts from the expression of the noise current $I_n$ for a detector:

$$I_n = \sqrt{2eIB} \quad (27)$$

where I is the total current, i.e., the sum of i(t) plus the detector dark current, $I_d$. Equation 27 is identical to Equation 18 for a unitary gain and neglecting the noise resistor term. It is possible to demonstrate that if $P_l$ is made high enough, the SNR (i.e., $I_s/I_n$) can be expressed as follows:[62]

$$SNR = \sqrt{\frac{P_s\eta}{Bh\nu c}} \quad (28)$$

The value of $P_l$ for which this equation holds has been evaluated in Reference 63:

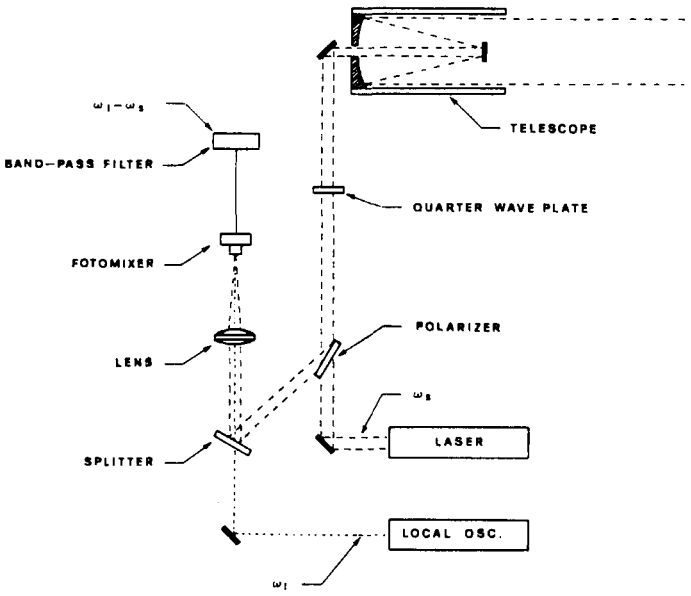


**FIGURE 14.** Block diagram for heterodyne detection. The laser beam is polarized in the plane of the figure so that it is completely transmitted by a polarizer (generally, a germanium plate at a brewster angle in the case of a $CO_2$ laser). A quarter-wave plate transforms the linear polarization of the laser beam into the circular polarization of the transmitted beam, and again, the circular polarization of the received beam in linear polarization, but now normal to the plane of the figure. With this expedient, the return signal is reflected by the polarizer in the receiver branch of the lidar. The bandpass filter transmits the intermediate frequency only.

$$P_l > \frac{A}{h\nu c D^{*2}} \quad [W] \tag{29}$$

where A is the detector-sensitive area.

Equation 28, which is similar to Equation 20, corresponds to quantum-limited detection and is valid for photoemissive (photomultipliers) and photovoltaic detectors. For photoconductors, the SNR is equal to this value divided by the square root of 2.[62] The following features of heterodyne detection are worth being stressed:

1. As it is clear from Equation 26, the signal current is proportional to the square root of the optical power; hence, the dynamic range of the electrical signal is greatly reduced when compared to direct detection where the signal is proportional to the received optical power. This results in a great benefit in the analog-to-digital conversion.
2. As the signal current is proportional to the square root of the optical power, it must be squared for a proper averaging and for the concentration evaluation according to Equation 6.
3. The SNR defined in Equation 28 is relevant to the signal current; it can be easily demonstrated that the SNR of the optical power is half of this value.
4. The SNR has a much slower behavior with range in comparison with the case of infrared direct detection, therefore, it is much more similar to the UV-visible case.
5. The effective SNR is not completely described by Equation 28, which could strictly hold only in the case described by Figure 2A). With a scatterer as a retroreflector, one has to deal with the speckle noise which produces a strong fluctuation of the signal. This term is described in the next section.
6. Heterodyne detection with a $CO_2$ laser still compares favorably with the visible direct detection because even if the scattering coefficents are one or two magnitudes lower,[15,122] this drawback is well compensated by a typical emission energy one magnitude higher and by photon energies about 20 times smaller (see the term h ν c in the denominators of Equations 28 and 20).

In Table 2, the parameters of a typical coherent system are reported.[184]

## E. Speckle Noise

When a target is struck by a laser beam, the backscattered light produces speckles on the observer plane (in this case, the telescope aperture), i.e., areas of higher illumination, whose average diameter is given by the following Equation:[104,105]

$$d = \frac{2\lambda r}{s} \quad [m] \tag{30}$$

where

**Table 2**
**Typical System Parameters of a Coherent DIAL (MAPM-Mobile Atmospheric Pollution Monitoring System of JPL)**

| | |
|---|---|
| Transmitter | |
| Laser system: | Two $CO_2$ lasers |
| Pulse energy: | 60 mJ |
| Pulse duration: | 0.5 to 2 μs |
| Operating wavelength: | 9.2 to 10.7 μm |
| Laser bandwidth: | Single longitudinal mode |
| Repetition rate: | 50 to 150 Hz |
| Receiver | |
| Telescope configuration: | Off-axis parabolic |
| Telescope diameter: | 0.3 m |
| Telescope focal length: | 1.5 m |
| Detector type: | HgCdTe cooled at 77 K |
| Detector size: | 0.25 mm |
| Intermediate frequency: | 30 Mhz |
| Transient recorder | |
| Type: | HP 5182A |
| Nominal precision: | 10 bit |
| Selected sampling rate: | 5 Mhz |
| Overall specifications | |
| Range: | Up to 1 to 3 km with direct detection<br>Up to 5 to 10 km with heterodyne detection |
| Range resolution: | 300 m |

λ = laser wavelength (m)

r = distance of the target (m)

s = laser spot diameter on the target (m)

The normalized statistical fluctuations of the light signal collected by the telescope are inversely proportional to the square root of the number, M, of speckles contained in the telescope area:

$$\sigma = M^{-1/2} \tag{31}$$

that is

$$\sigma = \frac{d}{D} = \frac{2\lambda r}{Ds} \tag{32}$$

where D is the telescope diameter.

In the far field s is given by

$$s = \theta r \quad [m] \tag{33}$$

where θ is the laser divergence, hence:

$$\sigma = \frac{2\lambda}{D\theta} \tag{34}$$

σ is generally less than 1% for typical direct-detection

systems, as can be easily verified with the parameters reported in Table 1. For coherent detection, $\sigma$ is 1 because the divergence of the transmitted beam is about the diffraction limit imposed by the telescope aperture,[154-156] here also used as a transmitter:

$$\theta \approx \frac{2\lambda}{D} \quad [\text{rad}] \tag{35}$$

These conditions maximize the previously defined SNR; their relaxation in order to get more speckles does not produce any improvement. At a different wavelength, a different speckle configuration can be observed. Hence, in the case of multimode lasers, often utilized in direct detection, this fact produces a further reduction of the signal variance.[104]

For range-resolved measurements, we have this situation:

1. For one shot, a speckle configuration lasts until the laser pulse has completely moved forward to cover another set of scatterers, i.e., it lasts for a period equal to the pulse duration (coherence time). The coherence times of the atmosphere depend on wavelength and the random velocity of the aerosol particles. They are generally longer[152,153] than the typical laser pulses and are on the order of microseconds.
2. The speckle pattern changes from shot to shot due to the scatterers' motion. Hence, in this case, averaging improves the SNR with the square root of the number of shots;[91] a further improvement is possible by integrating the signal over many coherence times.

## VII. CONCENTRATION SENSITIVITY

From Equation 6 and from the evaluation of the SNR of the four optical signals under logarithm, the minimum detectable concentration $\Delta N$ can be evaluated as follows:

$$\Delta N = \frac{2}{SNR}\frac{1}{2\Delta\sigma\Delta r} \quad [\text{cm}^{-3}] \tag{36}$$

where SNR is the signal-to-noise ratio associated with the four optical signals, here assumed identical. Their cumulative effect is contained in the factor 2 at the numerator of Equation 36, which is justified if the four signals are statistically uncorrelated. This is strictly true only for the noise sources relevant to the detection process. In the real case, fluctuations and correlations arising from the interaction of light with the atmosphere must be taken into account, such as the speckle noise described before. Aerosol scattering has been demonstrated to be temporally uncorrelated from shot to shot,[91] while for measurements with topographic reflectors, temporal correlation plays a more important role.[43,104,206] However, in this section, we only want to set a limit to detection sensitivity and these considerations play a secondary role.

As can be seen from Figure 13, the SNR can be as high as 100 when a suitable number of laser shots is averaged (a typical averaging ranges from a few tens to a few hundreds of shots). In this case, the system is able to measure a differential absorption of 1% and the detection sensitivity for a particular pollutant can be evaluated from Equation 36:

$$\Delta N = \frac{1}{100}\frac{1}{2\Delta\sigma\Delta r} \quad [\text{cm}^{-3}] \tag{37}$$

In Table 3, the detection sensitivity for some pollutants is reported by assuming an optical path or spatial resolution, $\Delta r$, of 100 m.

Coherent detection is characterized by quantum noise-limited conditions, but it is affected by 100% signal fluctuation due to the presence of speckle noise. Also, in this case, the SNR can be increased by averaging, but the number of shots required for 1% differential absorption detection is substantially higher than before and a longer time is required for the measurements unless a high PRF laser is used. This fact can render the measurement impractical or can introduce other noise terms due to the change of atmospheric parameters. For this reason, heterodyne detection should be preferred when a sufficiently high optical absorption is expected or when direct detection has a SNR of less than one.

The sensitivities listed in Table 3 should be considered an indicative parameter only since in the case of a real system, these values must be scaled to the spatial resolution really needed and other parameters, such as spectral interferences by other gases or particular conditions of operation (i.e., range, visibility, backscattering coefficients, etc.), must be carefully considered.

## VIII. FIELDS OF APPLICATION

The applications of the DIAL method cover a wide spectrum according to sensing range, system location (mobile on ground, fixed, on an aircraft, on a ship, or, in the future, on a satellite), field of measurement (troposphere or stratosphere), and kind of application: meteorological on a small or large scale, monitoring of the atmospheric pollution and emissions of an industrial plant, survey of pipelines and chemical plants, monitoring of gases emitted by the soil, vegetation, or volcanoes (Figure 15), etc. Table 4 collects the main applications of the DIAL method.

Such a wide field of applications is possible because of the strength of the backscattered signal. In fact, it has been demonstrated that tropospheric and stratospheric aerosols can give rise to a measurable return signal from a distance of up to many kilometers when a laser source of suitable energy is used. For example, now a common routine is the detection of volcanic aerosols (with lidars) in the range between 15- and 30- km height utilizing Nd:YAG and ruby laser-based systems.[114] These volcanic aerosols can also be detected in less

**Table 3**
**Minimum Detectable Concentration (MDC) for Various Pollutants for 1% Differential Absorption over 100-m Path (Double Trip)**

| Laser | Molecule | Laser lines or wavelengths (μm) | Differential absorption coefficients ($atm^{-1}$ $cm^{-1}$) | MDC (ppb) | Ref. |
|---|---|---|---|---|---|
| $CO_2$ | $SF_6$ | 10P(16)/10P(10) | 620 | 0.8 | 184 |
| $CO_2$ | $NH_3$ | 10P(32) | 17 | 30 | 63 |
| $CO_2$ | $C_6H_6$ | 9P(30)/9P(26) | 1.6 | 310 | 184 |
| $CO_2$ | $C_2H_4$ | 10P(14)/10P(12) | 30.7 | 16 | 184 |
| $CO_2$ | $O_3$ | 9P(14)/9P(22) | 11.1 | 45 | 184 |
| $CO_2$ | $N_2H_4$ | 10P(32)/10P(34) | 3.3 | 151 | 184 |
| DF | HCl | 3.6362 | 5.04 | 100 | 53 |
| DF | $N_2O$ | 3.8902 | 1.19 | 420 | 53 |
| Dye[a] | $NO_2$ | 0.45 | 10 | 50 | 140 |
| Dye[a] | $SO_2$ | 0.3 | 25 | 20 | 145 |
| Dye[a] | $O_3$ | 0.28 | 30 | 17 | 78 |
| Dye[a] | NO | 0.226 | 50 | 10 | 143 |

[a] Thanks to dye-laser tunability, the choice of the best pair of wavelengths or absorption coefficients is, to a certain extent, arbitrary.




**FIGURE 15.** CISE-ENEL DIAL system. This picture was taken in 1983 during the campaign for the detection of sulfur dioxide emitted by the fumaroles of a volcano in Vulcano Island (Italy).

**Table 4**
**Field Applications of DIAL**

| | UV | VIS | Near IR | Middle IR |
|---|---|---|---|---|
| Troposphere | | | | |
| Pollutants | $O_3$,NO,Hg, $SO_2$,$Cl_2$ | $NO_2$ | | $CH_4$,HCl,$NH_3$ $SF_6$,$C_6H_6$,$O_3$ $C_2H_4$,$N_2H_4$,CO $N_2O$,$CO_2$, |
| Meteorology | | | $H_2O$,p,T | $H_2O$ |
| Airborne | $O_3$,$SO_2$ | | $H_2O$ | $SF_6$ |
| Stratosphere | | | | |
| On ground | $O_3$ | | | |
| Airborne | $O_3$ | | | |
| Space-borne (prospective) | $O_3$ | | $H_2O$,p,T | |

favored spectral regions, such as the middle infrared, by means of coherent $CO_2$ lidars.[115,122] In the UV spectral region, molecular backscattering is the main source of signal for DIAL measurements of ozone up to 40 km in height.[35,37,61,116] It can therefore be stated that whenever sufficient backscattered laser energy is available, DIAL measurements are possible even from a very long distance, such as a space platform at an altitude of several hundred kilometers. This cannot be said for the Raman scattering approach.

### A. Spaceborne Lidars

Laser remote sensing activity from space is actually oriented toward the achievement of these primary goals:

1. Measurement of water vapor concentration
2. Measurement of pressure and temperature atmospheric profile[67,68]
3. Measurement of ozone concentration
4. Measurement of aerosol backscattering
5. Measurement of wind velocity (by measuring the Doppler frequency shift of aerosol backscattered light)
6. Measurement of trace species in the stratosphere[168,169] (by flourescence, see Section IX)

The first three activities are to be made with the DIAL method. In this case, the system requirements about laser energy or telescope diameter (which are the main parameters limiting the maximum range) are not much more severe than for on-ground-based systems. The main problems are instead system mass, reliability, power consumption, and component lifetimes. ESA and NASA programs in this field are nearly identical, aiming at demonstrating the possibility to perform these measurements with a lidar from a satellite.

### B. Stratospheric Measurements

DIAL measurements in the stratosphere are restricted to ozone. Most of them have been performed with fixed on-ground stations.[35,37] Only one system, i.e., that of NASA,[36,77,116,120] is airborne, with the possibility of both nadir (tropospheric) and zenithal (stratospheric) operation (see Figures 16 and 17, Plate 1,* and Table 5).

### C. UV-Visible DIALs

Pollution monitoring in the troposphere has been mainly devoted to ozone, sulfur dioxide, and nitrogen dioxide. The measurements are performed in the ultraviolet for $SO_2$[149,150,163-167,203] and $O_3$[38,120,164,165,171] and in the blue for $NO_2$.[147,164,203] With this kind of device, measurements could be performed (with little modifications) also on mercury[125,151] at 253 nm, nitric oxide (NO)[148,203] at 226 nm, chlorine[180] at about 300 nm, and water vapor at 720 nm.[183] These systems, of which several units exist in the world, have successfully overcome the phase of feasibility demonstration prototype and are now intensively utilized in many field trials. They are generally mounted on a truck or a trailer (see Figures 15 and 18 to 23), only the earlier mentioned NASA system being airborne. The main characteristics of these systems are reported in Tables 1 and 5.

### D. Meteorological Lidars

With the term "meteorogical lidar" is usually indicated a DIAL system able to perform measurements of water vapor concentration, atmospheric temperature,[67] and pressure profiles;[68] the two last quantities are to be performed by measuring the absorption on the center and wings of oxygen absorption lines in the NIR which are sensitive to them (see Section V.B). Up to now, this kind of system, which operates in the near infrared (in the range 720 to 770 nm), has been really utilized only for humidity measurements and only demonstrated for temperature and pressure[157] since the laser requirements for the last two applications are rather severe in terms of frequency bandwidth and stability. Up to now, at least two ground-based DIAL systems are routinely working for water vapor detection: one fixed (see Table 6 and References 123 and 158) and the

*Plate 1 follows page 302.

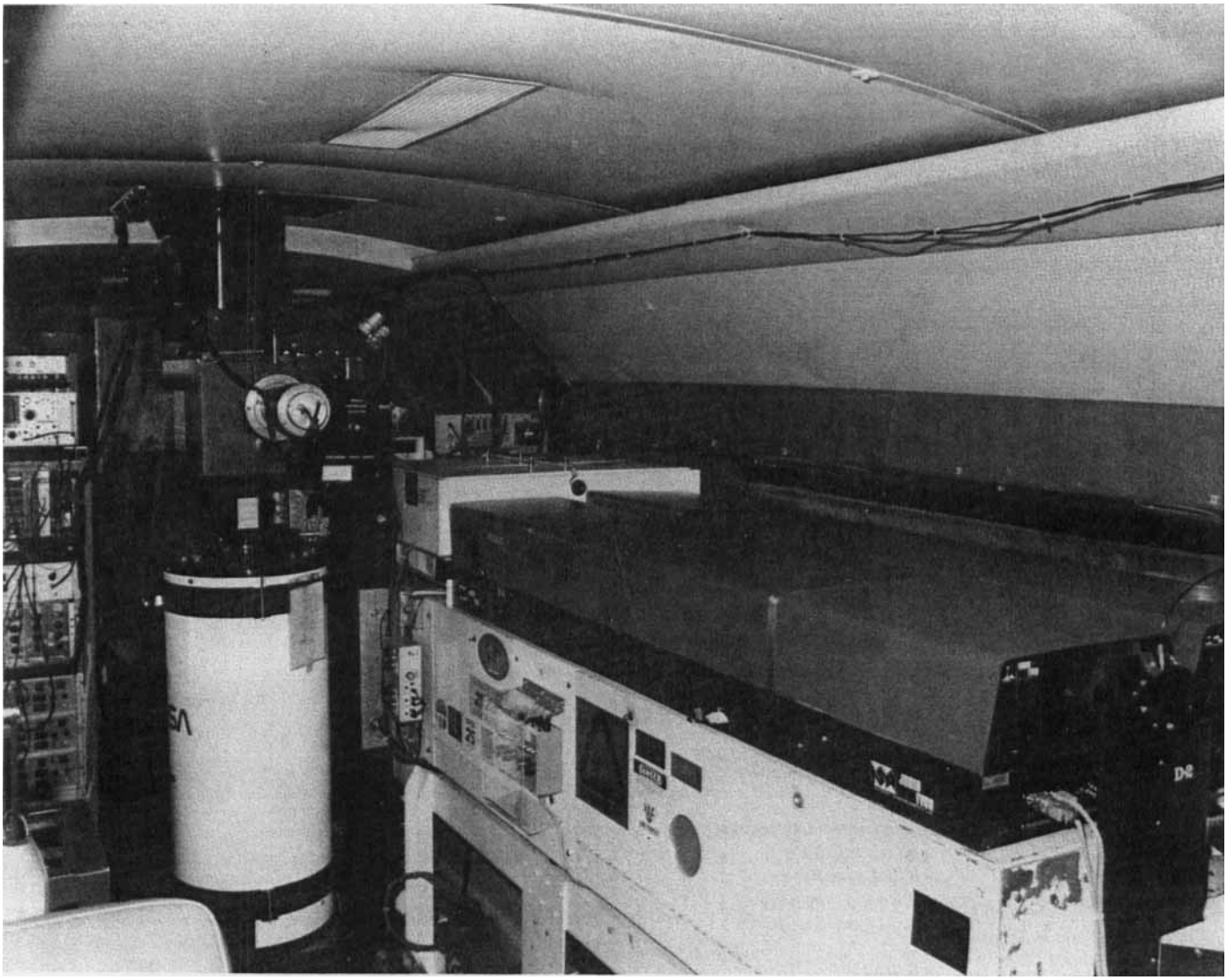

**FIGURE 16.** Airborne NASA DIAL system. The telescope tube, the receiver, and the two lasers systems (Nd:YAG pumped-dye lasers) are shown. (Courtesy of A. F. Carter and E. V. Browell, NASA Langley Research Center.)

other mobile.[76] An airborne lidar has recently been assembled by NASA[128,157] for performing all three kinds of measurements as an intermediate step to space-borne systems. The first of these devices utilizes an excimer pumped-dye laser, while the other two use the newly developed, solid-state, Alexandrite laser which offers better performance in terms of efficiency and maintenance.

### E. Infrared DIALs

Infrared DIAL systems have demonstrated the possibility to monitor a great number of pollutants; most of them utilize $CO_2$ lasers with direct or heterodyne detection. A $CO_2$ laser indeed offers real advantages thanks to its high efficiency, high energy output (of the order of 0.1 to 1 J), and reliability. However, also in this case, we have to note that only a few of them have been utilized outside laboratories for routine measurements. A general characteristic of all DIAL systems in operation nowdays is to require skilled operators with a deep knowledge of the machine and its related problems: this fact greatly limits the practical utilization of the technique.

Among the DIALs we mention, the ship-borne system of GKSS, based on a DF laser, utilized for HCl detection near incenerization ships in the North Sea,[46] the Mobile Atmosphere-Pollution and Mapping System (MAPM)[184] of the Jet Propulsion Laboratory (see Figures 24 and 25 and Table 2), the infrared airborne system of NASA (which utilizes backscatter of laser pulse from terrain surface),[121] the system of the University of Munich for ethylene detection[45] and the NPL infrared system.[204]

Infrared systems, with direct detection, are often operated

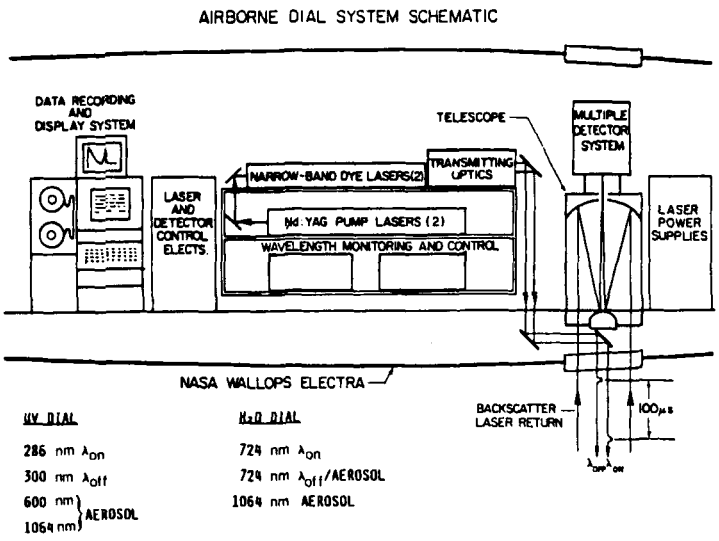


**FIGURE 17.** Block diagram of the airborne NASA DIAL. This system has been utilized for sulfur dioxide, ozone, water vapor, and aerosol detection. (Courtesy of A. F. Carter and E. V. Browell, NASA Langley Research Center.)

## Table 5
## NASA Airborne DIAL System Characteristics

| | |
|---|---|
| Transmitter | |
| Laser system: | Two Nd:YAG pumped-dye lasers |
| Pulse separation: | 100 μs |
| Nd:YAG pulse energy: | 350 mJ at 532 nm |
| Pulse duration: | 15 ns |
| Repetition rate: | 10 Hz |
| Dye Laser: | Two Jobin-Yvon model HP-HR |
| Dye output energy: | 63 mJ at 720 nm |
| | 47 mJ near 300 nm |
| Laser Linewidth: | <0.4 $cm^{-1}$ at 300 nm |
| | <0.04 $cm^{-1}$ at 720 nm |
| Receiver | |
| Telescope area: | 0.086 $m^2$ |
| Receiver efficiency: | 28% at 300 nm |
| | 29% at 720 nm |
| Detector type: | Photomultiplier |
| Detector quantum efficiency: | 29% at 300 nm |
| | 4.8% at 720 nm |
| Receiver field of view: | 2 mrad |

utilizing a topographic reflector,[121] which offers a better sensitivity at the expense of range resolution. This is the case of small systems which have to operate at short ranges or do not use high-energy lasers. Typical is the case of mobile systems used in an urban environment for local pollution control or detecting methane leaks from the distribution pipelines; among them, we mention the system made by SRI, which is based on three $CO_2$ lasers with frequency mixing in order to match the 3-μm absorption band of the gas, and the system made by CISE.[95,96] This last instrument (Figures 26 and 27), based on an optical parametric oscillator pumped by a Nd:YAG laser, is interesting because of its particular detection method — the gas-correlation.[207] Instead of utilizing two wavelengths (as in

**FIGURE 18.** UV-visible DIAL system made by CISE for Instituto de Investigaciones Electricas, Mexico (IIE) for the detection of ozone and sulfur dioxide. The system parameters are reported in Table 1.

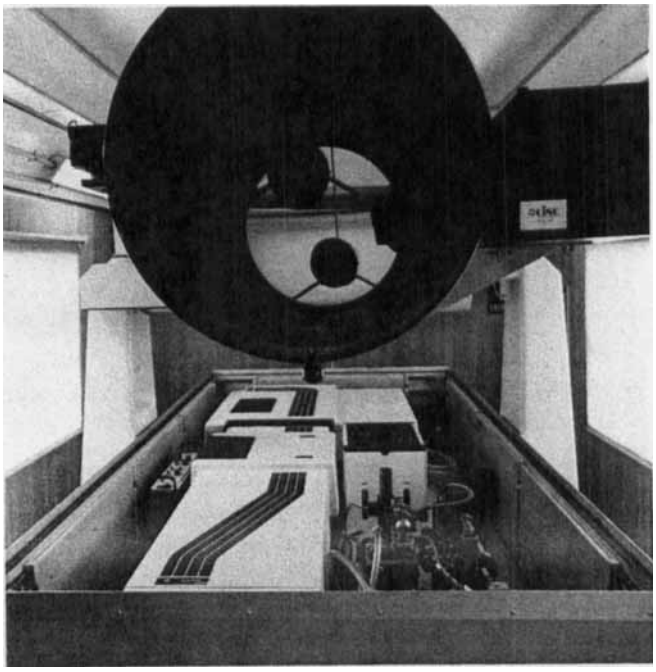

**FIGURE 19.** Inside of the IIE DIAL showing the laser-telescope assembly.

standard DIAL), the laser fires only one broadband (about one wavenumber) pulse centered at the selected methane absorption line. The on and off wavelengths are obtained by splitting the collected lidar return into two portions; one being directly detected by an infrared sensor and representing the "on-line" signal, and the other one being detected by another sensor

**FIGURE 20.** Inside of the IIE DIAL showing the computer console and electronics.

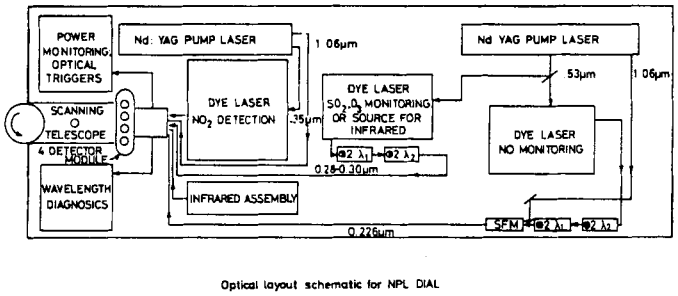


**FIGURE 21.** Block diagram of the mobile DIAL of National Physical Laboratory, Teddington, UK (NPL). (Courtesy of National Physical Laboratory.)

located behind a cell filled with a large amount of methane. This cell fully depletes the center of the broadband signal and transmits only its wings, which are weakly absorbed. The resulting signal therefore represents the "off-line" signal. This method simplifies the construction of the laser and is suitable when the measurements are to be performed from a moving platform (truck or aircraft).

## XI. COMPARISON WITH OTHER METHODS

As stated before, the three selective ways in which the light can interact with a particular atmospheric constituent are absorption, Raman scattering,[75] and fluorescence.[201] A detection method based on one of them can be usefully adopted only if the relative light signals have enough strength. In the case of DIAL, we have previously defined a sensitivity criterium by assuming to detect a particular molecule with a relevant differential absorption over a given path of 1%, therefore, tacitly implying to be able to obtain a SNR of 100. This assumption is generally satisfied for standard visibilities and useful ranges as it can be seen in Figure 13, whose results can be further improved by averaging over many laser shots.

Now, if one compares the cross sections corresponding to the three methods (and reported for a few molecules in Tables 7 through 9), it is evident that the Raman cross sections are much weaker than the Rayleigh scattering cross sections. If we work in the UV, most of the lidar return signal is due to molecular scattering of nitrogen and oxygen. In order to achieve a S/N of 100, we must detect around 10,000 photons. Since the Raman scattering coefficients are about three orders of magnitude lower; nitrogen, for example, would give a signal of a few photons only, with a SNR close to 1. If the gas concentration were at the parts-per-million or parts-per-billion levels, the signal would be even lower. For this reason, Raman lidars are not suitable to be utilized for the detection of trace gases but only for relatively high concentrations or in short-range applications. There is only one advantage for this technique: as laser tunability is not required, powerful sources can be utilized; for example, excimers, doubled ruby or tripled Nd:YAG lasers. The literature reports successful utilization of Raman lidars for water vapor concentration with a few kilometers range[159-161] and for methane.[209]

As far as the fluorescence technique is concerned, a distinction should be made between atoms and molecules. The former case is favored because the fluorescence-quenching factor is lower, the cross-section is larger, and the emission is not spread out over a large spectral band, but is rather concentrated on a narrow line at the same wavelength as the excitation. This last property, however, is not very useful in the troposphere because the fluorescence signal can be hidden by the strong backscattering of molecules and aerosols also occurring at the same wavelength.

Quenching factors are dependent on the collision rate between the molecules and therefore are much larger in the troposphere, where they can reach values as high as $10^5$. For these reasons, detection by fluorescence[201] has only been successfully utilized for measuring the concentration of alkali metals in the high stratosphere[9,127,197] and has also been proposed for space-borne applications.[168,169] In this case, the relevant signals dominate the molecular and aerosol backscattered signals which are too weak for an efficient utilization of the DIAL method.

About the molecules, the OH has been successfully detected with a balloon-borne lidar with excitation at 282 nm.[126]

The instrumentation for fluorescence detection is nearly the same as that for DIAL applications. Stratospheric alkali metals are detected by means of photon-counting techniques as for stratospheric ozone. The DIAL method is generally more sensitive in the troposphere, but not in the stratosphere, where backscattering coefficients are much lower.

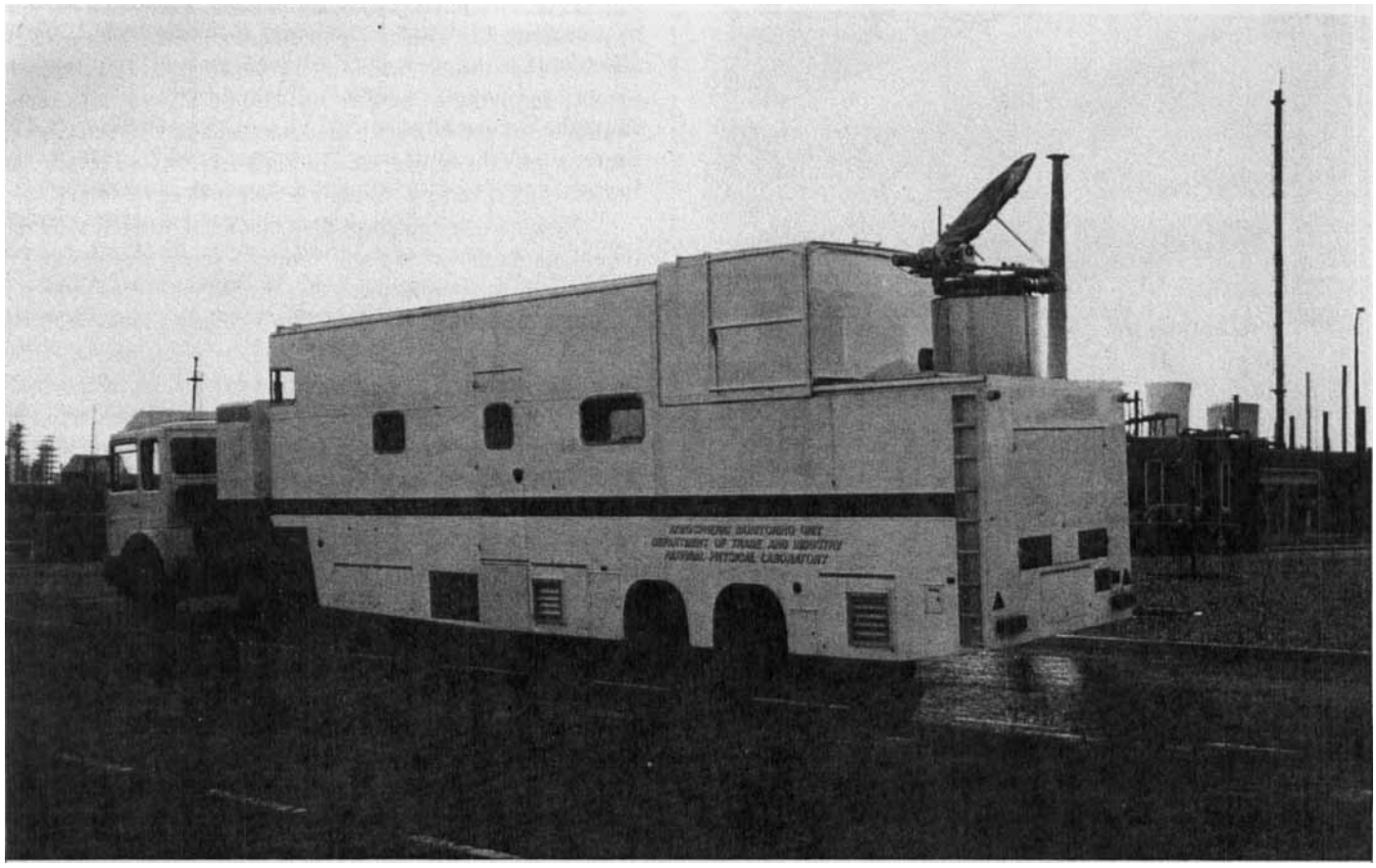

**FIGURE 22.** NPL DIAL. In this picture, it is possible to see the telescope tube and the large steering mirror. (Courtesy of National Physical Laboratory.)



## X. DIAL METHOD: PROBLEMS AND INSTRUMENTATION

The reasons why DIAL systems or lidars in general are not as widely used as one would expect, based upon their attractive potentialities, are many. One set of problems is inherent to the characteristics of the currently available lidar instrumentation and deals with the concepts of reliability, ease of use, and maintenance. Other problems arise when the DIAL method is applied to atmospheric targets which are highly variable (in time, height, and composition). Another set of problems is connected with the real complexity of the full system, made by many parts which are themselves complex systems and whose mutual matching has to be carefully controlled according to the particular measurement conditions on hand. We shall discuss these subjects in the following sections.

### A. Problems Related to the Method

As can be seen from Equations 1 to 6, the DIAL method permits to cancel out from the lidar signal the backscattering and absorption terms not dependent on absorption by the molecular species of interest by normalizing the lidar return "on" with the lidar return "off." Moreover, in Equation 6, every instrumental contribution, such as telescope transmission, laser energy, etc., is eliminated. Only the shape of the two lidar signals is required for evaluating the concentration, i.e., the system is self calibrated. This great feature of the DIAL method can fail in a few cases:

1. The two wavelengths are not close enough.

2. The two wavelength are not fired simultaneously, or the target is moving.

The first situation is typical of tropospheric measurements of ozone in the ultraviolet. The UV ozone absorption spectrum[78,92] is characterized by a broad and structureless band centered at 255 nm and ranging from 200 to 300 nm (see Figure 5). A sufficiently high differential absorption coefficient is obtained by choosing the two DIAL wavelengths about 5 to 15 nm apart in the 280- to 300-nm range. In this case, differences in the scattering parameters are no longer negligible and the molecular and aerosol contribution to the lidar signal must be evaluated in order to correct the resultant systematic errors[35-38,113,120] (see also Section V.C). This item is particularly important in the troposphere because the earlier contribution

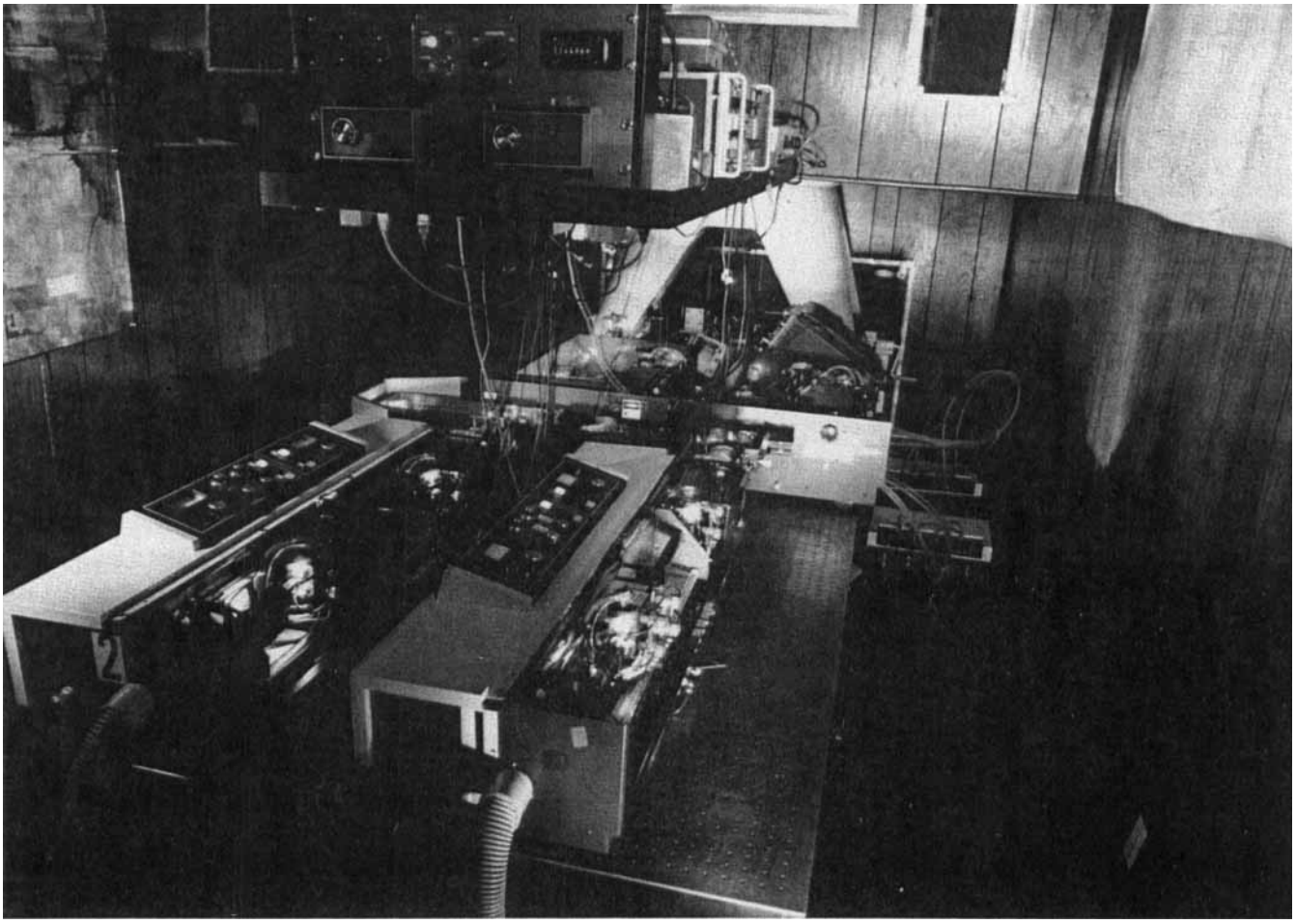

**FIGURE 23.** Inside of the UV-visible DIAL system made by SRI (now property of SAIC). It is possible to see the two Nd:YAG pumped-dye lasers. (Courtesy of J. G. Hawley.)



is of the same order and the aerosol content is highly variable. Its evaluation is therefore not straightforward and requires information about the visibility and some assumptions about aerosol composition. In the stratosphere, the influence of aerosol scattering is smaller (10% according to Reference 37) because the molecular term dominates. This term is inversely dependent on the fourth power of the wavelength and can be easily taken into account by evaluating the air density profile with height.

It has been found that aerosol presents a strong differential backscattering in the infrared,[81,82] particularly at about 9.5 μm, where a significant dependence on wavelength was observed. A similar problem exists for measurements of the integral content of pollutants produced from aircrafts utilizing the earth's surface as a topographic target. Large systematic errors can be made because of the differential reflectance of terrains (for example, water, asphalt, sand, vegetation, etc.)[79-81], which can be as high as 20% for $7cm^{-1}$ separation between the two wavelengths for quartz.[79]

The differential backscattering effect is enhanced when a discretely tunable laser (for example, a gas laser) is utilized. In fact, the gas laser emission lines, spaced by several wavenumbers, must be chosen to minimize spectral interferences by other gases. This procedure can result in a choice of a well-separated couple of frequencies.

The Doppler broadening of the linewidth of the Rayleigh backscattered light is another effect that, in some cases, must be taken into account. This fact has been evidenced about water vapor measurements[181,182] in the upper troposphere in the near infrared where the molecular contribution to the lidar signal is not negligible in comparison with the aerosol term. This broadening effect is of the same order of magnitude of the water vapor absorption linewidth and is expected to be important for pressure and temperature measurements, too.

When the atmosphere is not stationary, i.e., in the presence of strong winds or turbulences, signal differences between a pulse-pair arise because of beam wandering, atmospheric lens effects, motion of the pollutant cloud or plume, and change of scatterers.[216] These effects, which are of a statistical nature (thus leading to a negligible concentration error if averaged over many shots), can be a source of noticeable errors when

**Table 6**
**Characteristics of a Water Vapor DIAL[123,158]**

| | |
|---|---|
| Transmitter | |
| Laser type: | Two excimer pumped-dye lasers |
| Output energy: | 40 mJ at about 720 nm |
| Laser bandwidth (FWHM): | 0.023 to 0.038 $cm^{-1}$ |
| Spectral impurity: | 1 to 2% |
| Beam dimensions: | 2 mm |
| Beam divergence: | 1.5 mrad |
| Repetition rate: | 12 Hz |
| Bandwidth control: | Multibeam Fizeau interferometer with 0.015 $cm^{-1}$ resolution |
| Frequency stability and tuning control: | Photoacoustic cell at low pressure |
| Receiver | |
| Telescope: | 0.28 m Cassegrain |
| Separation transmission receiver: | 0.3 m |
| Filter bandwidth: | 8 nm |
| Telescope: | 0.5 m newtonian |
| Separation transmission receiver: | 3 m |
| Filter bandwidth: | 0.6 nm |
| Digitizer precision: | 12 bit |
| Selected digitizer sampling rate: | 20 MHz |
| Data storage: | 100 shot averages on magnetic tape |

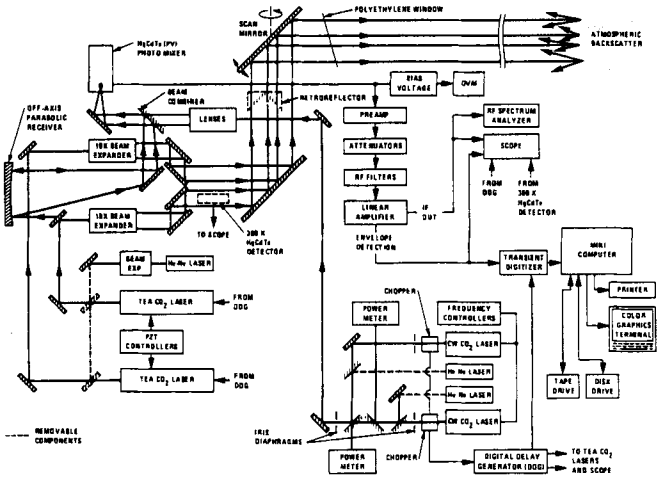


**FIGURE 24.** Block diagram of the Mobile Atmospheric Pollution and mapping system (MAPM) coherent DIAL system developed by the Jet Propulsion Laboratory, Pasadena (JPL). It is based on two $CO_2$ lasers (see Table 2) alternately switched at different wavelengths. Heterodyne detection is achieved by combining on one HgCdTe photomixer the return signals with one of the two CW $CO_2$ lasers (local oscillators) alternately chopped. (Courtesy of W. B. Grant.)

averaging is not possible or the measurement is to be performed on a single pair of shots. This problem appears more evident in the case of a lidar system installed on a fast-moving platform, i.e., aircrafts or (in the near future) satellites. A commonly adopted solution[77,164,166,167] consists of utilizing two lasers fired at the two different wavelengths with a temporal delay, short enough to "freeze" the atmosphere, but long enough to clearly distinguish the two correspondent lidar returns on the same detector with no temporal overlap. Another possible solution consists in the simultaneous firing of the lasers with spectral separation of the two signals on two separate detectors, but it is rarely adopted because the very narrow gap between the two wavelengths makes difficult a complete separation without cross-talk between them and because it implies a two-channel receiver. When only one laser is utilized, the solution of an alternate switching between the two frequencies is generally adopted;[150,163] a simultaneous two-frequency emission is rarely preferred[198] (see also Section XI.A.1).

# XI. INSTRUMENTAL APPARATUS

## A. Laser

The possibility to detect a particular pollutant strictly depends upon the existence of suitable laser frequencies in coincidence with convenient absorption bands. Therefore, we list first the main requirements that a laser system must fulfill for DIAL applications and then we give a list of the actually available sources, placing more emphasis on those features that are important for lidar investigations.

### *1. Laser Requirements*

#### a. PULSE ENERGY

High-pulse energy means a better signal-to-noise ratio on the received signal which, in turn, offers the advantages of a greater range and requires a lower number of shots for signal averaging (and hence, a shorter measurement time). This property is particularly useful when the atmospheric target is not stationary (e.g., for tracking plumes in the presence of strong winds). The output power of today's lasers is not always satisfactory for DIAL applications thus a compensation in terms of a very large telescope size is often needed.

#### b. REPETITION RATE

A high repetition rate permits a faster signal averaging, with the earlier mentioned advantages. Typical rates are of the order of 10 or 20 pulses per second; much higher rates can imply problems in the acquisitions system for the high flux of data from the transient recorder (see also Section XI.D). In general, one has to choose the best compromise between emission energy and repetition rate. In principle, for heterodyne or UV-visible direct detection, the SNR improves as the square root of pulse energy and number of pulses, hence, the only important parameter is the average laser power, i.e., the product of repetition rate and emission energy. For infrared direct detection, instead, the SNR is directly proportional (see Equation 21) to the emitted energy; in this situation, it is better to concentrate the available laser average power in a few shots of high energy. This can also be true in the former cases if, for example, there is a high solar background radiation or other strong noise sources due to the laser discharge and the related equipment or due to the detector amplifier chain. In conclusion, where possible, it is generally better to enhance the output

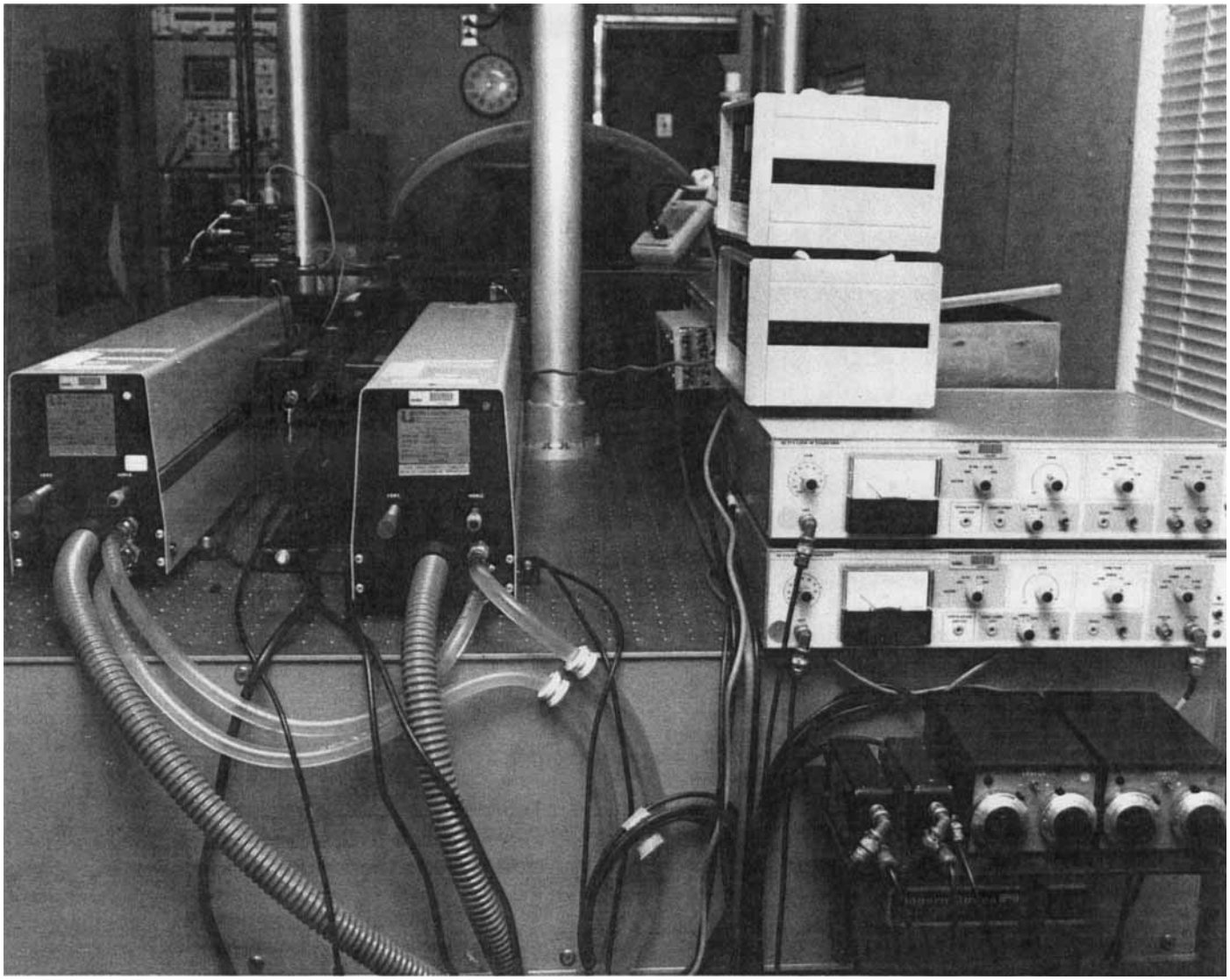

**FIGURE 25.** Inside the van housing of the MAPM. It is possible to see the optical bench with the two local oscillators and the large mirror (rear part) which transmits the laser beams upward. (Courtesy of W. B. Grant.)



energy instead of the repetition rate. Other factors to be taken into account in this choice are eye safety problems, which can limit the available laser energy, and the temporal delay between the two DIAL wavelengths, which is directly related to repetition rate in those systems where only one laser with alternate emission is utilized.

#### c. PULSE DURATION

The only effect of a long pulse duration is to reduce the spatial resolution, which, in most cases, is limited by the electronic bandwidth of the receiver and the transient recorder. In fact, typical pulse duration is 10 nsec for Nd:YAG lasers, excimers lasers, or dye lasers pumped by them. Longer pulses are supplied by lower-gain lasers such as Alexandrite (100 to 200 ns) and Co:$MgF_2$ lasers (300 ns). Typical pulse durations of a $CO_2$ laser can range from 0.1 to above 1 μsec (depending on the composition of the laser gas mixture) with a corresponding spatial resolution of 15 to above 150 m.

#### d. LASER TUNING

Tunable lasers are generally utilized in DIALs, but this is not strictly necessary because two single frequency lasers or one laser plus a frequency shifter or converter can also be utilized (see Section XI.A.2). Laser tuning can be achieved in many ways. Gratings are the most common choice because of their high dispersion even if, in the visible, they present larger losses and lower thresholds for optical damage in comparison with other tuning elements, such as birefringent filters. They are commonly utilized with high-gain devices like dye lasers, which are made by a low-energy output oscillator and two or

**FIGURE 26.** IR DIAL system made by CISE for AEM of Milan for the detection of methane leaks from the urban distribution network. The system is based on a Nd:YAG pumped Optical Parametric Oscillator (OPO), emitting at about 3300 nm. The range of the instrument is up to 100 m with a topographic reflector; its sensitivity is equivalent to the natural methane background (1.6 ppm).

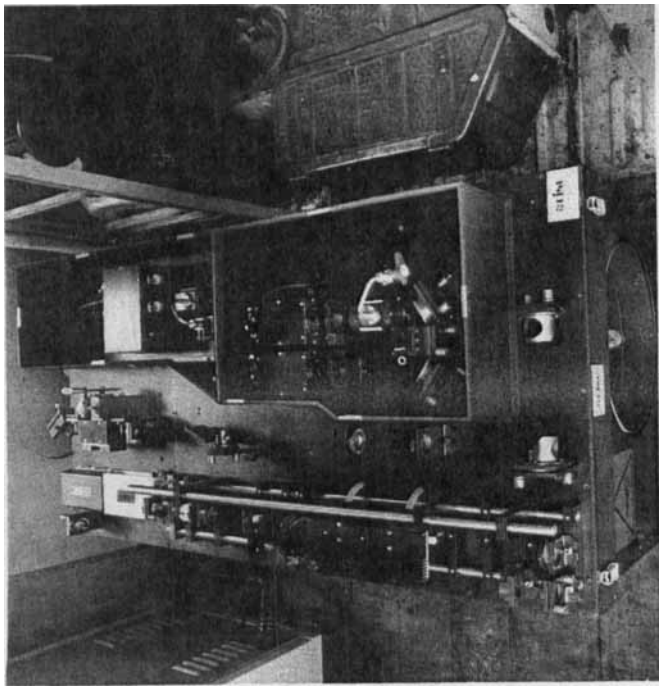

**FIGURE 27.** Inside of the IR DIAL system of Figure 26. This figure shows the laser, housed on a plane over the receiver telescope (25-cm diameter).

**Table 7**
**Comparison Between Raman and Rayleigh Cross-Sections (Data Relevant to 337 nm)[129]**

| Molecule | Raman shift $cm^{-1}$ | Differential cross-sections: Raman $10^{-30}$ $cm^2$ $sr^{-1}$ | Differential cross-sections: Rayleigh $10^{-27}$ $cm^2$ $sr^{-1}$ |
|---|---|---|---|
| $N_2$ | 2330.7 | 3.5 | 3.9 |
| $O_2$ | 1556 | 4.6 | 3.3 |
| $O_3$ | 1103.3 | 6.4 | |
| $NO_2$ | 1320 | 51 | |
| $SO_2$ | 1151.5 | 17 | |
| $CH_4$ | 2914 | 21 | |
| $H_2$ | 4160.2 | 8.7 | |
| $H_2O$ | 3651.7 | 7.8 | |

**Table 8**
**Absorption and Fluorescence Cross-Sections for Some Molecules at Atmospheric Pressure[75]**

| Molecule | Excitation wavelength (nm) | Absorption cross-section $10^{-19}$ $cm^2$ | Fluorescence diff. cross-section $10^{-24}$ $cm^2$ $sr^{-1}$ |
|---|---|---|---|
| $SO_2$ | 300.1 | 5 | 2 |
| $NO_2$ | 435.8 | 3 | 0.7 |
| NO | 226.5 | 13 | 300 |
| OH | 282.6 | 120 | $10^3$—$10^4$ |

**Table 9**
**Fluorescence Cross-Sections for Some Molecules in the Stratosphere[201]**

| Species | Excitation wavelength (nm) | Fluorescence wavelength (nm) | Fluorescence cross-section ($cm^2$) |
|---|---|---|---|
| Li | 670.78 | 670.78 | $1.3 \times 10^{-11}$ |
| Na | 588.995 | 588.995 | $1.8 \times 10^{-11}$ |
| K | 766.491 | 766.491 | $3.1 \times 10^{-11}$ |
| Cl | 134.724 | 134.724 | $8.6 \times 10^{-13}$ |
| O | 130.217 | 130.217 | $1.5 \times 10^{-13}$ |
| Fe | 371.994 | 371.994 | $1.1 \times 10^{-12}$ |
| Ca II | 393.366 | 393.366 | $1.6 \times 10^{-11}$ |
| $NO_2$ | 532 | 633—646 | $1.6 \times 10^{-21}$ |
| NO | 215 | 215—260 | $3 \times 10^{-15}$ |
| OH | 286.6 | 308—314 | $6.2 \times 10^{-15}$ |

three amplifiers utilized in saturation regime. In the visible or near infrared, with low-gain devices or when a high-energy output must be obtained by a laser with a single oscillator configuration, (for example, with Alexandrite or Co:$MgF_2$), birefringent filters are preferred because of their negligible losses and better resistence to optical damage. However, in this case, another element, such as an etalon, must be utilized if a very narrow band is needed.[157] The line selection of the gas lasers in the infrared is easily obtained by means of gold-

coated gratings with a moderate dispersion which offer a very high efficiency and good resistance to damage.

The DIAL method requires the emission of two wavelengths, preferably in a very short time in order to minimize the effects of the change of the atmospheric optical properties due to the wind or to the turbulence. The most obvious way for emitting two wavelengths is to utilize two different lasers which can be fired nearly simultaneously.[77,165-167] A cheaper solution consists in the alternate emission of two wavelengths from a single tunable laser, utilizing a fast wavelength switching device. Many possible solutions exist: rocking of the tuning grating at half of the laser repetition rate,[150] inserting at alternate shots a prism in the oscillator cavity before the grating for shifting the laser frequency by a given amount,[163] splitting the oscillator cavity in two halves, each one set at the right wavelength,[164] and alternately chopped. With this last configuration, a simultaneous two-frequency emission is also possible.[198]

For stationary systems, no important difference exists between the performances of the two classes of solutions because the repetition rate of today's lasers (more than 10 Hz) is high enough to consider the atmosphere frozen between two successive laser pulses. This is particularly true for the concentration content of a gas or for the scattering parameters of the atmosphere, which are slow phenomena in absence of strong winds. Turbulence effects are much faster, of the order of milliseconds, but the relevant fluctuations of the signal are lower and can be reduced by averaging. For airborne or satellite-borne systems, this is not true because of the change of the atmospheric target and therefore, the time separation between the on and off pulses must be as short as possible, that is, there must be just enough delay to avoid the overlapping of the trailing edge of the first signal with the leading edge of the successive one.

#### e. SPECTRAL PURITY

This parameter can be defined as the ratio between the laser energy emitted in the useful bandwidth and the total emitted energy. How much this term is important can be easily understood with the following example: let's suppose to have a purity of 99%; this means that 1% of the "on" wavelength is not in the center of the absorption line. If the on-line atmospheric absorption is 99%, then the relevant signal is detected with a 100% error. Pratically, the tolerated spectral "impurity" should be less than the digitizer precision, that is less than 1% (see Section XI.D).

#### f. BANDWIDTH

The general prescription about laser bandwidth is to be narrower than the gas absorption lines so that the expected transmission over a given atmospheric path is not noticeably different from the monochromatic case.[208] In the UV-visible, spectral bandwidths of about 0.1 to 1 wavenumber are generally sufficient and this requirement is well met by existing dye lasers.

The absorption spectra in the infrared often consist of separated narrow lines, hence, in these cases, the laser bandwidth must be kept about ten times smaller than before and in a few cases (e.g., for pressure and temperature measurements), it should be better than 0.02 wavenumbers. Dye lasers with such requirements are now commercially available. The construction of a pulsed-dye system operating in a single longitudinal mode (0.015 wavenumbers) has been recently reported;[170] the same performances for a tunable pulsed solid-state laser are yet under development. Equally severe requirements are set for the center wavelength position stability so that a calibration system should be provided: precise wavemeters, transmission cell, and photoacoustic cells filled with the gas to be detected are generally utilized.[74]

The bandwidth of tunable gas lasers in the infrared is much more narrow than typical absorption lines, and the emission frequency is also very stable. Heterodyne detection requires single longitudinal mode emission, with a bandwidth of a few megahertz (1 wavenumber is equivalent to 30 GHz). This condition is easily achieved with gas lasers.

#### g. BEAM QUALITY

Except for the case of heterodyne detection, where near diffraction-limited beams are necessary, this requirement is not severe; the only rule to be followed being that of making the beam divergence lower then the telescope field of view. Beam expanders are commonly utilized for this purpose. A peculiar problem exists for dual laser systems because small differences in laser shape or divergence can produce false concentration burdens[210] particularly in the near field (the same effect is produced by an imperfect alignment between the two laser beams).

In conclusion, laser systems are expected to improve in terms of overall efficiency, output power, lifetime, reliability, and maintenance. For mobile systems, particular care must be devoted to design the mechanical mounts of the cavity so that the device is resistant to vibrations and temperature-dependent effects.

### 2. Type of Lasers Utilized in Remote Sensing

#### a. DYE LASERS

The UV, visible, and near infrared regions (from 200 to 1000 nm) are well covered by the spectrum of the direct emission of the second harmonic of tunable dye lasers. In fact, the success of UV-visible DIAL systems (which up to now are the only devices routinely utilized for field measurements) is based on them. They have now reached a high level of reliability and efficiency at a relatively low cost. They provide enough output energy for this application together with sufficient frequency stability and narrow bandwidth. They have only one drawback: they require nearly a daily substitution of the dye solution. This feature is not dramatic in itself, but does not permit an automatic or unattended operation for long period. The dye lasers can be excited by flashlamps or other lasers; this second

choice being generally adopted because of many advantages, such as higher repetition rate, shorter pulse emission, longer flashlamp lifetime (at least one magnitude better for Nd:YAG laser pumping), etc.

#### b. EXCIMER LASERS

These devices can emit a set of discrete frequencies in the UV, each corresponding to a particular gas mixture. The active medium is a binary molecule composed by a halogen and a rare gas atom which exists only in the excited state. Their characteristics are listed in Table 10. In lidar applications, they can be utilized indirectly to pump dye lasers,[158,203] but in this case, the more compact Nd:YAG, doubled and tripled, is generally preferred. They can also be used directly for ozone[37,109] or $SO_2$[109] monitoring, possibly utilizing Raman shift for the generation of the wavelengths. Excimer lasers have now reached a good level of reliability, and the main maintenance consists in the periodic replacement of the gas mixture and the electrodes.

#### c. SOLID-STATE LASERS

The first lidars[2,3] were based on ruby lasers (emission at 694.3 nm). This kind of source is able to provide several pulses per minute, with emission energies of the order of 1 J, delivered in 20 to 30 ns. The ruby has been widely utilized for monitoring aerosols and clouds in Raman systems[5-8] and also for DIAL measurements of water vapor, exploiting its very small tunability range, due to temperature tuning, accidentally coincident with some water vapor absorption lines.[162] Now it has been replaced almost everywhere by the Nd:YAG laser (emission at 1064 nm), which can provide a slightly lower energy per pulse, but with a much higher repetition rate (10 to 30 pulses per second) thanks to its much better efficiency. It is largely used (doubled and tripled in frequency) as a pumping source for dye lasers, but its direct utilization in DIAL applications in conjunction with Raman shifting techniques has also been proposed (see Reference 171 for Nd:YAG and Reference 108 for Nd:glass). Beside ruby and Nd:YAG, which are well-developed active materials and commercially available for many years, many other crystals have been investigated as possible laser sources; some of them are tunable on a large spectral range and will be discussed later. Among those which emit on a narrow line, one can cite the erbium: YAG, and the osmium: YAG. The GSGG[87] can be codoped with neodimium and chromium for emission at 1061 nm; in comparison with Nd:YAG, it presents the advantage of a better flashlamp pumping efficiency, but with the drawback of worse thermal properties.

**Table 10**
**Lasers Utilized in Lidar Systems**

| Type | Wavelength (μm) | Typical energy (J) | Pulse duration (μs) | Repetition rate (Hz) |
|---|---|---|---|---|
| Gas | | | | |
| $CO_2$ | 9—11 | 0.1—1 | 0.1—2 | 10—50 |
| CO | 5–6 | 0.01—0.05 | 10 | 10 |
| HF | 2.7—3 | 0.1—0.5 | 0.1—1 | 1—10 |
| DF | 3.7—4 | 0.1—0.5 | 0.1—1 | 1—10 |
| Excimer | | | | |
| ArF | 0.193 | 0.1 | 0.01 | 10—100 |
| KrCl | 0.222 | 0.1 | 0.01 | 10—100 |
| KrF | 0.249 | 0.1—0.5 | 0.01 | 10—100 |
| XeBr | 0.282 | 0.1 | 0.01 | 10—100 |
| XeCl | 0.308 | 0.1—0.5 | 0.01 | 10—100 |
| XeF | 0.352 | 0.1 | 0.01 | 10—100 |
| Solid State | | | | |
| Alexandrite | 0.71—0.8 | 0.1—1 | 0.1—0.2 | 10 |
| Ruby | 0.6943 | 1 | 0.02 | 0.1 |
| Nd:YAG | 1.06 | 0.5—1 | 0.01 | 10—30 |
| Nd:YAG ×2 | 0.532 | 0.2—0.5 | 0.01 | 10—30 |
| Nd:YAG ×3 | 0.355 | 0.1—0.2 | 0.01 | 10—30 |
| Co:$MgF_2$ | 1.5—2.3 | 0.01 | 0.3 | 10 |
| *Dye Laser* | | | | |
| Visible-NIR | 0.4—0.8 | 0.1—0.01 | 0.01 | 10—30 |
| UV | 0.2—0.4 | 0.001—0.01 | 0.01 | 10—30 |

#### d. TUNABLE SOLID-STATE LASERS

A real improvement of the DIAL systems will consist in the replacement of dye lasers with tunable and maintenance-free solid-state sources. Among the materials recently developed, vibronic materials[211] show interesting properties of tunability and efficiency, which are due to the simultaneous transition between electronic and vibrational states. Good quality materials, in particular the alexandrite,[83] i.e., the chromium-doped chrysoberilium (Cr:$BeAl_2O_4$), has been particularly taken in consideration because it can be tuned in the 700 to 800-nm range, where the measurements of water vapor, temperature, and pressure can be performed. Ground-based DIAL systems have already been realized;[76] also airborne and space applications are now under project.[124,157,172]

Titanium-doped sapphire (Ti:$Al_2O_3$) is another interesting new material because it can emit in the range of 650 to 1000 nm, which is much larger than the tuning range of any other material. It can be pumped by the second harmonic of Nd:YAG with up to 30% efficiency.[84,196] For operation in the region of 1000 to 4000 nm, many tunable solid-state lasers have been developed. As an example, the Co:$MgF_2$ laser,[85] tunable in the range from 1500 to 2280 nm and pumped by the 1320-nm emission of Nd:YAG laser. It has been recently utilized for methane, carbon dioxide, and water vapor concentration measurements.[86] Some vibronic lasers have to be cooled at liquid nitrogen temperatures for operation and, due to their relatively long storage times, can be flashlamp or laser pumped as well. Room temperature operation of Co:$MgF_2$ has been obtained in pulsed operation with 50% slope efficiency.[173]

#### e. GAS LASERS

They are currently used because of their large output energy: hundreds of millijoules or, in the case of $CO_2$, of 1 J. Other commonly utilized gas lasers are CO (tunable around 5

μm) HF (2.7 to 3 μm) and DF (3.7 to 4 μm). In Table 10, the typical characteristics of these devices are reported. The He-Ne laser has also been utilized at 3.3 μm in CW emission for short-range applications.[104] The future development of high-pressure gas lasers, which can be continuously tunable,[93] will probably avoid the present problem of a reduced tunability (limited to a set of several tens of lines). The most interesting molecules are $CO_2$, $N_2O$, and $CS_2$, which permit laser operation in the ranges from 9 to 11, 10 to 11, and 11 to 12 μm respectively.

#### f. COLOR-CENTER LASERS

Such lasers, which are continuously tunable in a broad tuning range, have been developed for the visible and near infrared region,[94] from about 400 to 2000 nm. Their operation is very similar to that of dye lasers, which are similar in terms of gain and type of pumping: laser pumping is preferred. The only actual drawback, for most of them, is the need to operate and be stored at low temperatures (about 70 K). Up to now, they have not been utilized for lidar applications because of their small output power and because they still are in a developmental stage. Only one commercial device exists, operating in the range from 1000 to 1400 nm, with an output power of only some microwatts. Among the crystals able to work at room temperature,[200] the most promising, thanks to their excellent thermal and mechanical properties, are diamonds, which provide emission in the 500- to 600 - nm range, and sapphires, tunable in many bands in the visible and near IR, of which has been recently reported pulsed operation at a relatively high output energy, about 0.1 J. The most important problem yet to solve is the photostability of their color centers.

#### g. WAVELENGTH CONVERTERS

This name indicates those devices which are able to shift or convert, towards longer or shorter wavelengths, the tuning range or the emission frequencies of one or more lasers. Raman shifting[202,212] is now a commonly used technique. It is obtained by focusing the primary laser beam in a cell containing the gas whose vibrational or rotational transition corresponds to the designed frequency shift. In general, one uses hydrogen, deuterium, or methane because they offer high-frequency Raman-active vibrational modes: 4155, 2986, and 2917 $cm^{-1}$ respectively. The typical cell length is 1m, and the gas pressure is of the order of 10 atm. They are generally utilized in the first Stokes mode, that is for down-shifting the frequency once, and in this case, the conversion efficiency is easily 30%, while the first anti-Stokes or the higher-order Stokes are generally of a few percents. Raman shifts are to be considered a simple, inexpensive and reliable device. They have been proposed for obtaining high spectral purity emission at 720 and 940 nm, starting from a dye laser,[107] for tropospheric and stratospheric measurements of water vapor. Emission at 940 nm can also be obtained from Raman shifting of a Nd:glass laser.[108] UV radiation for ozone and sulfur dioxide monitoring is achieved in the same way, starting from an excimer laser[109] or a Nd:YAG laser.

Another kind of wavelength converter is represented by the well-known harmonic generators or mixing crystals. Second harmonic generation (SHG) of Nd:YAG (generally performed with KD*P or CD*A, i.e., potassium dideuterium phosphate and cesium dideuterium arsenate) can be made with a typical conversion efficiency of 40%, while the third harmonic conversion is larger than 15%. The SHG of visible lasers into the UV is generally performed with potassium dihydrogen phosphate (KDP), with an efficiency better than 20%. Recent technological development has improved the crystal quality in terms of damage resistance to light intensity and has led to the discovery of new kinds of materials with high nonlinear coefficients. Typical is the case of β-Barium Borate (BBO),[135,136] tunable in the range of 200 to 3000 nm, with a laser damage threshold larger than 1 $GW/c^2$ and a nonlinear coefficient four times higher than that of KDP. In the infrared range, for doubling, tripling, and mixing of $CO_2$ wavelengths, crystals having a much lower quality in comparison with the visible devices are used, generally $AgGaS_2$ and AgGaSe.[174] A more efficient material, $ZnGeP_2$, has been recently grown in good quality boules, whose size is large enough to be useful for this kind of application; conversion efficiencies of up to 80% have been reported,[175] but the crystal is not yet commercially available.

#### h. OPTICAL PARAMETRIC OSCILLATOR (OPO)

These sources[97,213,214] can provide a few millijoules of energy output continuously tunable in a wide range. They are generally pumped by the Nd:YAG laser or by its harmonics and can be temperature or angle tuned. Even if these devices are very attractive because of their compactness (cavities with lengths of 20 cm or less), they have not been widely utilized up to now for several reasons, such as the difficulty to get crystals of good quality, optical damage problems (which seem to be less severe if the earlier-described BBO crystals[135,136] are used), and, finally, the high quality required to the pump beam. The crystals more suited for OPO operation are $LiNbO_3$ (angle tuned with tunability range from 1.5 to 4 μm when pumped by a Nd:YAG[97]), urea,[102] and BBO[177-179] (both angle-tunable from UV to near infrared when pumped by the third and fourth harmonics of Nd:YAG). The potentiality of the OPO in DIAL systems has been demonstrated by a few authors,[98-101] but these works have to be considered as a proof of feasibility, rather than a real demonstration of utility. Indeed, for $SO_2$ detection,[99] there is a lack of sensitivity because of the low absorption cross section in the OPO emission range and, moreover, the low output power of this device makes it suitable only for small-system and short-range applications of tens or hundreds of meters.[95,96]

#### i. GaAs DIODE LASERS

This family of diode lasers has been particularly developed for communications and has now reached an high level of

reliability. The emission wavelength of available components can be tailored in three large spectral windows: at about 750 to 900 nm (gallium aluminium arsenide), at 1200 to 1550 nm (indium gallium arsenide phosphide), and, recently, in the visible at about 650 to 690 nm (gallium indium phosfide). They can be assembled in an array for increasing the output power of the overall device: arrays with 1-W average power are commercially available with efficiencies of more than 30% and lifetimes of $10^4$ h.

Despite these performances, their use in DIAL applications can be only indirect, restricted to the pumping of solid-state lasers, such as Nd:YAG. The specific advantage in the use of laser crystals is the possibility of energy storing due to the long lifetime of the upper laser level in the crystal itself. This property makes possible Q-switching, i.e., the release in a very short time of a few nanoseconds, of the energy stored in a period of hundreds of microseconds. The emission of short powerful pulses is, in turn, necessary for the lidar requirement and for getting an efficient wavelength conversion in the pumping of other lasers. The diode pumping efficiency of Nd:YAG with radiation at 808 nm can be as high as 50%, one order of magnitude better in comparison with the standard flashlamp pumping. Other great advantages are in terms of component lifetime and in terms of safety since the high voltage capacitors of the flashlamp driver are eliminated.

For a typical lidar application, a diode with a peak output power of several kW is required; unfortunately, devices with this performance are not yet available, but they may become available in a few years at a reasonable cost. In fact, the development in this field is very rapid: arrays with 12-W average output power and 40% efficiency,[176] and arrays with 300-W peak power has been recently announced.[195] A very promising application of CW laser diodes is connected with the possibility to achieve a very narrow band, single-mode emission. This property allows the use of them for the injection seeding of tunable solid-state lasers; for example, alexandrite,[185] for obtaining high-power pulses with the same spectral properties.

## B. Receiver Telescope

The function of this device is to efficiently collect the scattered light. Since, in many cases, it is less expensive and easier to increase the signal power by utilizing a larger telescope rather than using a more powerful laser; it is a general rule to utilize a very large telescope. Hence, 50-cm-diameter telescopes are nearly standard for UV-visible DIAL systems. Heterodyne detection requires a smaller size because of its good sensitivity and the large power commonly available for this application ($CO_2$ lasers). Moreover, there is nothing to gain, in this case, in utilizing a telescope larger than the transmitted beam or the transverse coherence length of the atmosphere.[51,60,106,154-156] Reflective optics are almost exclusively utilized because they can operate in every wavelength range without problems of chromatic aberrations or transparency of glasses. An aluminium-coated mirror, for example, can be utilized from the UV to the far IR as well. Furthermore, standard reflective telescopes, developed for astronomical use and easily available on the market, have an optical quality which is better than that required for lidar operation. Even for coherent detection, where diffraction-limited optics are required, there exists no particular problems because of the long wavelengths utilized (about 10 μm).

The choice of the focal length is primarily determined by requirements of compactness. The telescope f-number (i.e., the ratio between focal length and diameter of primary mirror) is generally of the order of three; lower f-numbers rise the cost of the mirrors and increase the optical aberrations. The telescope field of view is limited by means of an iris placed in the focal plane or close to it. This parameter, which must be evaluated in connection with laser divergence, solar background, and lidar signal dynamic range, is discussed here.

### *1. Steering of the Telescope*

If the optical components themselves do not represent a critical part of the system, a little more care should be devoted to the system used to steer the optical beam. Measurements performed on board aircraft or moving vans are usually made with the telescope pointing in a fixed direction, generally upwards or downwards. Measurements performed from a fixed location (and also from satellite) usually require beam scanning, particularly when pollution concentration in plumes is monitored. Beam scanning can be performed in many ways:

1. By moving the telescope and laser, fixed together on a common table
2. By keeping the telescope and laser fixed and using one or two flat steering mirrors for both transmission and reception
3. By keeping the laser fixed and steering together beam and telescope
4. Other combinations of these schemes

There are advantages and disadvantages for each of these solutions, which represent the best compromise between measurement requirements, problems of cost, range of solid angle scanned, easy alignment, size, and stability limitations. The first scheme poses some alignment problems of the laser components because it requires tilting in an inclined plane and hence, is rarely adopted. The second solution is more common. With one scanning mirror only,[150,164,203] the telescope is pointing upwards and the maximum elevation angle is limited by the size of the major axis of the mirror (see Figure 22); vertical measurements are possible by completely removing the mirror. A two-mirror geometry permits scanning in every direction but is more cumbersome and is generally adopted with a telescope of moderate aperture (about 30 cm).[51,52,184] The third scheme

is more complicated from the point of view of the alignment of the beam with the optical axis of the telescope, which has to be kept within a fraction of milliradiant during beam steering. Other solutions, adopted for van-mounted systems, use the laser fixed and the telescope with one scanning mirror rotating on the roof of the truck[166] or the laser mounted on the fork of the telescope, rotating with it around the vertical axis and the telescope scanning in elevation[163] (see Figures 15, 18, and 19.) For these systems, the steering is under computer control by means of stepping motors and suitable encoders. An angular precision of a few milliradians is generally sufficient for standard pollution measurements. An automatic alignment control between the laser (or lasers) and the telescope should be particularly welcome by all people having some experience of field campaigns.

### 2. Wavelength Filtering and Separation

Together with the lidar signal, an unwanted background radiation is always collected by the telescope. This radiation is composed of the infrared thermal contribution of the surroundings, centered at about 10 μm, and of the visible daylight, which extends from 300 nm to about 2 μm.

The infrared background radiation (black body radiation of the environment) is the main component of the receiver noise, given by the detectivity D*, earlier. This term can only be attenuated by reducing the detector size, bandwidth, and detector field of view (by means of a cold field stop), and by a cooled spectral filter. Visible radiation can be easily eliminated in the infrared systems by means of a proper detector window or a long pass filter. The long wavelength cutoff of visible-UV detectors [photomultipliers (PMT)] make them insensitive to thermal radiation. Due to the fact that solar radiation is completely absorbed by the stratospheric ozone, UV systems below 300 nm (the solar-blind region) behave as if they were operated in nighttime conditions. However, in this case, a good shielding against the daytime visible light, which also offers a good transmission at the DIAL wavelengths, must be provided. An interference filter with a bandwidth of about 3 to 10 nm is the common choice, even if the UV transmission is not very high (20%), and the blocking of the visible radiation is not always satisfactory (degree of blocking of $10^{-6}$ is standard, but sometimes not sufficient). A better solution in term of transmission efficiency and spectral contrast can be represented by a polychromator, which, on the other hand, is more cumbersome and expensive.

For measurements in the visible, some amount of background light is unavoidable because the spectral width of the filter must be as large as the separation between the two wavelengths (which can be 1 nm) and, in any case, it cannot be narrower than 1 to 3 nm, for practical reasons. Unless some other narrow band filtering device is also utilized (for example, a Fabry-Perot), this fact can limit the useful range of daylight measurements.[147]

### 3. Field of View and Laser-Telescope Coupling

For optimum performances, the field of view must match the laser beam direction and divergence. The principles to follow in the design of the transmitter-receiver optics are

1. Maximization of the collecting efficiency at a given range
2. Dynamic compression of the lidar signal
3. Rejection of the unwanted background radiation
4. No detector saturation for large near-field return

These items are mutually dependent and are strictly dependent on operational features, the choice of the detector, spectral region, and laser characteristics. The parameters to consider in the design are[129,192,199]

1. Type of propagation of the laser beam with regard to the telescope axis: coaxial, parallel, nonparallel
2. Obscuration of the secondary mirror of the telescope
3. Width of the field of view
4. Position of the field stop along the telescope axis
5. Laser divergence
6. Laser beam diameter
7. Size and position of the last laser beam-transmitting mirror

In some applications, one problem is the detector saturation by the near-range backscattered light; the simplest solution is the choice of a parallel beam propagation far from the telescope axis together with the use of a small field stop (see Table 6). In this case, the detector is blind for several kilometres up to an altitude where the laser beam overlaps the field of view. For stratospheric ozone measurements an equivalent result has been obtained using a rotating chopper.

In the troposphere, near-field operation from a few tens of meters to several kilometers is often required. The minimum range is limited by the obscuration of the transmitting mirror or the telescope secondary mirror for coaxial systems.

Maximization of the signal return from a given distance is obtained by positioning the field stop in the image plane corresponding to that range. A small field of view, just of the same size of the laser divergence, is useful to reduce the dynamic range of the lidar return: a complete correction of the geometric quadratic range dependence of the signal has been achieved in this way coupled to a noncollinear transmission of the beam.[191] An objection to small fields of view is the more critical alignment and the possible errors that can arise if the beams at the two wavelengths have a different spatial profile (in particular, when a dual laser system is utilized). In this case, false concentration burdens can be measured because of the different light-collecting efficiency vs. range.

The most-used solution in ground-based systems is a coaxial or near-coaxial propagation of the laser beam. For heterodyne systems, the receiving telescope is often used as a transmitter;[51,52] more rarely, a two-coaxial telescope configuration is adopted.[193]

Typical fields-of-view are of the order of 1 mrad. For wavelengths below 1 μm, a small field stop is useful to reduce solar background in conjunction with interference filters, monocromators, or other similar devices.

For IR wavelengths, thermal background noise dominates and can be reduced by means of cold filters, cold stops, and small detector size (for improving NEP, see Equation 21). The field of view is limited by the size of the detector, which is typically 1-mm diameter.

For heterodyne detection, useful fields of view are about 0.2 mrad (for $CO_2$-laser wavelengths), dictated by the requirement of diffraction-limited operation.

## C. Detectors

The detectors, together with the laser, are the most critical parts of a DIAL system; they will be treated according to their classification into direct and heterodyne detection. For exhaustive discussions about these items, see References 187 and 188.

### *1. Direct Detection*

Photomultipliers, providing virtually noise-free signal amplification, are ideal (and trouble-free) detectors and offer a sensitivity (defined as the minimum detectable optical power, i.e., relevant to SNR = 1) better by several orders of magnitude in comparison with the direct-detection infrared receivers. PMTs with over 20% quantum efficiencies are available in the UV and the visible. In the near infrared, the efficiency decreases and does not surpass a few percent, except for the gallium arsenide types in which it is over 10% up to 900 nm. This last device, although attractive, is not widely utilized because it is believed to be very delicate and other less efficient PMTs or silicon avalanche photodiodes are preferred in the region above 700 nm.

Above 1.1 μm, silicon is no more sensitive and other kinds of detectors, progressively noisier as the wavelength increases, are to be used, i.e., InAs, InSb, HgCdTe. These last detectors also present limitations and problems in terms of bandwidth (which affects spatial resolution), small detector size (they must be small to reduce noise and increase the bandwidth), requirement of cooling down to liquid nitrogen temperatures, and difficulties connected with signal amplification. In any case, every kind of detector requires hard work for shielding the signal from electromagnetic interferences, which are typical of lasers (due to the power supply, capacitor discharge, Pockel's cell switching, etc.). A common feature of DIAL systems is the utilization of battery-powered detectors and preamplifiers to decrease electrical pick-up.

An important characteristic of DIAL signals lies in their wide dynamic range, through many decades, which brings about problems of detector linearity and imposes techniques of dynamic compression in order to precisely digitize the signal in a transient recorder. In fact, this last device has a maximum dynamic range of 1000 or 4000 (with 10- or 12-bits analog to digital conversion, respectively). This problem is amplified even more by the high variability (in time and space) of the atmospheric backscattering and extinction coefficients. Many solutions have been devised to solve this problem, namely:

1. Gain modulation or gain switching of the detector amplifier.
2. Gain modulation or gain switching of the photomultipliers by changing the polarization voltage of dynodes.[150,163]
3. Use of log amplifiers. Actually, they are widely utilized for standard lidar applications, but not for DIALs because of the high precision required for this application and because their use does not allow versatility in choosing the most correct signal-averaging technique (see also Section XI.E).
4. Manipulation of the telescope function, which is performed by choosing a suitable iris, located close to the focal plane[129,192,199] (see also Section XI.B).
5. Use of two different transient recorders or two channels (if available) of the same transient recorder with two different voltage input range.
6. Use of microprocessor-controlled transient recorder for the automatic change of the input scale as a function of the range or signal amplitude.[76]

### *2. Heterodyne Detection*

When compared to these light sensors, heterodyne detection presents peculiar properties. It behaves like a PMT because of its quantum noise-limited operation, and in the same time, it is inherently amplified by the beat between the local oscillator field and the signal field. On the other hand, in comparison with direct infrared detection, it suffers from the drawback of a greater complexity, even lower useful detector size (which involves problems of alignment), and the same requirements of cooling. As the heterodyne signal is proportional to the electric field amplitude and not to the intensity of the light signal, its dynamic range is advantageously reduced. On the other hand, a proper averaging of this signal can be performed only after its quadrature,[184] which, therefore, requires a more complicated acquisition software. Averaging is mandatory with this technique because of the high signal fluctuations, due to speckle noise.

Further complications arise from the need of two local oscillators for the two wavelengths (whose output power must be stable during the lidar return to avoid modulations of the signals). Generally, only one detector is utilized, with the two local oscillator beams alternatively chopped and directed upon it.[184] At $CO_2$ wavelengths, a mercury cadmium telluride (PV) detector is utilized, with a useful size of less than 0.5 mm and a bandwidth of a few tens of megahertz, the local oscillator being offset by 20 to 30 MHz, typically.

### D. Transient Recorder

A transient recorder (or transient digitizer) is the standard instrument utilized to digitize a lidar signal. It is normally based on a fast video analog-to-digital converter (flash converter type[112]) which samples and converts the input signal at the rate given by a clock. The less significant bit of the converter must be of the order of magnitude of the baseline noise. The data are transferred in a random access memory (RAM) for successive transfer to the external computer or for data logging on a display. Its general requirements are a sufficient precision and a bandwidth compatible with the desired spatial resolution. This instrument is replaced by photon counting techniques[112,216] in the UV-visible range only in those applications where the arrival rate of the photons is very low: typically, for monitoring the stratosphere from a ground-based system (for the ozone with the DIAL technique or the alkali metals with the resonant fluorescence technique). In these cases, lidar signals from the PMT are composed of current spikes, each of them corresponding to the detection of a single photon. When their rate is lower than (typically) 5 MHz, then it is more convenient in terms of recording precision to count them instead of to integrate the relevant current and measure its value. The total counts for each time intervals are then stored and averaged over many shots for on and off wavelengths for the evalutation of the concentration in the standard way.

Up to 10 years ago, only a few models of digitizers were available on the market and almost all systems were based on the same devices. Now, many instruments have been developed, each of them able to store a digitized signal in a 1000-word memory capacity and equipped with plenty of mathematical options and functions, such as signal averaging, sum, subtraction, FFT, etc. It is worthwhile to say that such improvements are not really significant for DIAL applications. On the contrary, in many cases, their presence causes a slowing of the acquisition speed of the instrument (in terms of number of lidar signals per second that it is able to digitize and transfer to the computer) and a raise of cost. The more important input requirements concern bandwidth and precision. A bandwidth of a few megahertz and a sampling time of 10 or 20 MHz (equivalent to a spatial resolution of 15 or 7.5 m, respectively) is more than adequate for pollution monitoring.

Concerning the digitizer precision, one has to distinguish between the normal precision, evaluated in terms of the number of bits in which the waveform is digitized, and the real precision, which is generally a pair of bits lower than this value and is strongly dependent on the bandwidth of the signal. The absolute digitizer precision is not so important in itself, as the standard quality offered by the available instruments is good enough, but the biggest problem arises from the large dynamic range of the lidar return, which varies with range with an inverse square law and can then span over several decades. As a consequence, it is impossible to record with enough precision or, in some cases, over the level of the low significant bit, the tail of the signal, corresponding to the farthest range. This problem is generally solved by a dynamic compression of the signal in the detector or the amplifier, as stated earlier. In some cases, the same signal is fed in two channels of the same digitizer, each set with a different input sensitivity range corresponding to the large near-field signal and the low far-field one. In another case,[123,158] two different telescopes with two different PMTs are utilized for the near and the far range (see Table 6).

In any case, a digitizer with a high number of bits is always advisable; actually, digitizer with a 20-MHz sampling rate and 12-bit precision are available, while most of the present DIALs utilize 10-bit/10-MHz instruments. Further improvements of this device could be found not in an increase of the number of bits, but in the ability to digitize small and large signals with the same precision; for example, with some sort of automatic gain control or by programming the input scale according the expected amplitude of the signal vs. time. One example of such an instrument has already been realized with success,[76] and it is expected to be commercially available.

Another important parameter that must be carefully considered is the overall acquisition speed, defined as the number of signals per second that the instrument is able to digitize and transfer to the computer. This term is dependent on the organization of the mainframe of the digitizer, the speed of the digital interface, the matching characteristics with the computer interface card, and on the software. This very critical point is often a source of troubles and is not satisfactorily solved even in a large number of expensive, commercially available instruments. A real-time display of the digitized signal on a scope is the most useful information for a visual check of the system operation (it also gives immediate information about the intensity of the signal, beam alignment, presence of plumes or obstacles in the atmospheric path, etc.) and should be provided for a system devoted to field campaigns.

### E. Computer and Data Acquisition System

Computers have enabled DIAL systems to make the jump from laboratory devices to really useful tools for atmospheric analysis, the reasons being essentially the possibility to handle a great deal of data in a short time and to perform automatically some control functions such as telescope positioning. As an example of the amount of data dealt with, for a system working with 3-km range, 15-m resolution, and a laser running at 10-pulse pairs per second, the number of data bytes are of the order of 16 kbytes/s, including background subtraction. This is not a very high number but it is impossibile to handle the data in a different way and not every computer is suited for this application. In the existing DIAL systems, the computer and most of the software are substantially dedicated to data acquisition from the digitizer and data storing in internal or external memory devices for later analysis, with only a few mathematical operations of data processing and data averaging.

The computer control of the system mainly consists in the steering of the telescope or in getting additional data such as laser energy or travel parameters for mobile systems.

The complete data processing, including graphic plots and two dimensional maps, is generally performed after the field campaign and normally takes three or four times the time necessary for the campaign itself. A great deal of time is lost because of the limited performances of the computers which were available when these systems were developed. Now, for the same prices, computers are available which are much more powerful in terms of computing speed, internal and external memory, graphic display, and available software. In view of the progress that can be done and should be made in the future, it is easy to foresee the advent of a completely computer-controlled DIAL system. For doing so, an "intelligent software" is to be developed which has to take into account most of the situations that can happen during the measurement.

In terms of system control, many tests and calibrations that can now be performed only by a skilled operator, could be made through proper software. Widespread use of a DIAL system will be possible only if such system will be made accessible to personnel not expert in the laser field, nor in electronics or optics. If this will not be the case, then we would assist again to the rather common fate of complicated lidar systems left in the garage because of the lack of skilled operators. The items that really need to be made computer controlled are

1. Laser frequency tuning and calibration
2. Detector gain
3. Transient recorder input range

The operation of a computer-controlled system should be really user oriented so that one has not to worry about the real parameters of the measurements, except for a few practical ones such as the kind of gas to be monitored or the directions in which to fire the laser.

About the mathematical "on-line" processing; it is strictly dependent on the particular features of the experience and there are no rules about the best way to do it, so only a few guidelines can be given:

1. For an airborne system, where the pair of laser shots is fired quasi-simultaneously, generally only background subtraction is performed on the return signals and every pair is later individually analyzed (on ground) to derive a concentration profile.
2. For measurements from a fixed location, on-line averaging of the return signals is usually performed for reducing the amount of data and for simplifying later analysis. The averaging can be performed separately on the "on" and "off" resonance signals or on their ratio (if it is supposed that a strong correlation between signals is existing only on a shot-pair basis), or on the logarithm of the signals, if it is supposed that gas concentration is by far the most fluctuating parameter. Usually, the first kind of processing is adopted because it best fits most of the pratical situations and because of its simplicity. In the case of negligible noise and stationary atmosphere, all the methods give the same results, otherwise noise-dependent or systematic concentration errors can arise.
3. Measurements carried out from a ground-based mobile system are generally performed by averaging the signals in some of the earlier-mentioned ways. In this case, the laser repetition rate is fast in comparison with the speed of the vehicle and acceptable horizontal spatial resolution is compatible with averaging over a limited number of shots.

For a user-oriented system, most mathematical processing should be performed in real time in order to give to the operator immediate information as close as possible to the final one. Up to now, only in one case[163] are the concentration profiles evaluated in real time together with the measurement error, based on the calculation of the root mean square fluctuations of the signal. In other cases, only the averaged lidar returns are generally available after the measurements.

The final data processing is the most wearisome process. This phase can include further data corrections needed for taking into account a particular system or some physical parameters (needed, for example, for ozone monitoring), but usually a great deal of work deals with aspects which have strictly nothing to do with the DIAL method, such as graphics, editing, etc. Nevertheless, these time-consuming aspects are very important as the final output of a lidar campaign consists of a set of tables, two-dimensional pollutant maps or a pollutant profile vs. time, or a set of data, suitably formatted, to be fed as input to mathematical models of pollution diffusion or meteorological forecasting programs.

Today, minicomputers, which can possess an internal memory of megabytes in comparison with the few tens of kilobytes of the early DIAL systems, are well endowed with graphic hardware (graphic display, plotters, graphic printers, etc.) and software to support these facilities. It is evident that such options require a larger effort in software development than that required by the data acquisition and system control only.

### *1. Hardware and Software*

Table 1 reports, as an example, the typical components of a range-resolved DIAL computer system (taken from the configuration of the mobile systems made by CISE for ENEL-CRTN of Milan and the Instituto de Investigaciones Electricas of Mexico (IIE).

The hardware has been chosen by taking into account several practical reasons:

1. The need to use a widely diffused computer model in order to get data format compatibility with computers of other institutions interested in utilizing the results.
2. The need, expressed by the customer, to dispose of graphic hardware and software facilities on board a truck in order to be able to get a nearly immediate and complete data analysis and printing of the results during the dead times of the campaign.

The software is strictly dependent on the particular measurement procedure that has been adopted; that is, from a fixed location with the telescope pointing over a set of directions. For each direction, a number of shot pairs ranging from 20 to 500 are typically averaged. Concentration profiles and measurement error are then evaluated before turning to the next direction. The concentration data are calculated according to the desired spatial resolution, set before the beginning of the experience. The digitizer sampling rate is always set at 10 MHz, corresponding to 15 m spatial resolution; hence, if the spatial resolution really needed is larger than this value, then a digital triangular filter[215] is applied to adjacent concentration values for a further smoothing of the data and improving the precision of the measurement.

For each concentration data, an evaluation of the relative error, based on the root mean square of the signal fluctuations at that range, is made. A set of four values, i.e., concentration, error, "on," and "off" signals, is stored for each 15-meters range step in the hard disk or the streamer tape. Additional stored informations concern experience parameters, directions, date, time, lidar location, etc. The controls performed by the computer consist in the laser energy monitor, the system calibration utilizing a transmission cell containing a given amount of the gas to be monitored, and the steering of the telescope. With this described measurement procedure, the graphic output consists of two-dimensional maps such those reported in Figures 28 and 29. These plots are obtained by tracing isoconcentration levels at the values desired by the operator. The area to be plotted is automatically cut by the program in order to blank the data corresponding to far ranges where the concentration error is too high in comparison with the required sensitivity. The plot is completely performed on the graphic terminal, the hardcopy of the video being obtained by means of a plotter or graphic printer.

## XII. SAFETY PROBLEMS

Safety problems are of concern here because of the possibility of skin and eye exposure to high-intensity laser beams. Lidars, in particular, present the problem of beam transmission into the open atmosphere to a range of many kilometers. Care should be taken that in the beam path no people could be hit or that, if the case arises, the beam intensity is not at a dangerous level. The safety criterion can be defined in terms of maximum permissible exposure levels (MPE) which have been

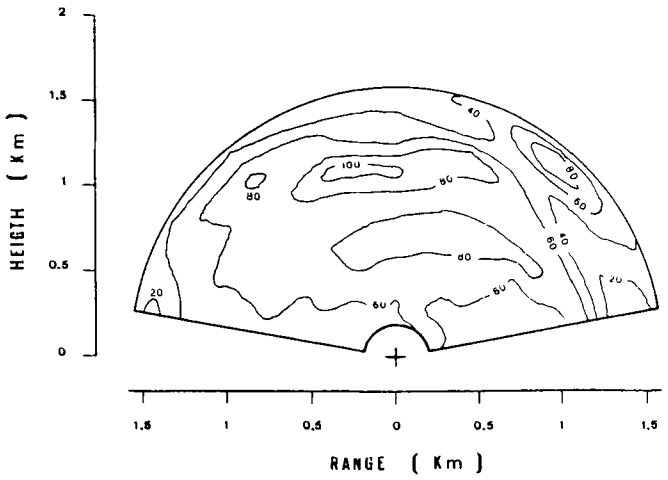


**FIGURE 28.** Vertical map of ozone concentration obtained with the CISE-ENEL system of Figure 15. The measurements have been made during an experimental campaign performed in the north of Italy in July 1987. The system has been oriented in a set of nine directions lying on a vertical plane. The concentration is expressed in parts per billion.

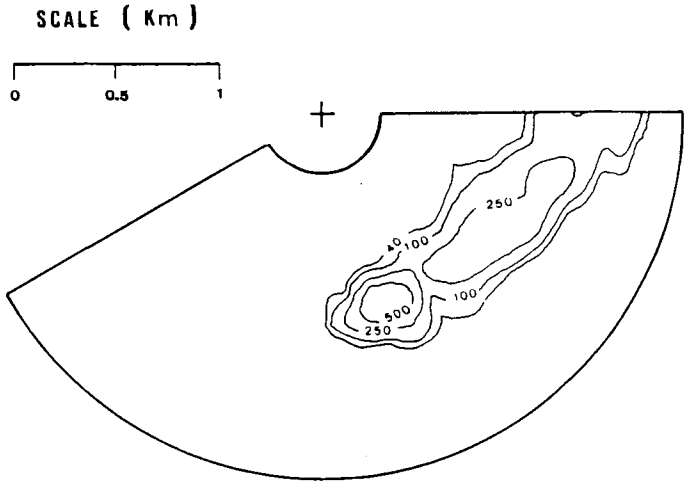


**FIGURE 29.** Horizontal map of sulfur dioxide performed with the CISE-ENEL DIAL. The figure shows the intersection of a plume emitted by a power plant with a set of lidar directions lying on a conical surface with 10° elevation over the horizontal. The concentration is expressed in parts per billion.

studied and classified by many institutions, formerly by the American National Standards Institute (ANSI),[88] whose standards are almost universally accepted. (For an exhaustive description of the matter, we recommend Reference 194.) The MPEs concerned with this application are primarily those relative to an occasional direct viewing of the laser beam, which are by far the more severe.

In order to evaluate the main aspects of the problem, it is useful to distinguish three spectral regions:

1. Ultraviolet (wavelengths under 400 nm). Here the light absorption occurs within a small depth on the surface of the cornea, and the MPE are 1 mJ/cm$^2$ with some de-

pendence on wavelength. Both heating and phototoxic effects are effective in eye damage. A complete light absorption occurs in the eye surface according to ANSI,[88] but in the region from 300 to 400 nm, some discrepancies exist between different authors: in Reference 89, a small amount of light can reach the retina and hence, the MPE is much lower.

2. Visible-near infrared (from 400 to 1400 nm). The cornea is transparent in this region, and the radiation is focused into a very small spot (nearly diffraction limited if the eye is focused to infinity) on the retina where the irradiation can reach very high levels if compared with the light intensity on the eye surface. For typical laser pulse durations of a few nanoseconds, MPEs are100 $nJ/cm^2$, constant in the range 400 to 700 nm, and with a little wavelength dependence from 700 to 1400 nm.
3. Infrared over 1400 nm. Here, the MPEs levels are about 10 $mJ/cm^2$. Only heating effects on the cornea are considered.

Once the MPE for a particular system have been evaluated (the MPE also depend on laser repetition rate), it is to be compared with the output energy density of the transmitted laser beam vs. range, taking possibly into account the lens effects of the atmospheric turbulence. The results of this comparison give an indication of the range over which the system can be considered eye-safe. For infrared systems with heterodyne detection, the need to enlarge the transmitted beam to about the telescope size results in a very small energy density, even with output energy of the order of 1 J.

For the other infrared systems (over 1400 nm) with a smaller transmitted beam, generally there is a range at which the laser divergence (of the order of 1 mrad.) has widened the beam to the point that sufficiently low-energy densities are achieved. This range depends on laser parameters and can be of tens or hundreds of meters. In the case of very low-power lasers, the system can be considered always safe.

A similar situation exists in the UV, while, for the visible and infrared under 1400 nm, the MPEs are so low that even after many kilometers propagation, the beam is still dangerous.

The safety aspects are strictly dependent on operational features and surroundings of the system; no particular rule can be given here, except for the obvious suggestions to carefully design laser energy, beam diameter, and beam divergence in order to optimize this aspect. A useful device that is quite standard, not only for safety purposes but also for system operation, is a telecamera mounted on the telescope, which permits to avoid firing against people.

## XIII. CONCLUSIONS

The DIAL method has demonstrated its ability to perform remote atmospheric analyses and measurements which are hardly possible with conventional tools. Its main advantage is the capability to sound large regions of many kilometers extent.

Many systems are now routinely utilized for pollution monitoring and atmospheric studies, but their use is up to now confined in research laboratories and in experimental "on-the-field" facilities. Problems of cost, system complexity, and overall reliability have not yet allowed a wider use. The high cost of such instruments, $1 million or more, is mainly due to the cost of the design, development, and software, which are often charged on only one prototype. The technique itself and the related phenomena are well understood, but the instrumental apparatus needs further development and engineering, in particular, the laser transmitter and detection electronics. The expected progress in the laser field is in terms of new devices with broader frequency coverage, efficiency, output power, durability, frequency stability, and control. Detection electronics should improve in terms of higher dynamic range and automatic control to overcome the problems connected with the high variability of the atmospheric target.

We are confident that, thanks to the fast evolution in progress in these fields, in a few years, the construction of really user-oriented systems will be possible, whose costs (initial and maintenance), can be substantially lowered to encourage a wider use of lidars, thanks to a larger-scale production and better reliability of the components.

## ACKNOWLEDGMENTS

The author wishes to thank the researchers who have granted permission to reproduce the figures in this paper. The author is also very grateful to A. Sona, I. Carrer, L. Fiorina, E. Galletti of CISE, A. Marzorati of ENEL-CRTN, and A. Raspa of Quanta System, for their helpful cooperation, Professor N. Omenetto of JRC-Ispra, and W. B. Grant of the NASA Langley Research Center for a critical reading of the manuscript.

## REFERENCES

1. **Bureau, R.,** *Meteorologie*, 3, 292, 1946.
2. **Fiocco, G. and Smullin, L. O.,** Detection of scattering layers in the upper atmosphere (60-140 Km) by optical radars, *Nature*, 199, 1275, 1963.
3. **Ligda, M. G. H.,** Proc. 1st Conf. Laser Technol., U.S. Navy Office of Naval Research, 1964.
4. **Leonard, D. A.,** Observations of raman scattering from the atmosphere using a pulsed nitrogen ultraviolet laser, *Nature*, 216, 142, 1967.
5. **Cooney, J. A.,** Measurements of the raman components of laser atmospheric backscatter, *Appl. Phys. Lett.*, 12, 40, 1968.
6. **Inaba, H. and Kobayasi, T.,** Digest of technical papers, N° 12-1, 1970, in Int. Quant. Electron Conf., Kyoto, Japan, 1970.
7. **Kobayasi, T. and Inaba, H.,** Spectroscopic detection of $SO_2$ and $CO_2$ molecules in polluted atmosphere by laser-Raman radar technique, *Appl. Phys. Lett.*, 17, 139, 1970.

8. **Kobayasi, T. and Inaba, H.,** Laser-Raman radar for air pollution probe, *Proc. IEEE,* 58, 1568, 1970.
9. **Bowman, M. R., Gibson, A. J., and Sandford, M. C. W.,** Atmospheric sodium measured by a tuned laser radar, *Nature,* 221, 456, 1969.
10. **Rothe, K. W., Brinkman, U., and Walter, H.,** Applications of tunable dye lasers to air pollution detection: measurements of atmospheric $NO_2$ concentrations by differential absorption, *Appl. Phys.,* 3, 115, 1974.
11. **Rothe, K. W., Brinkman, U., and Walter, H.,** Remote sensing of $NO_2$ emission from a chemical factory by the differential absorption technique, *Appl. Phys.,* 4, 181, 1974.
12. **Grant, W. B., Hake, R. D., Jr., Liston, E.M., Robbins, R. C., and Proctor, E. K., Jr.,** Calibrated remote measurement of $NO_2$ using differential absorption backscatter technique, *Appl. Phys. Lett.,* 24, 550, 1974.
13. **Collis, R. T. H.,** Lidar, *Appl. Opt.,* 9, 1782, 1970.
14. **Collis, R. T. H. and Russel, P. B.,** Lidar measurements of particles and gases, in *Laser Monitoring of the Atmosphere,* Hinkley, E. D., Ed., Springer-Verlag, Berlin, 1976.
15. **McClatchey, R. A. and D'Agati, A. P.,** Atmospheric Transmission of Laser Radiation: Computer Code LASER, AFGL-TR-178-0029, 1978.
16. **Etterman, L.,** Atmospheric Attenuation Model, 1964, in the Ultraviolet, Visible and Infrared Regions for Altitudes to 50 Km, Tech. Rep. AFCRL-64-740, ERP N°46, 1964.
17. **Mie, G.,** *Ann. Phys.,* 25, 377, 1908.
18. **Van de Hulst, H. C.,** *Light Scattering by Small Particles,* John Wiley & Sons, New York, 1957.
19. **Kerker, M.,** *The Scattering of Light,* Academic Press, New York, 1969.
20. **Deirmendjan, D.,** *Electromagnetic Scattering on Spherical Polydispersion,* American Elsevier, New York, 1969.
21. **Elterman, L.,** An Atlas of Aerosol Attenuation and Extinction Profiles for the Troposphere and Stratosphere, Tech. Rep. AFCRL-66-828, 1966.
22. **Elterman, L.,** UV, Visible, and IR Attenuation for Altitudes up to 50 Km, 1968, Tech. Rep. AFCRL-68-0153, ERP N°285, 1968.
23. **Elterman, L.,** Vertical Attenuation Model with Eight Surface Meteorological Ranges 2 to 13 Kilometres, Tech. Rep. AFCRL-70-0200, 1970.
24. **Elterman, L.,** Relationships between vertical attenuation and surface meteorological range, *Appl. Opt.,* 9, 8, 1970.
25. **Shettle, E. P. and Fenn, R. W.,** Models of the atmospheric aerosols and their optical properties, in AGARD Conf. Proc. N°183, Lingby, Denmark, October 27 to 31, 1975.
26. **Selby, J. E. A., Kneizys, F. X., Chetwynd, J. H., Jr., and McClatchey, R. A.,** Atmospheric Transmittance/Radiance: Computer Code Lowtran 4, Tech. Rep. AFGL-TR-78-0053, ERP N°626, 1978.
27. **McClatchey, R. A., and Selby, J. E. A.,** Atmospheric Attenuation of Laser Radiation from 0.76 to 31.25 μm, Tech. Rep. AFCRL-TR-74-0003, ERP N°460, 1974.
28. **McClatchey, R. A., Benedict, W. S., Clough, S. A., Burch, D. E., Calfee, R. F., Fox, K., Rothman, L. S., and Garing, J. S.,** AFCRL Atmospheric Absorption Line Parameters Compilation, Tech. Rep. AFCRL-TR-73-0096, ERP 434, 1973.
29. **Hamilton, P. M.,** The application of a pulsed-light rangefinder (lidar) to the study of chimney plumes, *Philos. Trans. R. Soc. London Ser.,* A:265, 153, 1969.
30. **Selby, J. E. A. and McClatchey, R. A.,** Atmospheric Transmittance from 0.25 to 28.5 μm: Computer Code LOWTRAN 2, Tech. Rep. AFCRL-TR-72-0745, 1972.
31. **Selby, J. E. A. and McClatchey, R. A.,** Atmospheric Transmittance from 0.25 to 28.5 μm: Computer Code LOWTRAN 3, Tech. Rep. AFCRL-TR-75-0255, 1975.
32. U.S. Standard Atmosphere 1976, U.S. Government Printing Office, Washington, D.C., 1976.
33. **Kruse, P. W., McGlauchin, L. D., and McQuistan, R. B.,** *Elements of Infrared Technology,* John Wiley & Sons, New York, 1963.
34. **Measures, R. M.,** Lidar equation analysis allowing for target lifetime laser pulse duration, and detector integration period, *Appl. Opt.,* 16, 1092, 1977.
35. **Pelon, J. and Megie, G.,** Ozone monitoring in the troposphere and lower stratosphere: evaluation and operation of a ground-based lidar station, *J. Geophys. Res.,* 87, 4947, 1982.
36. **Browell, E. V., Ismail, S., and Shipley, S. T.,** Ultraviolet DIAL measurements of $O_3$ profiles in regions of spatially inomogeneous aerosols, *Appl. Opt.,* 24, 2827, 1985.
37. **Uchino, O., Maeda, M., Shibata, T., Hirono, M., and Fujiwara, M.,** Measurements of stratospheric vertical ozone distribution with a Xe-Cl lidar; estimated influence of aerosols, *Appl. Opt.,* 19, 4175, 1980.
38. **Sutton, S.,** Differential Lidar Measurements of Ozone in the Lower Troposphere, Cent. Electr. Res. Lab. Note TPRD/L/2967/N85, Her Majesty's Stationery Office, London, 1986.
39. **Byer, R. L.,** Review remote air pollution measurement, *Opt. Quant. Electron.,* 7, 147, 1975.
40. **Kildal, H. and Byer, R. L.,** Comparison of laser methods for the remote detection of atmospheric pollutants, *Proc. IEEE,* 59, 1644, 1971.
41. **Byer, R. L. and Garbuny, M.,** Pollutant detection by absorption using Mie scattering and topographic targets as retroreflectors, *Appl. Opt.,* 12, 1496, 1973.
42. **McCormick, M. P., Lawrence, J. D. Jr., and Crownfield, F. R. Jr.,** Mie total and differential backscattering cross sections at laser wavelengths for Junge aerosol models, *Appl. Opt.,* 7, 2424, 1968.
43. **Menyuk, N., Killinger, D. K., and Menyuk, C. R.,** Limitations of signal averaging due to temporal correlation in a laser remote-sensing measurement, *Appl. Opt.,* 21, 3377, 1982.
44. **Murray, E. R., Hake, R. D. Jr., Van der Laan, J. E., and Hawley, J. G.,** Atmospheric water vapour measurements with an infrared differential absorption lidar system, *Appl. Phys. Lett.,* 28, 542, 1976.
45. **Rothe, K. W., Walther, H., and Werner, J.,** Differential-absorption measurements with fixed-frequency IR and UV lasers, in *Optical and Laser Remote Sensing,* Killinger, D. K. and Mooradian, A., Eds., Springer-Verlag, Berlin, 1983.
46. **Heinrich, H. J., Weitkamp, C., Baugart, R., Boie, H. O., Koehler, S., and Michaelis, W.,** Shipborne DF laser lidar for depth-resolved measurements of hydrogen chloride in 12th Int. *Laser Radar Conf.,* Aix en Provence, France, August 13 to 17, 1984.
47. **Flamant, P. H., Menzies, R. T., and Kavaya, M. J.,** Evidence for speckle effects on pulsed $CO_2$ lidar signal returns from remote targets, *Appl. Opt.,* 23, 1412, 1984.
48. **Foord, R., Jones, R., Vaughan, J. M., and Willets, D. V.,** Precise comparison of experimental and theoretical SNRs in $CO_2$ laser heterodyne systems, *Appl. Opt.,* 23, 3787, 1983.
49. **Killinger, D. K. and Menyuk, N.,** Remote probing of the atmosphere using a $CO_2$ DIAL system, *IEEE J. Quant. Electron.,* QE-17, 1917, 1981.
50. **Murray, E. R.,** Remote measurements of gases using discretely tunable infrared lasers, *Opt. Eng.,* 16, 284, 1977.
51. **Hardesty, R. M.,** Measurement of Range-Resolved Water Vapor Concentration by Coherent $CO_2$ Differential Absorption Lidar, NOAA Tech. Memo. ERL WPL-118, National Oceanic and Atmospheric Administration, Boulder, CO, 1984.
52. **Hardesty, R. M.,** Coherent DIAL measurements of range-resolved water vapor concentration, *Appl. Opt.,* 23, 2545, 1984.
53. **Murray, E. R., Van der Laan, J. E., and Hawley, J. G.,** Remote

measurent of HCL, $CH_4$, and $N_2O$ using a single-ended chemical-laser lidar system, *Appl. Opt.*, 15, 3140, 1976.
54. **Menyuk, N., Killinger, D. K., and DeFeo, W. E.,** Laser remote sensing of hydrazine, MMH, and UDMH, using a differential-absorption $CO_2$ Lidar, *Appl. Opt.*, 21, 2275, 1982.
55. **Asai, K. and Igarashi, T.,** Detection of ozone by differential absorption using $CO_2$ laser, *Opt. Quant. Electron.*, 7, 211, 1975.
56. **Menyuk, N., Killinger, D. K., and DeFeo, W. E.,** Remote sensing of NO using a differential absorption lidar, *Appl. Opt.*, 19, 3282, 1980.
57. **Persson, U., Johansson, J., Marthinsson, B., and Eng, S. T.,** Ethylene mass flow measurements with an automatic $CO_2$ laser long-path absorption system, *Appl. Opt.*, 21, 4417, 1982.
58. **Murray, E. R. and Byer, R. L.,** *Remote Measurements of Air Pollutants*, SRI International, 1980.
59. **Murty, R.,** Refractive turbulence effects on truncated gaussian beam heterodyne lidar, *Appl. Opt.*, 23, 2498, 1984.
60. **Lading, L., Hanson, S., and Skov Jensen, A.,** Diffraction-limited lidars: the impact of refractive turbulence, *Appl. Opt.*, 23, 2492, 1984.
61. **Megie, G. J., Ancellet, G., and Pelon, J.,** Lidar measurements of ozone vertical profiles, *Appl. Opt.*, 24, 3454, 1985.
62. **Yariv, A.,** *Introduction to Optical Electronics*, 2nd ed., Holt, Rinehart, & Winston, New York, 1976.
63. **Menzies, R. T.,** Laser Heterodyne Detection Techniques, in *Laser Monitoring of the Atmosphere*, Hinkley, E. D., Ed., Springer-Verlag, Berlin, 1976.
64. **Pratt, W. K.,** *Laser Communication Systems*, John Wiley & Sons, New York, 1969.
65. **Killinger, D. K., Menjuk, N., and DeFeo, W. E.,** Experimental comparison of heterodyne and direct detection for pulsed differential absorption $CO_2$ lidar, *Appl. Opt.*, 22, 682, 1983.
66. **Kalshoven, J. E. Jr., Korb, C. L., Schwemmer, G. K., and Dombrowski, M.,** Laser remote sensing of atmospheric temperature by observing resonant absorption of oxygen, *Appl. Opt.*, 20, 1967, 1981.
67. **Korb, C. L. and Weng, Chi Y.,** A theoretical study of a two-wavelength lidar technique for the measurement of atmospheric temperature profiles, *J. Appl. Meteorol.*, 21, 1346, 1982.
68. **Korb, C. L. and Weng, Chi Y.,** Differential absorption lidar technique for measurement of the atmospheric pressure profile, *Appl. Opt.*, 23, 3759, 1983.
69. **Grossmann, B. E., Cahen, C., Lesne, J. L., Benard, J., and Leboudec, G.,** Intensities and atmospheric broadening coefficients measured for $O_2$ and $H_2O$ absorption lines selected for dial monitoring of both temperature and humidity. I. $O_2$, *Appl. Opt.*, 25, 4261, 1986.
70. **Cahen, C., Grossmann, B. E., Lesne, J. L., Benard, J., and Leboudec, G.,** Intensities and atmospheric broadening coefficients measured for $O_2$ and $H_2O$ absorption lines selected for dial monitoring of both temperature and humidity. II. $H_2O$, *Appl. Opt.*, 25, 4268, 1986.
71. **Ritter, K. J. and Wilkerson, T. D.,** Strength, width, and pressure shift measurements of 54 lines in the oxygen A-Band, in 13th Int. Laser Radar Conf., NASA Conf. Publ. 2431, Toronto, Canada, August 11 to 15, 1986.
72. **Wilkerson, T. D., Schwemmer, G., and Gentry, B.,** Intensities and $N_2$ collision-broadening coefficients measured for selected $H_2O$ absorption lines between 715 and 732 nm, *J. Quant. Spectrosc. Radiat. Transfer*, 22, 315, 1979.
73. **Amstrong, H.,** Spectrum line profiles: the voight function, *J. Quant. Spectrosc. Radiat. Transfer*, 7, 61, 1967.
74. **Bosenberg, J.,** Measurements of the pressure shift of water vapour absorption lines by simoultaneous photoacoustic spectroscopy, *Appl. Opt.*, 24, 3531, 1985.
75. **Inaba, H.,** Detection of atoms and molecules by Raman scattering, in *Laser Monitoring of the Atmosphere*, Hinkley, E. D., Ed., Springer-Verlag, Berlin, 1976.
76. **Cahen, JC., Lesne, J. L., Deschamps, P., and Thro, P. Y.,** Testing the mobile DIAL system for humidity and temperature monitoring, in 14th Int. Laser Radar Conf., San Candido, Italy, June 20 to 24, 1988.
77. **Browell, E. V., Carter, A. F., Shipley, S. T., Allen, R. J., Butler, C. J., Mayo, M. N., Siviter, J. H., and Hall, W. M.,** Airborne DIAL system and measurements of ozone and aerosol profile, *Appl. Opt.*, 22, 522, 1983.
78. **Griggs, M.,** Absorption coefficients of ozone in the ultraviolet and visible regions, *J. Chem. Phys.*, 49, 857, 1968.
79. **Grant, W. B.,** Effect of differential spectral reflectance on DIAL measurements using topographic targets, *Appl. Opt.*, 21, 2390, 1982.
80. **Shumate, M. S., Lundqvist, S., Persson, U., and Eng, S. T.,** Differential reflectance of natural and man-made materials at $CO_2$ laser wavelengths, *Appl. Opt.*, 21, 2386, 1982.
81. **Bufton, J. L., Itabe, T., and Grolemund, D. A.,** Airborne remote sensing measurement with a pulsed $CO_2$ DIAL system, in *Optical and Laser Remote Sensing*, Killinger, D. K. and Mooradian, A., Ed., Springer-Verlag, Berlin, 1986.
82. **Petheram, J. C.,** Differential backscatter from the atmospheric aerosol: the implication for IR differential absorption lidar, *Appl. Opt.*, 20, 3941, 1981.
83. **Walling, G. C., Heller, D. F., Samelson, H., Harter, D. J., Pete, J. E., and Morris, R. C.,** Tunable alexandrite lasers: development and performance, *IEEE J. Quant. Electron.*, QE-21, 1568, 1985.
84. **Moulton, P. F.,** Spectroscopic and laser characteristics of Ti:$Al_2O_3$, *J. Opt. Soc. Am.*, 3, 125, 1986.
85. **Moulton, P. F.,** An investigation of the Co:$MgF_2$ system, *IEEE J. Quant. Electron.*, QE-21, 1582, 1985.
86. **Menyuk, N. and Killinger, D. K.,** Atmospheric remote sensing of water vapor, HCl and $CH_4$: using a continuously tunable Co:$MgF_2$ laser, *Appl. Opt.*, 26, 3061, 1987.
87. **Reed, E.,** A flashlamp-pumped, Q-switched Cr:Nd:GSGG laser, *IEEE J. Quant. Electron.*, QE-21, 1625, 1985.
88. American National Standards for the Safe Use of Lasers, *ANSI Rep.* Z136.1, American National Standards Institute, 1986.
89. Acceptable Levels of Micrometre Radiation, Rep. 65E, Health Council of Netherlands, Ministry of Health and Environment Protection, Rijswijk, Netherlands, 1978.
90. **Rothman, L. S., Gamache, R. R., Goldman, A., Brown, L. R., Toth, R. A., Pickett, H. M., Poynter, R. L., Flaud, J. M., Camy-Peyret, C., Barbe, A., Husson, N., Rinsland, C. P., and Smith, M. A. H.,** The HITRAN database: 1986 edition, *Appl. Opt.*, 26, 4058, 1987.
91. **Grant, W. B., Brothers, A. M., and Bogan, J. R.,** Differential absorption lidar signal averaging, *Appl. Opt.*, 27, 1934, 1988.
92. **Molina, L. T. and Molina, M. J.,** Absolute absorption cross-sections of ozone in the 185- to 350-nm wavelength range, *J. Geophys. Res.*, 91, 14501, 1986.
93. **Jaeger, T. and Wang, G.,** Tunable high-pressure infrared lasers, in *Tunable Lasers*, Mollenauer, L. F. and White, J. C., Eds., Springer-Verlag, Berlin, 1987.
94. **Mollenauer, L. F.,** Color center lasers, in *Tunable Lasers*, Mollenauer, L. F. and White, J. C., Eds., Springer-Verlag, Berlin, 1987.
95. **Galletti, E., Zanzottera, E., Draghi, S., Garbi, M., and Petroni, R.,** Gas correlation lidar for methane detection, in 13th Int. Laser Radar Conf., NASA Conf. Publ. 2431, Toronto, Canada, August 11 to 15, 1986.
96. **Galletti, E.,** Detection of methane leaks with a correlation lidar, in Topical Meeting Laser Opt. Remote Sensing: Instrum. Techn., *Opt. Soc.* Am. Tech. Digest Ser., Vol 18, North Falmouth, MA, September 28 to October 1, 1987.
97. **Brosnan, S. J. and Byer, R. L.,** Optical parametric oscillator threshold and linewidth studies, *IEEE J. Quant. Electron.*, QE-15, 6, 415, 1979.
98. **Brassington, D. J.,** Differential absorption lidar measurements of at-

mospheric water vapour using an optical parametric oscillator source, *Appl. Opt.*, 21, 4411, 1982.

99. **Baumgartner, R. A. and Byer, R. L.,** Continuously tunable IR lidar with applications to remote measurements of $SO_2$ and $CH_4$, *Appl. Opt.*, 21, 4411, 1982.
100. **Henningsen, T., Garbuny, M., and Byer, R. L.,** Remote detection of CO by parametric tunable laser, *Appl. Phys. Lett.*, 24, 242, 1974.
101. **Endemann, M. and Byer, R. L.,** Remote single-ended measurements of atmospheric temperature and humidity at 1.77 μm using a continuously tunable source, *Opt. Lett.*, 5, 452, 1980.
102. **Cheng, K., Rosker, M. J., and Tang, C. L.,** Urea parametric oscillator for the visible and near infrared, in *Tunable Lasers*, Mollenauer, L. F. and White, J. C., Eds., Springer-Verlag, Berlin, 1987.
103. **Alkemade, C. Th. J., Hollander, Tj., Snelleman, W., and Zeegers, P. J. Th.,** *Metal Vapours in Flames*, Pergamon Press, Elmsford, NY, 1981.
104. **Grant, W. B.,** He-Ne and $CO_2$ laser long-path systems for gas detection, *Appl. Opt.*, 25, 709, 1986.
105. **Goodman, J. W.,** Statistical properties of laser speckle patterns, in *Laser Speckle and Related Phenomena*, Dainty, J. C., Ed., Springer-Verlag, Berlin, 1975.
106. **Clifford, S. F. and Wandzura, S.,** Monostatic heterodyne lidar performance: the effect of turbulent atmosphere, *Appl. Opt.*, 20, 514, 1981.
107. **Grossmann, B. E., Singh, U. N., Higdon, N. S., Cotuoir, L. J., Wilkerson, T. D., and Browell, E. V.,** Linewidth characteristics of Raman shifted dye laser output at 720 and 940 nm, in 13th Int. Laser Radar Conf., Toronto, Canada, August 11 to 15, 1986.
108. **Kagann, R. H., Petheram, J. C., and Rosenberg, A.,** Tunable Nd:glass Raman laser for DIAL applications, in Proc. SPIE, Vol. 736, New Slab and Solid-State Laser Technologies and Applications, Los Angeles, January 15 to 16, 1987.
109. **Bristow, M.,** Design concepts for an airborne UV DIAL system for monitoring tropospheric $O_3$ and $SO_2$ in 1st Int. DIAL Data Coll. Anal. Workshop, Virginia Beach, VA, November 18 to 21, 1985.
110. **Hinkley, E. D., Ku, R. T., and Kelley, P. L.,** Techniques for detection of molecular pollutants by absorption of laser radiation, in *Laser Monitoring of the Atmosphere*, Hinkley, E. D., Ed., Springer-Verlag, Berlin, 1976.
111. **Berlman, I. B.,** *Handbook of Fluorescence Spectra of Aromatic Molecules*, 2nd ed., Academic Press, New York, 1971.
112. **Jenkins, T. E.,** *Optical Sensing Techniques and Signal Processing*, Prentice-Hall International, United Kingdom, 1987.
113. **Milton, M. J. T.,** Corrections for Differential Scattering by Aerosols in the Measurement of Ozone by DIAL, NPL Rep. Qu87, 1987.
114. **McCormick, M. P. and Swissler, T. J.,** Stratospheric Aerosol Mass and Latitudinal Distribution of the El Chicon Eruption Cloud for October 1982, *Geophys. Res. Lett.* 10, 1983.
115. **Post, M. J.,** Lidar Observations of the El Chicon Cloud at 10.6 micron, *Geophys. Res. Lett.* 9, 1984.
116. **Browell, E. V., Danielsen, E. F., Ismail, S., Gregory, G. L., and Beck, S. M.,** Tropopause fold structure determined form airborne lidar and in situ measurements, *J. Geophys. Res.*, 92, 2112, 1987.
117. **Killinger, D. K., Bufton, J. L., and McLellan, E. J.,** Enhanced direct-detection of $CO_2$ lidar returns using a laser pre-amplifier, in Topical Meet. Laser Opt. Remote Sensing: Instrum. Tech., North Falmouth, MA, September 28 to October 1, 1987.
118. **Van der Laan, J. E.,** Low presssure gain-cell laser-detector operation with a $CO_2$ transversely excited atmospheric (TEA) laser, in Topical Meet. Laser Opt. Remote Sensing: Instrum. Tech., North Falmouth, MA, September 28 to October 1, 1987.
119. **Kinpui, C. and Bufton, J. L.,** $CO_2$ laser pre-amplifier for lidar application, in Topical Meet. Laser Opt. Remote Sensing: Instrum. Tech., North Falmouth, MA, September 28 to October 1, 1987.
120. **Browell, E. D.,** Differential absorption lidar sensing of ozone, *Proc. IEEE*, 77, 419, 1989.
121. **Bufton, J. L., Toshikazu, I., and Grolemund, D. A.,** Airborne remote sensing measurements with a pulsed $CO_2$ DIAL system, in *Optical and Laser Remote Sensing*, Killinger, D. K. and Mooradian, A., Eds., Springer-Verlag, Berlin, 1983.
122. **Post, M. J.,** Aerosol backscattering profiles at $CO_2$ wavelengths: the NOAA data base, *Appl. Opt.*, 23, 2507, 1984.
123. **Bösenberg, J.,** A DIAL system for high resolution water vapor measurements in the troposphere, in 1st Int. DIAL Data Coll. Anal. Workshop, Virginia Beach, VI, November 18 to 21, 1985.
124. **Pelon, J.,** The Leandre Project: a french airborne lidar system for meteorological studies, in Topical Meet. Laser Opt. Remote Sensing: Instrum. Tech., Optical Soc. Am. Tech. Dig. Ser. Vol. 18, North Falmouth, MA, September 28 to October 1, 1987.
125. **Edner, H., Faris, G. W., Sunesson, A., and Svanberg, S.,** Mapping of Atmospheric Atomic Mercury using Differential Absorption Lidar Techniques, Paper TuL3, CLEO 88, Anaheim, CA, April 25 to 28, 1988.
126. **Heaps, W. S. and McGee, T. J.,** Measurement of stratospheric hydroxyl radical by ballon borne lidar, in 12th Int. Laser Radar Conf., Aix en Provence, France, August 13 to 17, 1984.
127. **Granier, C., Jegou, J. P., and Megie, G.,** Resonant lidar detection of Ca and $Ca^+$ in the upper atmosphere in 12th Int. Laser Radar Conf., Aix en Provence, France, August 13 to 17, 1984.
128. **Schwemmer, G. K., Dombrowsky, M., Korb, C. L., Milrod, J., Walden, H., and Kagann, R. H.,** A lidar system for measuring atmospheric pressure and temperature profiles, *Rev. Sci. Instrum.*, 12, 58, 1987.
129. **Measures, R. M.,** *Laser Remote Sensing: Fundamentals and Applications*, John Wiley & Sons, 1984.
130. **Camagni, P. and Sandroni, S.,** Joint Research Centre Ispra, in Optical Remote Sensing of Air Pollution, Elsevier, New York, 1984.
131. **Hinkley, E. D., Ed.,** *Laser Monitoring of the Atmosphere*, Springer-Verlag, Berlin, 1976.
132. **Killinger, D. K. and Mooradian, A., Eds.,** *Optical and Laser Remote Sensing*, Springer-Verlag, Berlin, 1986.
133. **Zuev, V. E.,** *Laser Beams in the Atmosphere* (transl.), Consultant Bureau, New York, 1982.
134. **Kobayashi, T.,** Techniques for laser remote sensing of the environment, *Remote Sensing Rev.*, 3, 1, 1987.
135. **Lin, J. T. and Chen, C.,** Choosing a nonlinear crystal, in *Laser and Optronics*, Gordon Publications, Dover, NJ, 1987.
136. **Eimerl, D., Davis, L., Velsko, S., Graham, E. K., and Zalkin, A.,** Optical, mechanical and thermal properties of barium borate, *J. Appl. Phys.*, 62, 1968, 1987.
137. **Warneck, P., Marmo, F. F., and Sullivan, J. O.,** Ultraviolet absorption of $SO_2$: dissociation energies of $SO_2$ and SO, *J. Chem. Phys.*, 40, 1132, 1964.
138. **Thompson, B. A., Harteck, P., and Reeves, R. R. Jr.,** Ultraviolet absorption coefficients of $CO_2$, CO, $O_2$, $H_2O$, $N_2O$, $NH_3$, NO, $SO_2$, and $CH_4$, between 1850 and 4000 A, *J. Geophys. Res.*, 68, 6431, 1963.
139. **Woods, P. T., Jolliffe, B. W., and Marx, B. R.,** High-resolution spectroscopy of $SO_2$ using a frequency-doubled pulsed dye laser, with application to the remote sensing of atmospheric pollutants, *Opt. Commun.*, 33, 281, 1980.
140. **Woods, P. T. and Jolliffe, B. W.,** Experimental and theoretical studies related to a dye laser differential lidar system for the determination of atmospheric $SO_2$ and $NO_2$ concentrations, *Opt. Laser Technol.*, 25, 1978.
141. **Hall, T. C. Jr. and Blacet, F. E.,** Separation of the absorption spectra of $NO_2$ and $N_2O_4$ in the range of 2400-5000 A, *J. Chem. Phys.*, 20, 1745, 1952.

142. **Jacobs, T. A. and Giedt, R. R.,** Absorption coefficients of $Cl_2$ at high temperatures, *J. Quant. Spectrosc. Radiat. Transfer*, 5, 457, 1965.
143. **Tajime, T., Saheki, T., and Ito, K.,** Absorption characteristics of the Γ-O band of nitric oxide, *Appl. Opt.*, 17, 1290, 1978.
144. **Brassington, D. J.,** Measurements of the $SO_2$ Absorption Spectrum Between 297 and 316 nm, Lab. Note Rd/L/N 184/79, Central Electricity Research Laboratories, 1980.
145. **Brassington, D. J.,** Tunable Dye Laser Measurements of the $SO_2$ Absorption Spectrum Between 290 and 317 nm, Lab. Note RD/L/2055N81, Central Electricity Research Laboratories, 1981.
146. **Ogawa, M.,** Absorption cross sections of $O_2$ and $CO_2$ continua in the Shumann and far-UV regions, *J. Chem. Phys.*, 54, 2550, 1971.
147. **Fredriksson, K. A. M. and Hertz, H. M.,** Evaluation of the DIAL technique for studies on $NO_2$ using a mobile lidar system, *Appl. Opt.*, 23, 1403, 1984.
148. **Alden, M., Edner, H., and Svanberg, S.,** Laser monitoring of atmospheric NO using ultraviolet differential-absorption techniques, *Opt. Lett.*, 7, 543, 1982.
149. **Egeback, A., Fredriksson, K. A., and Hertz, H. M.,** DIAL technique for the control of sulfur dioxide emissions, *Appl. Opt.*, 23, 722, 1984.
150. **Edner, H., Fredriksson, K., Sunesson, A., Svanberg, S., Uneus, L., and Wendt, W.,** Mobile remote sensing for atmospheric monitoring, *Appl. Opt.*, 26, 4330, 1987.
151. **Alden, M., Edner, H., and Svanberg, S.,** Remote measurement of atmospheric mercury using differential absorption lidar, *Opt. Lett.*, 7, 221, 1982.
152. **Ancellet, G. M. and Menzies, R. T.,** Atmospheric correlation-time measurements and effects on coherent doppler lidar, *J. Opt. Soc. Am.*, 4, 367, 1987.
153. **Hardesty, R. M., Keeler, R. J., Post, M. J., and Richter, R. A.,** Characteristics of coherent lidar returns from calibration targets and aerosols, *Appl. Opt.*, 21, 3763, 1981.
154. **Siegman, A. E.,** The antenna properties of optical heterodyne receivers, *Proc. IEEE*, 54, 1350, 1966.
155. **Klein, B. J. and Degnan, J. J.,** Optical antenna gain. I. Transmitting antennas, *Appl. Opt.*, 13, 2134, 1974.
156. **Degnan, J. J. and Klein, B. J.,** Optical antenna gain. II. Receiving antennas, *Appl. Opt.*, 13, 2397, 1974.
157. **Korb, C. L., Schwemmer, G. K., Dombrowski, M., Milrod, J., and Walden, H.,** Airborne lidar measurements of the atmospheric pressure profile with tunable alexandrite laser, in 13th Int. Laser Radar Conf., NASA Conf. Publ. 2431(abstr.), 1986, 52.
158. **Bösenberg, J.,** A DIAL system for high resolution water vapour measurements in the troposphere, in Topical Meet. Laser Opt. Remote Sensing: Instrum. Tech., Opt. Soc. Am. Tech. Digest Ser. Vol 18, North Falmouth, MA, September 28 to October 1, 1987.
159. **Melfi, S. H., Whiteman, D., Ferrare, R. R., and Falcone, V.,** Observation of frontal passages using a raman lidar, in 14th Int. Laser Radar Conf., San Candido, Italy, June 20 to 24, 1988.
160. **Melfi, S. H. and Whiteman, D.,** Observation of lower atmosphere moisture structure and its evolution using a Raman lidar, *Bull. Am. Meteorol. Soc.*, 16, 1288, 1985.
161. **Pourny, J. C., Renaut, D., and Orsag, A.,** Raman-lidar humidity sounding of the atmospheric boundary layer, *Appl. Opt.*, 18, 1141, 1979.
162. **Zuev, V. E.,** Laser-light transmission through the atmosphere, in *Laser Monitoring of the Atmosphere*, Hinkley, E. D., Ed., Springer-Verlag, Berlin, 1976.
163. **Marzorati, A., Corio, W., and Zanzottera, E.,** Remote sensing of $SO_2$ during field tests at Fos-Berre in June 1983, in 12th Int. Laser Radar Conf., Aix en Provence, France, August 13 to 17, 1984.
164. **Jolliffe, B. W., Felton, R. C., Swann, N. R., and Woods, P. T.,** Field measurements studies using a differential absorption lidar system, in 12th Int. Laser Radar Conf., Aix en Provence, France, August 13 to 17, 1984.
165. **Capitini, R., Ancellet, G., Megie, G., Pelon, J., and Renaut, D.,** DIAL lidar measurements of atmospheric pollutants ($SO_2$, $O_3$) during the Fos-Berre 83 experiment, in 12th Int. Laser Radar Conf., Aix en Provence, France, August 13 to 17, 1984.
166. **Hawley, J. G.,** Plume Model Validation and Development Project: Differential Absorption Lidar Measurements of $SO_2$ in Moderately Complex Terrain, EPRI EA-3758, Final Report, SRI International, 1985.
167. **Staehr, W., Lahman, W., Weitcamp, C., and Michaelis, W.,** Differential-absorption lidar system for $NO_2$ and $SO_2$ monitoring in 12th Int. Laser Radar Conf., Aix en Provence, France, August 13 to 17, 1984.
168. **Yeh, S. and Browell, E. V.,** Shuttle lidar resonance fluorescence investigations analysis of Na and K measurements, *Appl. Opt.*, 21, 2365, 1982.
169. **Yeh, S. and Browell, E. V.,** Shuttle lidar resonance fluorescence investigations. II. Analysis of thermospheric $Mg^+$ measurements, *Appl. Opt.*, 21, 2373, 1982.
170. **Littman, M. and Montgomery, J.,** Grazing-incidence designs improves pulsed dye lasers, in *Laser Focus/Electro Optics*, 1988.
171. **Papayannys, A., Ancellet, G., Pelon, J., and Megie, G.,** Tropospheric ozone DIAL measurements using a Nd:YAG laser and Raman shifters, in 14th Int. Laser Radar Conf., San Candido, Italy, June 20 to 24, 1988.
172. **Nava, E. and Malvicini, C.,** A tunable alexandrite laser for remote sensing in 14th Int. Laser Radar Conf., San Candido, Italy, June 20 to 24, 1988.
173. **Welford, D. and Moulton, P. F.,** Room-temperature operation of the Co:$MgF_2$ Laser, Paper ME5, CLEO 88, Anaheim, CA, April 25 to 28, 1988.
174. **Eckardt, R. C.,** Infrared frequency generation in chalcopyrite crystals $AgGaS_2$ and $AgGaSe_2$, in *Tunable Solid State Laser for Remote Sensing*, Byer, R. L., Gustafson, E. K., and Trebino, R., Ed., Springer-Verlag, Berlin, 1984.
175. **Andreev, Y. M., Voevodin, V. G., Geiko, P. P., Gribenyukov, A. I., Zuev, V. V., and Zuev, V. E.,** Effective source of coherent radiation based on $CO_2$ lasers and $ZnGeP_2$ wavelength converters, in Topical Meet. Laser Opt. Remote Sensing: Instrum. Tech., Opt. Soc. Am. Tech. Digest Ser. Vol. 18, North Falmouth, MA, September 28 to October 2, 1987.
176. **Sakamoto, M., Harnagel, G. L., Welch, D. F., Lennon, C. R., Streifer, W., Kung, H., Scifres, D. R.,** Continuous-wave 12.5 W monolithic laser diode arrays, Paper WB2, CLEO 88, Anaheim, CA, April 25 to 28, 1988.
177. **Fan, Y. X., Eckardt, R. C., Byer, R. L., Nolting, J., and Wallenstein, R.,** Visible Ba $B_2O_4$ optical parametric oscillator pumped at 355 nm by a single-axial-mode pulsed source, *Appl. Phys. Lett.*, 53, 2014, 1988.
178. **Komine, H.,** β-Barium borate optical parametric oscillator, Paper PD32-1, CLEO 88, Anaheim, CA, April 25 to 28, 1988.
179. **Cheng, L. K., Bosenberg, W. R., Edeltein, D. C., and Tang, C. L.,** Demonstration of optical parametric oscillation in β-$BaB_2O_4$ in the visible and near infrared Paper PD33-1, CLEO 88, Anaheim, CA, April 25 to 28, 1988.
180. **Edner, H., Fredriksson, K., Sunesson, A., and Wendt, W.,** Monitoring $Cl_2$ using a differential absorption lidar system, *Appl. Opt.*, 26, 3183, 1987.
181. **Ansmann, A.,** Errors in ground-based water-vapour DIAL measurements due to Doppler-broadened Rayleigh backscattering, *Appl. Opt.*, 24, 3476, 1985.
182. **Ansmann, A. and Bösenberg, J.,** Correction scheme for spectral

broadening by Rayleigh scattering in differential absorption lidar measurements of water vapour in the troposphere, *Appl. Opt.*, 26, 3026, 1987.
183. **Browell, E. V., Carter, A. F., and Wilkerson, T. D.,** Airborne differential absorption lidar system for water vapor investigation, *Opt. Eng.*, 20, 84, 1981.
184. **Grant, W. B.,** The mobile atmospheric pollutant mapping (MAPM) system: a coherent $CO_2$ DIAL system, SPIE Vol. 1062, *Laser Applications in Meteorology and Earth and Atmospheric Remote Sensing*, 1989, 172.
185. **Schwemmer, G.,** Frequency stabilized diode laser system for active control of DIAL lasers, wavemeters, and receiver filters, in 14th Int. Laser Radar Conf., San Candido, Italy, June 20 to 24, 1988.
186. **Measures, R. M., Ed.,** *Laser Remote Chemical Analysis*, John Wiley & Sons, New York, 1988.
187. **Dereniak, E. L. and Crowe, D. G.,** *Optical Radiation Detectors*, John Wiley & Sons, New York, 1984.
188. **Keyes, R. J. Ed.,** Optical and Infrared Detectors, in *Topics in Applied Physics* Vol. 19, Springer-Verlag, Berlin, 1980.
189. **Schotland, R. M.,** Some observations of the vertical profile of water vapour by a laser optical radar, in Proc. 4th Symp. Remote Sensing Environ., University of Michigan, Ann Arbor, April 12 to 14, 1966.
190. **Schotland, R. M.,** Errors in lidar measurements of atmospheric gases by differential absorption, *J. Appl. Meteorol.*, 13, 71, 1974.
191. **Harms, J., Lahman, Q., and Weitcamp, C.,** Geometrical compression of lidar return signals, *Appl. Opt.*, 17, 1131, 1978.
192. **Harms, J.,** Lidar return signal for coaxial and non-coaxial systems with central obstruction, *Appl. Opt.*, 18, 1559, 1979.
193. **Green, B. A., Masters, D., Rye, B. J., and Thomas, E. L.,** Antenna Considerations in Atmospheric Backscatter Coherent Lidar, Paper TuB3, Coherent Laser Radar for Atmospheric Sensing, Aspen, CO, July 15 to 17.
194. **Sliney, D. and Wolbarsht, M.,** *Safety with Lasers and Other Optical Sources — A Comprehensive Handbook*, Plenum Press, New York, 1980.
195. **Streifer, W., Scifres, D. R., Harnagel, G. L., Welch, D. F., Berger, J., and Sakomoto, M.,** Advances in diode laser pumps, *IEEE J. Quant. Electron.*, 24, 883, 1988.
196. **Egglestone, J. M., DeShazer, L. G., and Kangas, K. W.,** Characteristics and kinetics of laser-pumped Ti:Sapphire oscillators, *IEEE J. Quant. Electron.*, 24, 1009, 1988.
197. **Megie, G., Bos, F., Blamont, J. E., and Chanin, M. L.,** Simultaneous nightime lidar measurements of atmospheric sodium and potassium, *Planet. Space Sci.*, 26, 27, 1978.
198. **Fredriksson, K.,** DIAL technique for pollution monitoring: improvements and complementary systems, *Appl. Opt.*, 24, 3297, 1985.
199. **Sassen, K. and Dodd, G. C.,** Lidar crossover function and misalignment effects, *Appl. Opt.*, 21, 3162, 1982.
200. **Basiev, T. T., Mirov, S. B., and Osiko, V. V.,** Room-temperature color center lasers, *IEEE J. Quant. Electron.*, 24, 1052, 1988.
201. **McIlrath, T. C.,** Fluorescence lidar, *Opt. Eng.*, 19, 494, 1980.
202. **DeMartino, A., Frey, R., and Pradére, F.,** Near- to far-infrared tunable Raman Laser, *IEEE J. Quant. Electron.*, QE-16, 1184, 1980.
203. **Kolsch, H. J., Rairoux, P., Wolf, J. P., and Woste, L.,** New perspectives in remote sensing using excimer-pumped dye lasers and $\beta$-$BaB_2O_4$ crystals, in 14th Int. Laser Radar Conf., San Candido, Italy, June 20 to 24, 1988.
204. **Milton, M. J. T., Bradsell, R. H., Jolliffe, B. W., Swann, N. R. W., and Woods, P. T.,** The design and development of a near-infrared DIAL system for the detection of hydrocarbons, in 14th Int. Laser Radar Conf., San Candido, Italy, June 20 to 24, 1988.
205. **Liou, K. N. and Schotland, R. M.,** Multiple backscattering and depolarization from water clouds for a pulsed lidar system, *J. Atmos. Sci.*, 28, 772, 1971.
206. **Edner, H., Svanberg, S., Uneus, L., and Wendt, W.,** Gas-correlation lidar, *Opt. Lett.*, 9, 493, 1984.
207. **Brassington, D. J., Felton, R. C., Jolliffe, B. W., Marx, B. R., Moncrieff, J. T. M., Rowley, W. R. C., and Woods, P. T.,** Errors in spectroscopic measurements of $SO_2$ due to nonexponential absorption of laser radiation, with application to the remote sensing of atmospheric pollutants, *Appl. Opt.*, 23, 469, 1984.
208. **Houston, J. D., Sizgoric, S., Ulitsky, A., and Banic, J.,** Raman lidar system for methane gas concentration measurements, *Appl. Opt.*, 25, 2115, 1986.
209. **Lahmann, W., Staehr, W., Weitcamp, C., and Michaelis, W.,** Range-sensitivity optimization of range-resolved differential absorption lidar, in 12th Int. Laser Radar Conf., Aix en Provence, France, August 13 to 17, 1984.
210. **Walling, J. C.,** Tunable paramagnetic-ion solid state lasers, in *Tunable Lasers*, Mollenauer, L. F. and White, J. C., Eds., Springer-Verlag, Berlin, 1987.
211. **White, J. C.,** Stimulated Raman Scattering, in *Tunable Lasers*, Mollenauer, L. F. and White, J. C. Eds., Springer-Verlag, Berlin, 1987.
212. **Byer, R. L.,** Parametric oscillators and nonlinear materials, in *Nonlinear Optics*, Harper P. G. and Wherrett, B. S., Eds., Academic Press, New York, 1977.
213. **Baumgartner, R. A. and Byer, R. L.,** Optical parametric amplification, *IEEE J. Quant. Electron.*, QE-15, 432, 1979.
214. **Cappellini, V., Constantinides, A. G., and Emiliani, P.,** *Digital Filters and Their Applications*, Academic Press, London, 1978.
215. **Young, A. T.,** Photomultipliers: their cause and cure, in *Methods of Experimental Physics Vol. 12, Part A: Optical and Infrared*, Carleton, N. Ed., Academic Press, New York, 1974.
216. **Killinger, D. K. and Menyuk, N.,** Effect of turbulence-induced correlation on laser remote sensing errors, *Appl. Phys. Lett.*, 38, 968, 1981.